# Efficient Reconstruction Techniques for Compressively Sampled Magnetic Resonance Imaging



By

## Maria Murad

Reg. No. 88-FET/PHDEE/S15

A dissertation submitted to I.I.U. in partial fulfillment of the requirements for the degree of

## **DOCTOR OF PHILOSOPHY**

Department of Electrical and Computer Engineering Faculty of Engineering and Technology INTERNATIONAL ISLAMIC UNIVERSITY ISLAMABAD



Miles of setime in the series of the series

## Copyright © 2022 by Maria Murad

All rights reserved. No part of the material protected by this copyright notice may be reproduced or utilized in any form or by any means, electronic or mechanical, including photocopying, recording, or by any information storage and retrieval system, without permission from the author.

# **DEDICATED TO**

My Teachers and Family

# CERTIFICATE OF APPROVAL

Title of Thesis: Efficient Reconstruction Techniques for Compressively Sampled Magnetic

Resonance Imaging

Name of Student: MARIA MURAD

Registration No: 88-FET/PhDEE/S15

Accepted by the Department of Electrical and Computer Engineering, Faculty of Engineering and Technology, International Islamic University (IIU), Islamabad, in partial fulfillment of the requirements for the Doctor of Philosophy degree in Electronic Engineering.

#### Viva voce committee:

Prof. Dr. Abdul Jalil (Supervisor)

Professor DECE, FET IIU Islamabad

Dr. Muhammad Bilal (Co-Supervisor)

Lecturer DECE, FET IIU Islamabad

<u> Prof. Dr. Muhammad Amir (Internal Examiner)</u>

Professor DECE, FET, IIU Islamabad

Dr. Muhammad Zia (External Examiner-I)

Associate Professor Department of Electronics,

Quaid-i-Azam University, Islamabad.

Prof. Dr. Tanveer Ahmed Cheema (External Examiner-II)

Professor Department of Electrical Engineering,

Isra University, Islamabad.

Dr. Shahid Ikram (Chairman, DECE)

Assistant Professor DECE, FET, IIU Islamabad

Prof. Dr. Nadeem Ahmad Sheikh (Dean, FET)

Professor DME, FET, IIU Islamabad

12th September, 2022

iv

#### Abstract

Magnetic Resonance Imaging (MRI) is used to produce detailed images of body tissues and organs using strong magnets and radio waves, but with a very slow acquisition process. In multi-slice MRI hundreds of slices are acquired for just a single scan. Compressed Sensing (CS) has efficiently accelerated the MRI acquisition process by employing different reconstruction strategies using a fraction of the random Nyquist samples. The interpolated Compressed Sensing (iCS) techniques have further reduced this scan time by exploiting the strong inter-slice correlation of multi-slice MRI through interpolation.

The primary objective of this thesis is to propose several efficient interpolated Compressed Sensing MRI (iCSMRI) techniques based on highly under-sampled data and the most efficient, novel interpolation approaches. These novel interpolation techniques exploit the sampling trajectories of different under-sampling patterns and their combinations. The proposed techniques show improvement in terms of image quality and information content along with reduced scan time and lower computational complexity.

The first contribution is a novel Fast interpolated Compressed Sensing (FiCS) technique based on a 2D Variable Density Under-Sampling (2D-VRDU) scheme. The novel interpolation technique of FiCS takes two consecutive slices and estimates the missing samples of each target slice (T slice) from its corresponding left slice (L slice). Compared to the previous iCS methods, slices recovered with the proposed FiCS technique have a maximum correlation with their corresponding original slices using even half of their under-sampling ratio.

The second contribution is an improved Efficient interpolated Compressed Sensing (EiCS) technique using a non-Cartesian Radial under-sampling approach. The novel interpolation technique of EiCS uses three consecutive slices to estimate the missing samples of the central target slice from its two neighboring slices. The EiCS technique has improved image quality and performance compared to FiCS using both Golden-Angle (GA) and Uniform-Angle (UA) Radial under-sampling patterns, with sharper details and more improved results.

In the last part of this thesis, the previously proposed techniques have been combined to overcome their shortcoming, termed as Modified Fast interpolated Compressed Sensing (Mod-FiCS) technique. This technique has a three-step interpolation approach like EiCS and uses the Gaussian-Radial under-sampling scheme. This undersampling has an edge that, it neither shows any streaking artifacts like Radial nor any blurred edges like 2D-VRDU. The Mod-FiCS technique shows even more improved results and performance compared to the previous techniques using the same computational cost and under-sampling ratio.

In this thesis, the Non-linear Conjugate Gradient (NCG) algorithm has been used as a CS reconstruction approach for the proposed iCSMRI techniques. The evaluation has been performed using MATLAB simulation with different Vivo knee and brain multislice MRI datasets, all available online. The assessment has been performed using seven state-of-the-art evaluation parameters and compared with recent iCS techniques and CS for computing both qualitative and quantitative analysis.

### List of Publications

- [1]. Murad, M., Bilal, M., Jalil, A., Ali, A., Mehmood, K. and Khan, B., 2020. Efficient reconstruction technique for multi-slice CS-MRI using novel interpolation and 2D sampling scheme. IEEE Access, 8, pp.117452-117466.
- [2]. Murad, M., Jalil, A., Bilal, M., Ikram, S., Ali, A., Khan, B. and Mehmood, K., "Radial Undersampling-Based Interpolation Scheme for Multislice CSMRI Reconstruction Techniques," BioMed Research International, vol. 2021, p. 6638588, 2021/04/13 2021.
- [3]. Murad, M., Jalil, A., Bilal, M., Ikram, S., Ali, A., Mehmood, K. and Khan, B., "Gaussian-Radial Under-Sampling Based CSMRI Reconstruction using a Modified Interpolation Approach," International Conference on Electrical, Communication, and Computer Engineering (ICECCE), 2021, pp. 1-6.
- [4]. Khan, B., Ali, A., Jalil, A., Mehmood, K., Murad, M. and Awan, H., 2020.
  AFAM-PEC: Adaptive Failure Avoidance Tracking Mechanism Using Prediction-Estimation Collaboration. IEEE Access, 8, pp.149077-149092.
- [5]. Mehmood, K., Jalil, A., Ali, A., Khan, B., Murad, M., Khan, W.U. and He, Y., 2021. Context-Aware and Occlusion Handling Mechanism for Online Visual Object Tracking. Electronics, 10(1), p.43.
- [6]. Mehmood, K., Jalil, A., Ali, A., Khan, B., Murad, M., K. M. Cheema, AH Milyani "Spatio-Temporal Context, Correlation Filter and Measurement Estimation Collaboration Based Visual Object Tracking," Sensors, vol. 21, p. 2841, 2021.
- [7]. Mehmood, K., Ali, A., Jalil, A., Khan, B., K. M. Cheema, M. Murad, AH Milyani "Efficient Online Object Tracking Scheme for Challenging Scenarios," Sensors, vol. 21, p. 8481, 2021.
- [8]. B. Khan, A. Jalil, A. Ali, K. Alkhaledi, K. Mehmood, K. M. Cheema, M. Murad, H Tariq, AM El-Sherbeeny. "Multiple Cues-Based Robust Visual Object Tracking Method," Electronics, vol. 11, p. 345, 2022.

The research work presented in this dissertation is based on the first three publications.

## Acknowledgments

In the name of Allah (SubhanahuWaTa'ala), who is the most gracious and the most merciful. I would like to thank Allah for giving me the strength and patience to complete this research work. Peace and blessings of Allah be upon His last Prophet Muhammad (Sallallahu Alaihi wa Aalihi wa Sallam) and all his Sahaba (Razi Allah Tala Anhu) who dedicated their lives for Dawah and spread of Knowledge.

I am truly grateful to Dr. Ijaz Mansoor Qureshi (Late) and my supervisor Prof. Dr. Abdul Jalil, whose inspiration, ideas, and efforts make it possible for me to complete my higher studies. The role and support of my co-supervisor Dr. Muhammad Bilal during my Ph.D. research work was exceptional. His encouraging and never-ending support is always a source of motivation for me.

It has been an honor to be the student of Dr. Aqdas Naveed Malik, Dr. Abdul Basit, Dr. Jawad Ali Shah, Dr. Ihsanul Haq, Dr. Syed Zubair, Dr. Shahid Ikram, Dr. Shehbaz Khan, and Dr. Ahmad Ali from whom I learned and benefited a lot. I am very fortunate to receive their long-standing support at each stage of my Ph.D.

I would also like to acknowledge the support of International Islamic University Islamabad Pakistan for providing me one year of study leave and a full fee waiver during the Ph.D. studies.

The biggest thanks go to my family members: My mother and father. It is only because of their love, never-ending support, and prayers that I have completed my Ph.D. I owe a lot to my husband: Syed Saifullah Shah for his unending encouragement and patience. Lastly, I express my special graduate to my kids for always making me smile and allowing me to utilize their time in my research.

(Maria Murad)

# **Table of Contents**

Abstrac	:t		. v		
List of Publicationsvii					
Acknov	Acknowledgmentsviii				
Table o	f Co	ntents	ix		
List of	Figur	es	Xii		
List of	Table	es	ΧV		
List of	Abbr	eviations	cvi		
Chapter	r 1		. 1		
Introdu	ction		. 1		
1.1	Dis	sertation contribution	. 2		
1.2	The	esis organization	. 4		
Chapter	r <b>2</b>		. 6		
MRI A	cquis	ition and Reconstruction	. 6		
2.1	Intr	oduction	. 6		
2.2	MR	U Acquisition	. 7		
2.3	MR	I Reconstruction Techniques	10		
2.3	.1	Parallel MRI (pMRI)	11		
2.3	.2	CSMRI	12		
2.3	.3	iCSMRI	18		
2.4	Lite	erature Review	18		
2.5	Dat	a Sets	22		
2.6	Eva	duation Criteria and Simulation Environment	23		
2.6	.1	Subjective Assessment	23		
2.6	.2	Objective Assessment	23		
2.6	.3	Simulation Environment	26		
2.7	Sun	nmary	26		
Chapter	3		27		
		ated Compressed Sensing Technique using 2D Sampling Scheme for Multi	- 27		
3.1	Intr	oduction	27		
3.2	Rela	ated Work	27		
3.3	The	FiCS Technique.	28		

3.3.1	2D-VRDU Under-Sampling Scheme	29
3.3.2	Novel Fast Interpolation Scheme	31
3.3.3	CS Reconstruction	33
3.4 Si	mulation and Results	35
3.4.1	Evaluation of the Under-Sampling Scheme	35
3.4.2	Evaluation of the Fast Interpolation Scheme of FiCS	39
3.4.3	Evaluation of FiCS	44
3.5 St	ımmary	44
Chapter 4		47
	terpolated Compressed Sensing Technique using Radial Under-Samplin	_
	troduction	
	elated Work	
	on-Uniform Sampling	
	ne EiCS Technique	
4.4.1	Radial Under-Sampling Scheme	
4.4.2	The Novel Efficient Interpolation Scheme	
4.4.3	CS Reconstruction	
4.5 Si	mulation and Results	
4.5.1	Evaluation of the Radial Under-Sampling Scheme	
4.5.2	Evaluation of the Novel Efficient Interpolation Scheme	
4.5.3	Evaluation of the EiCS technique	66
4.5.4	Evaluation of EiCS for Increased Inter-Slice Gap	66
4.6 Su	mmary	68
Chapter 5		71
	adial Under-Sampling Based CSMRI Reconstruction using a Modified	
	troduction	
5.2 Re	elated Work	71
	e Mod-FiCS Technique	
5.3.1	Gaussian-Radial Under-Sampling	73
5.3.2	Modified Interpolation Scheme	75
5.3.3	CS Reconstruction	78

5.4	Simulation and results	78
5.5	Summary	81
	6	
-	sion and Future Work	
6.1	Thesis Conclusion	82
6.2	Directions for Future Work	84
REFER	FNCES	86

# **List of Figures**

	_
Fig. 2-1 MRI Applications	
Fig. 2-2 Planes used in modern imaging procedures [19].	
Fig. 2-3 Generation of RF waves in MRI acquisition [21]	
Fig. 2-4 Complete process of MRI scan [22]	. 9
Fig. 2-5 Magnetic Resonance Image of a single slice	10
Fig. 2-6 pMRI [25]	
Fig. 2-7 CS Reconstruction Scheme [11].	
Fig. 2-8 Reconstructed MRI images produced from different under-sampling patterns in	1
k-space. [46]	16
Fig. 2-9 Three steps of iCSMRI	19
Fig. 2-10 Under-sampling of 2D multi-slice sequence using 1D-VRDU masks [100]	21
Fig. 2-11 (a) 1D (b) 2D-VRDU Sampling patterns for three consecutive slices used in	
[16, 100]	23
Fig. 3-1 (a) Full k-space data and (b) under-sampled k-space data acquired using a 2D-	
VRDU mask	29
Fig. 3-2 2D-VRDU Sampling pattern for two consecutive slices	30
Fig. 3-3 The novel fast interpolation technique	33
Fig. 3-4 The Novel FiCS Technique	34
Fig. 3-5 Three consecutive (a) original and reconstructed images using (b) iCS-1D and	
(c) iCS-2D. New information is pointed by the arrow in a3 which is missed by iCS in	
both b3 and c3. The three consecutive slices of iCS (b1-b3 and c1-c3) show similar	
information to the central slice (b2 and c2) and are the same as in the original centered	
slice (a2). Secondly, iCS also shows large contrast variation among adjacent slices	36
Fig. 3-6 Three consecutive (a) original and reconstructed images using (b) FiCS-1D and	i
(c) FiCS-2D. New information is pointed by the arrow in a3 which was missed by iCS,	
while FiCS has retained that information in both 1D (b3) and 2D (c3). Similarly, FiCS	
also shows no contrast variation among adjacent slices while preserving the original	
information of their corresponding original slices.	37
Fig. 3-7 Slice-wise assessment of three consecutive slices on both knee and brain data	
sets. iCS-1D and iCS-2D show huge variations in values while the novel FiCS techniqu	е
has consistent values in both 1D and 2D like CS and is better than CS	38
Fig. 3-8 Comparing CS-1D, iCS-1D, FiCS-1D, CS-2D, iCS 2D, and FiCS-2D with 9%	
average sampling ratio. The assessment is done on 9 consecutive slices (slice number 74	4-
82) and averaged using four assessment parameters on knee dataset. Thus FiCS-2D	
	39
Fig. 3-9 Comparison of (a) Original brain Image with Reconstructed images using (b)	
CS-1D, (c) iCS-1D, (e) CS-2D, (f) iCS-2D and (d) FiCS-2D with 9% average sampling	5
ratio. Similarly, comparison of (g) Original knee Image with Reconstructed images usin	g
(h) CS-1D, (i) iCS-1D, (k) CS-2D, (l) iCS-2D and (j) FiCS-2D with 9% average	
sampling ratio. The reconstructed image using the novel FiCS technique has better	
quality compared to other techniques	42

Fig. 3-10 Comparison of (a) Original image with (b) iCS-1D-9%, (c) iCS-2D-9%, (d)
FiCS-1D-9%, (e) FiCS-2D-9%, (f) FiCS-2D-7% and (g) FiCS-2D-5%. The novel FiCS
shows better results with even 5% under-sampling ratio
Fig. 3-11 Evaluation of the novel FiCS-2D technique on 150 slices of knee dataset by
comparing it with iCS-1D, iCS-2D, and CS-2D using 9% average sampling ratios. It is
clear from the graphs that FiCS-2D has a consistent graph like CS with improved results
while iCS-1D and iCS-2D show huge fluctuation in values
Fig. 4-1 Gridding Radial samples on the Cartesian grid [122]
Fig. 4-2 (a) Original k-space and under-sampled k-space slices using (b) 1D-VRDU (c)
2D-VRDU (d) Radial and (e) Spiral mask
Fig. 4-3 Two different Radial under-sampling approaches used in EiCS technique 53
Fig. 4-4 Three consecutive Radial under-sampling masks with non-overlapping spokes 54
Fig. 4-5 The three-step efficient interpolation technique
Fig. 4-6 The novel EiCS Technique57
Fig. 4-7 Comparison of (a) Original Image with (b-f) reconstructed images using
different reconstruction strategies and under-sampling ratios. (b) iCS reconstructed image
has sharper details but with loss of information (c) FiCS 2D-VRDU has preserved the
original information but has a blurring effect which becomes more prominent when the
under-sampling ratio is reduced (d) CS reconstruction using the Radial under-sampling
also shows severe degradation when the under-sampling ratio reduces (e) FiCS-Radial
and (f) EiCS-Radial has improved results compared to CS-Radial but the sharpness
degrades for (e) FiCS with 3% samples while (f) EiCS has improved results with clear
and sharp details as pointed by the red arrow
Fig. 4-8 Comparison of the novel EiCS averaged assessment parameters with iCS, FiCS,
and CS. iCS 1D-VRDU has 9%, FiCS 2D-VRDU has 5% while CS-Radial, FiCS-Radial,
and EiCS-Radial have 3% samples. Thus, the novel EiCS-Radial technique outperforms
all with even 3% average samples
Fig. 4-9 Comparison of the original image with reconstructed images using FiCS 2D-
VRDU 3%, FiCS-Radial 3%, and EiCS-Radial 3%. It is clear from the comparison of the
selected zoomed portions that the EiCS technique outperforms FiCS by retaining sharper
details
Fig. 4-10 Evaluation of EiCS using the seven assessment parameters with GA-Radial
under-sampling for 3%, 5%, 7%, and 9% samples. The evaluation has been done on 150
centered slices of the knee dataset and compared slice-wise
Fig. 4-11 Comparison of FiCS and EiCS for different inter-slice gaps and under-sampling
ratios
Fig. 5-1 UA and GA Gaussian-Radial sampling approach
Fig. 5-2 Three Consecutive Gaussian-Radial under-sampling masks using both
approaches
Fig. 5-3 The novel interpolation technique
Fig. 5-4 Interpolated slices using both approaches
Fig. 5-5 Average assessment of iCS. FiCS and Mod-FiCS.

Fig. 5-6 Comparison of the reconstruction results of FiCS and Mod-FiCS with the	
original image. It is clear from the figure that Mod-FiCS has sharper and clear results	
compared to the FiCS technique	81

# List of Tables

Table 3-1 Comparison of iCS with the novel FiCS technique using 9%, 7%, and 5%
under-sampling ratios41
Table 4-1 Comparison of the Radial under-sampling schemes with 1D-VRDU and 2D-
VRDU schemes. The assessment has been done on 3 consecutive slices and averaged
(slice 165-167 of knee dataset)
Table 4-2 Comparison of %age number of samples of different interpolation techniques
and CS
Table 4-3 Comparison of the novel EiCS technique with CS, FiCS, and iCS for different
under-sampling ratios64
Table 5-1 Comparison of the novel Mod-FiCS technique with FiCS and CS using
different under-sampling schemes

## List of Abbreviations

ADMM Alternating Directions of Multiple Multipliers

CNN Convolutional Neural Network

**CORR** Correlation

CS Compressed Sensing

dB Decibel

**DCF Density Compensation Function** 

**DCT Discrete Cosine Transform** 

**DFT Discrete Fourier Transform** 

**DWT Discrete Wavelet Transform** 

EiCS Efficient interpolated Compressed Sensing

FCSA Fast Composite Splitting Algorithm

FFT Fast Fourier Transform

FiCS Fast interpolated Compressed Sensing

FISTA Fast Iterative Shrinkage-Thresholding Algorithm

FOV Field of View

FR Full Reference

FSIM Feature Similarity Index Measurement

GA Golden-Angle

GPU Graphics Processing Unit

GRAPPA Generalized Auto-calibrating Partial Parallel Acquisition

iCS Interpolated Compressed Sensing

IFFT Inverse Fast Fourier Transform

**IQ** Image Quality

ISTA Iterative Shrinkage Thresholding Algorithm

IWTMRI Iteratively Weighted Wavelet Tree sparsity MRI

1-BFGS Limited-memory Broyden-Fletcher-Goldfarb-Shanno

Mod-FiCS Modified Fast interpolated Compressed Sensing

MRI Magnetic Resonance Imaging

MSE Mean Square Error

NCG Non-linear Conjugate Gradient

NR Non-Reference

NUFFT Non-Uniform Fast Fourier Transform

PDF Probability Density Function

PIQE Perceptual Image Quality Evaluator

pMRI Parallel Magnetic Resonance Imaging

POCS Projection Onto Convex Sets

PSNR Peak Signal-to-Noise Ratio

RF Radio Frequency

SENSE SENSitivity Encoding

SI Sharpness Index

SNR Signal-to-Noise Ratio

SSIM Structural Similarity Index

TE echo time

TR repetition time

TV Total Variation

UA Uniform-Angle

VRDU Variable Density Under-Sampling

WaTMRI Wavelet Tree Sparsity MRI

## Chapter 1

## Introduction

Magnetic Resonance Imaging (MRI) is a highly useful medical imaging technique for clinical diagnosis and research because it generates a very detailed picture of an inside body organ and soft tissues without using any damaging ionizing radiation like X-rays. The scan time of an MRI acquisition mainly depends on the raw k-space or Fourier data that are to be acquired to fulfill the Nyquist criteria [1]. Multiple lines of k-space are acquired to generate a single slice and Multi-slice MRI needs hundreds of such slices for just one MRI scan [2]. The speed of the data acquisition in MRI is fundamentally slow which heightens the feelings of claustrophobia due to being in an enclosed and uncomfortable space for prolonged durations, especially for pediatric patients. Secondly, it is very difficult for a patient to remain motionless and even hold their breath for abdominal and cardiac scans, for that long [2, 3].

To speed up the MRI acquisition process, the data collection has been accelerated using efficient sampling trajectories. Compressed Sensing (CS) is an emerging technique that enables the reconstruction of an image from even 10% of the random Nyquist samples, provided the basic constraints of CS are fulfilled [4-8]. MRI is a good candidate for the application of CS due to implicit sparsity in MR images, and inherently slow data acquisition process [9]. With the edge of this reduced scan time, Compressed Sensing MRI (CSMRI) requires some slow non-linear reconstruction techniques [10-14], which

are an additional computational overhead. But this computational load is just a postacquisition process and takes lesser time for MRI scan.

A single multi-slice MRI scan acquires hundreds of slices. Therefore their consecutive slices have a very strong inter-slice correlation, because of having very narrow inter-slice gaps [15]. This correlation has been exploited to reduce the under-sampling ratios of CSMRI through interpolation called interpolated Compressed Sensing (iCS) in the literature [15, 16]. An efficient interpolated Compressed Sensing MRI (iCSMRI) technique mainly depends on a good under-sampling scheme with minimum samples, an efficient interpolation approach to collect enough samples, and a fast CS reconstructed technique to reconstruct a sharper and clear image with minimum processing time. Such efficient iCSMRI reconstruction techniques are essential due to the following reasons which are addressed in this thesis:

- To enable higher resolution MR imaging in clinically acceptable scan times to be applicable in emergency and accidental cases.
- To have an MRI scan with real-time monitoring
- To improve patient care by minimizing the scan time and claustrophobic feeling,
   especially for pediatric patients.
- The reduced scan time will be helpful for telemedicine and save battery power and storage sizes.
- The reduced scan time will be helpful in dynamic cardiac MR scans as it will help to reduce the motion artifacts due to respiratory motions and cardiac cycles.

#### 1.1 Dissertation contribution

The primary contributions of this thesis are to reduce the scan time of multi-slice CSMRI acquisition, with even improved image quality, and lower computational complexity.

The proposed novel interpolation techniques along with CS exploit different undersampling trajectories for multi-slice MRI reconstruction. Thus, preserving the original information in every reconstructed slice along with consistency in the slice-wise image quality, and improved results.

The under-sampled k-space data of multi-slice MRI are acquired with only 3% and 5% of the total Nyquist samples from each slice using different under-sampling trajectories, each having its benefits. The uniformity of the under-sampling ratio for consecutive slices results in consistent slice-wise image quality and therefore, helps to preserve maximum samples and information of the original slices.

The proposed novel interpolation techniques are computationally efficient with only a set difference and addition operation and interpolate the slices by exploiting the strong, interslice correlation between them. These interpolated slices are then CS reconstructed to have improved image quality and performance with even reduced scan time, lower computational complexity, and maximum information content.

### Contributions of this dissertation can be summarized as follows

- 1. This thesis proposes a novel FiCS technique for efficient reconstruction of multi-slice MRI datasets using 2D-VRDU under-sampling, and a fast interpolation scheme. The FiCS technique has the highest under-sampling ratio and the most efficient two-step interpolation approach for CSMRI Reconstruction. The evaluation reveals that FiCS has improved performance with maximum information content and the lowest under-sampling ratio.
- 2. This thesis also proposes a novel EiCS technique based on a Radial undersampling scheme and a novel three-step interpolation approach for improved

CSMRI Reconstruction. The EiCS technique is computationally efficient like FiCS with only set a difference and addition operation and with a more practical non-Cartesian Radial under-sampling scheme. The proposed EiCS technique has more improved results compared to FiCS using an even lower under-sampling ratio.

3. This dissertation also proposes a Modified FiCS (Mod-FiCS) technique. This technique combines the 2D-VRDU and Radial under-sampling schemes of FiCS and EiCS called Gaussian-Radial under-sampling. The efficient three-step interpolation approach of Mod-FiCS has improved results compared to the previous techniques. The Mod-FiCS technique has the benefits of both the previous schemes as it neither shows blurring like FiCS nor any streaking artifacts like EiCS with improved results along with consistency in slice-wise image quality and information content.

### 1.2 Thesis organization

This thesis has been organized as follows

Chapter 2 describes the MRI acquisition process and the physics involved in it. The reconstruction of MR images from the acquired k-space data is also discussed. Many advanced MR reconstruction methods along with the CS techniques related to this thesis are elaborated followed by the assessment parameters and datasets used.

Chapter 3 discusses an efficient 2D-VRDU under-sampling strategy and the novel twostep interpolation technique for Multi-slice CSMRI reconstruction. This new technique is termed as FiCS, exploiting the correlation among consecutive slices of multi-slice CSMRI reconstruction. Chapter 4 provides an improved three-step interpolation approach using Radial undersampling schemes for iCS reconstruction. This technique is termed as Efficient iCS (EiCS). The proposed EiCS technique is a practical scheme from the current hardware point of view with even more improved results from FiCS and a reduced under-sampling ratio.

Chapter 5 discusses a modified FiCS (Mod-FiCS) technique using the Gaussian-Radial Under-Sampling scheme. The Mod-FiCS technique gathers the benefits of both the previous techniques with improved reconstruction results.

Chapter 6 provides the concluding remarks about the current research followed by some future directions of this research.

## Chapter 2

## **MRI** Acquisition and Reconstruction

This chapter discusses the fundamentals of MRI acquisition. It also provides a brief description of CS reconstruction techniques in the context of MRI acquisition. The background works related to the recent trends of CSMRI along with iCSMRI are also presented. Finally, the multi-slice MRI datasets and different assessment parameters used for simulation are elaborated.

#### 2.1 Introduction

Magnetic Resonance Imaging (MRI) is used to produce detailed images of body tissues and organs using strong magnets and radio waves [17, 18]. Different types of MRI scans help doctors to diagnose various diseases. The MRI scan is useful for the detection of multiple diseases occurring in different parts of the body, some of which are mentioned in Fig. 2-1.

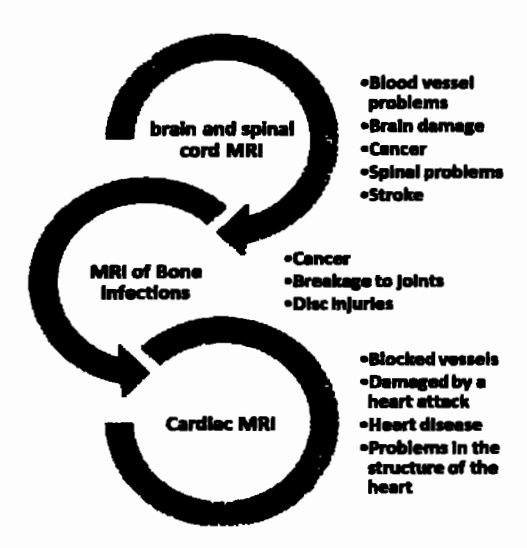


Fig. 2-1 MRI Applications

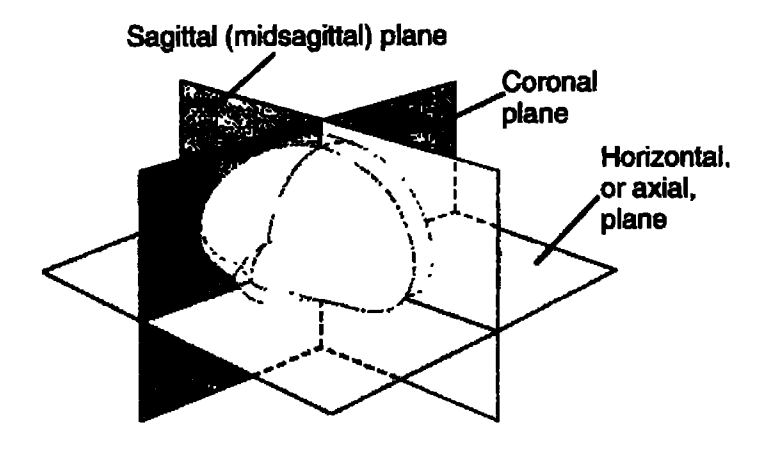


Fig. 2-2 Planes used in modern imaging procedures [19].

MRI is itself a non-ionizing and non-invasive multi-planar imaging modality generating images to visualize anatomy along the three different planes called sagittal, axial, and coronal [19] as shown in Fig. 2-2. Therefore, it is a very valuable tool in medical diagnosis and treatment monitoring.

## 2.2 MRI Acquisition

MRI scanners use radio waves and strong superconducting magnets of 1.5-3.0 Tesla (T) flux density, for acquisition. Most of the Human body is comprising of water, having hydrogen and oxygen atoms [20]. In the absence of any magnetic field, all the protons of the hydrogen atoms have random orientation and therefore have zero magnetic movements. When an external magnetic field is applied, most of them align themselves in the direction of the applied field resulting in a net magnetic movement called longitudinal magnetization. Next, a brief RF pulse is applied which systematically alters this magnetization alignment. When this RF pulse is removed, a signal is generated in the RF coils due to the change in the magnetic moments of the hydrogen nuclei. The process of generating RF waves during MRI acquisition is shown in Fig. 2-3. The multidimensional spatially encoded data matrix, generated by RF receiving coils, is called k-space data which consists of Fourier coefficients.

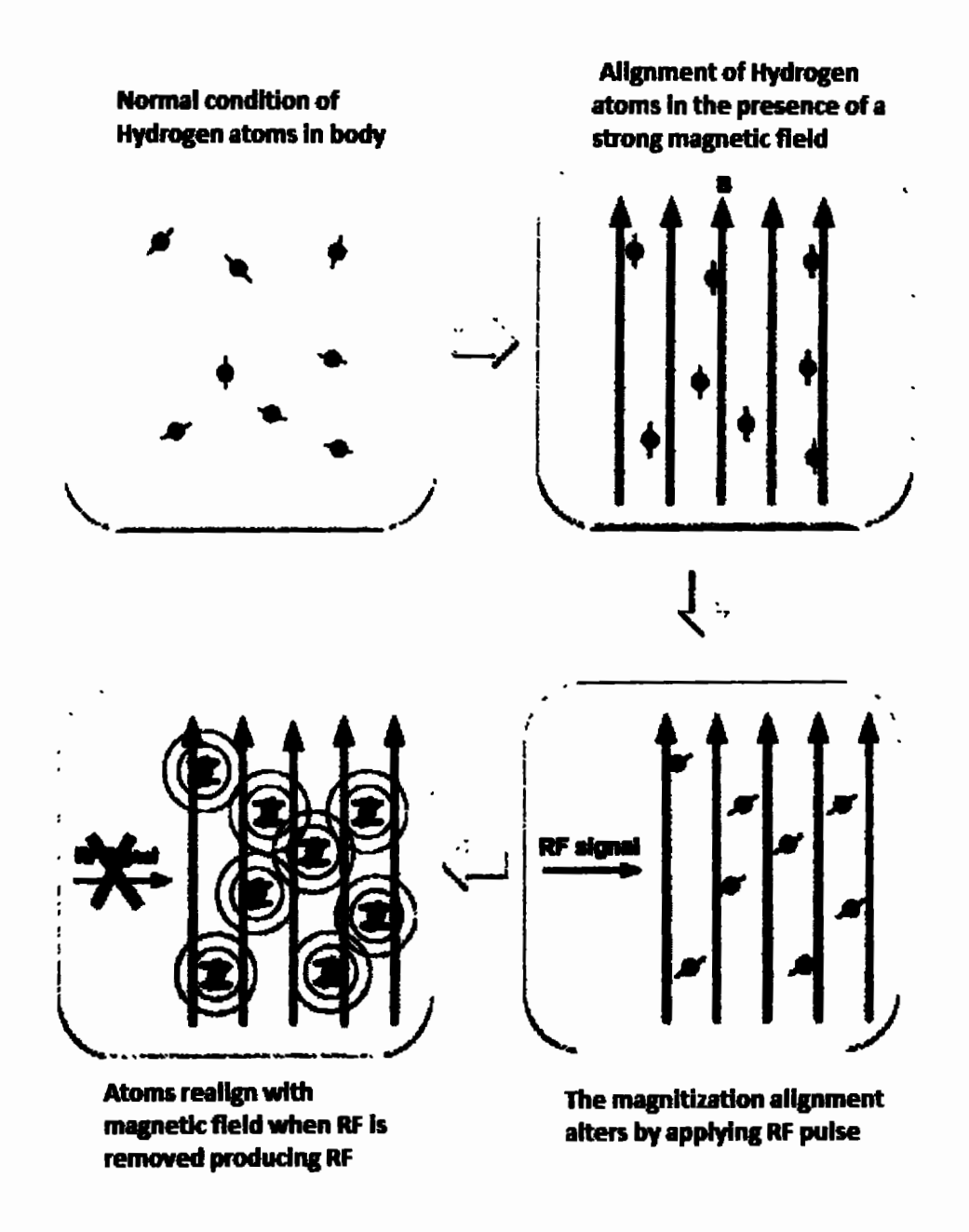


Fig. 2-3 Generation of RF waves in MRI acquisition [21]

In MRI, the important part is the spatial encoding, which is the connection of the produced signal with its spatial locations. This spatial localization depends upon the differences in frequency, phase, timing, and location on the receiving coil. MRI is a slow imaging method because it requires multiple scans to generate a single slice and multi-

slice MRI has hundreds of such slices. This process is also slow due to nerve stimulation and the limited slew rate of the gradient fields. The complete process of generating an MR image is shown in Fig. 2-4

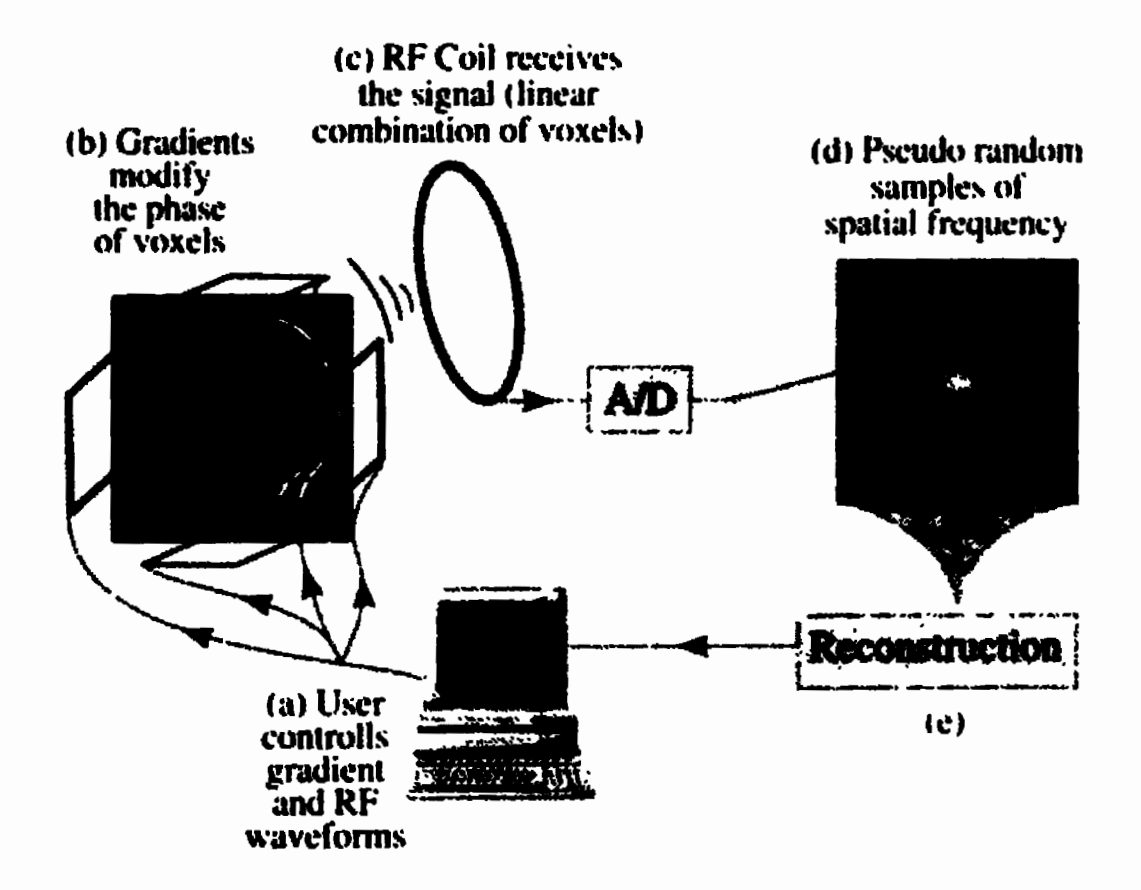


Fig. 2-4 Complete process of MRI scan [22]

The technician varies the gradient and radio frequencies to control the pixels/voxels phase of the image. An RF coil receives the signal in an encoded form (samples in k-space) as shown in Fig. 2-4. Finally using a relevant reconstruction technique, an MRI image can be recovered [22].

The traditional MRI scanner acquires the k-space data in the form of Fourier coefficients and thus requires only inverse Fourier transform to get the MRI slices in the spatial domain.

## 2.3 MRI Reconstruction Techniques

In MRI, the three spatial encodings generated are frequency encoding, phase encoding, and slice selection [23]. The acquisition time of MRI is mainly dependent on the number of phase encoding steps because the frequency encoding steps are fast.

During the acquisition of a single slice, other slices cannot be selected as they have different frequencies because of the gradient fields. The slice thickness mainly depends on the bandwidth of the applied RF pulse. The generated radio frequencies of a single slice are originated from the transverse magnetization [22]. This acquisition is sampled in k-space following the Nyquist criteria and adopted on the Cartesian grid on straight lines. Traditional MRI takes fully sampled Fourier encoded data points and reconstructs the MR image using only inverse Fourier Transform as shown in Fig. 2-5.

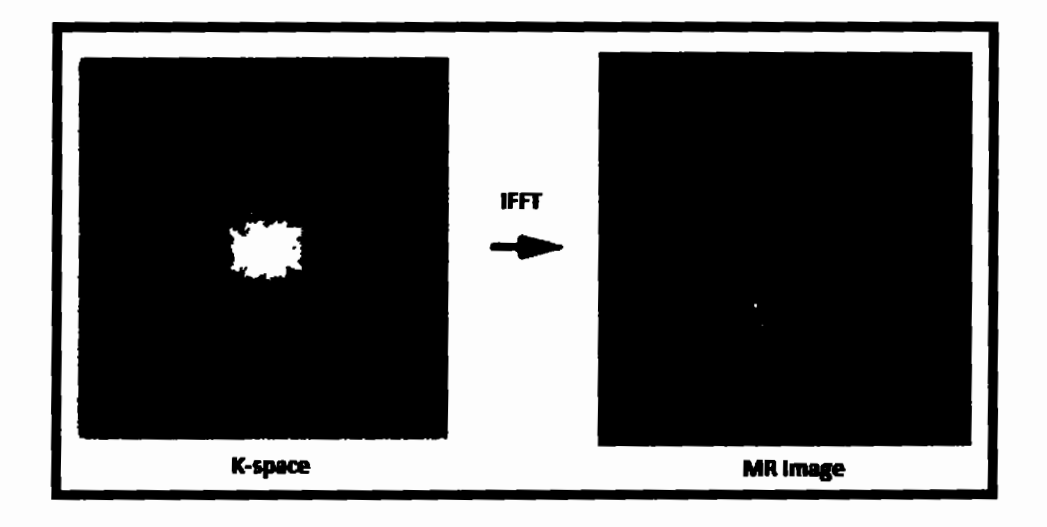


Fig. 2-5 Magnetic Resonance Image of a single slice

## 2.3.1 Parallel MRI (pMRI)

The speed of the data acquisition in MRI is fundamentally slow because of physical (gradient amplitude and slew-rate) and physiological (nerve stimulation) constraints. This slow imaging process can be accelerated using multiple coils that work in parallel called Parallel MRI (pMRI) [24-32]. But multiple coils require parallel imaging techniques, like sensitivity encoding (SENSE) [33] and generalized auto-calibrating partial parallel acquisition (GRAPPA) [34] for the reconstruction of artifact-free images [16]. pMRI is a robust technique to reduce the acquisition time of MRI scans [35] and has opened new ways for MRI applications. In pMRI, an array of multiple coils is used and thus accelerates the acquisition time of the k-space data [26]. Thus the main advantage of pMRI is the reduction of the scan time which provides comfort for patients of all ages because they have lesser interaction with the claustrophobic design of the MRI machine [24]. Moreover, the difficulty of breath-holding for a long time is also reduced especially in abdominal and cardiac MRI scans [25].

The acquisition of pMRI needs a phased array that consists of multiple independent receiver coils. The sensitivity of the coils with magnetization depends upon the distance from the magnetizing part. A coil closer to the magnetizing part will receive a strong RF signal as compared to the coil farther from the targeted part [25, 27, 28]. The idea is shown in Fig. 2-6. Finally, the knowledge of the individual coil sensitivities is used to combine the data from each of the coils using some special algorithms to get a reconstructed image with a full Field Of View (FOV) [26].

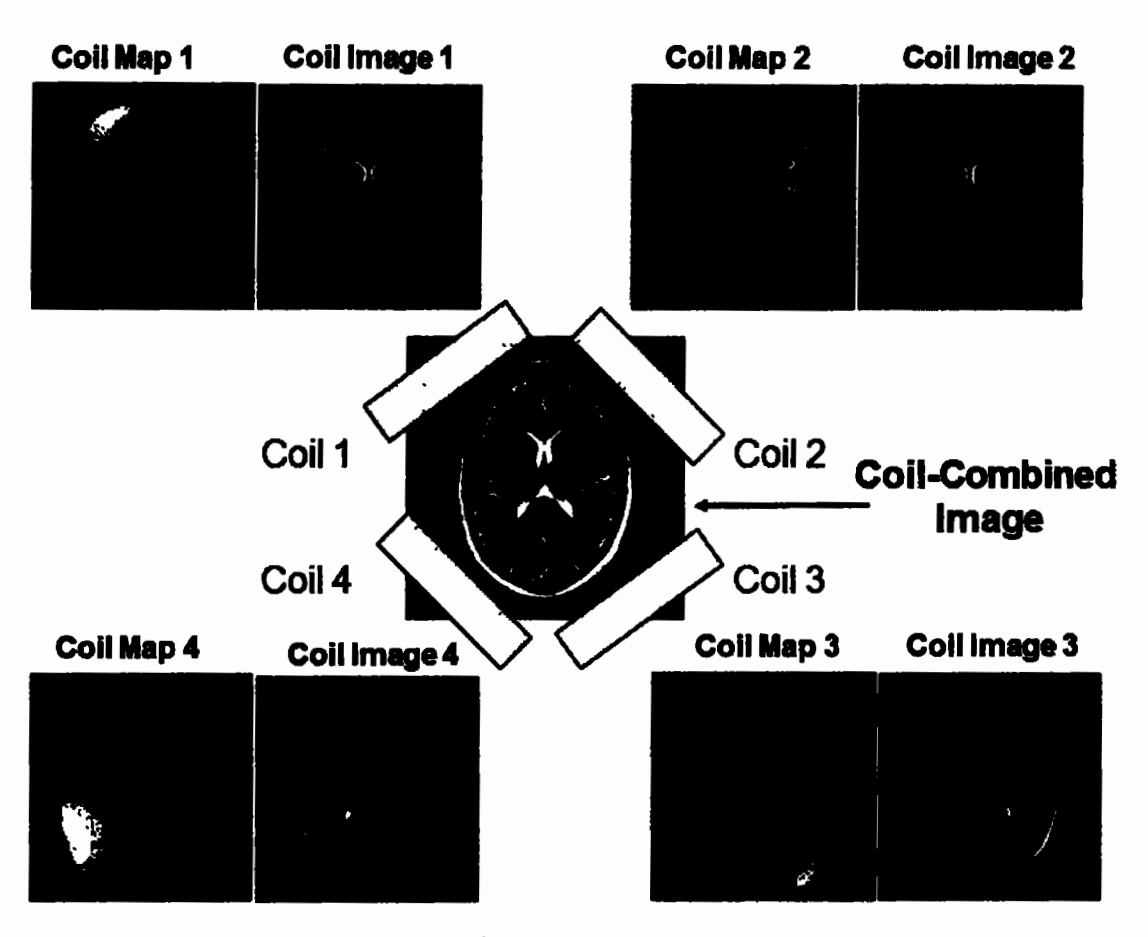


Fig. 2-6 pMRI [25].

### **2.3.2 CSMRI**

Shannon Nyquist theorem states that to reconstruct a signal we have to initially sample it through a rate that is twice the highest frequency component in that signal [1]. This acquired signal when converted into a particular transform domain, like Discrete Cosine Transform (DCT), DFT (Discrete Fourier Transform), or Wavelet Transform, will have few of its coefficients with larger values, and most of them with smaller values that are near to zero. Hence a signal is said to be sparse if it has numerous zero and some nonzero coefficients. But most of the real-world signals are not sparse although they can be compressible. Thus compressible signals can be sparse by enforcing its smaller valued coefficient to be zero [36, 37]. Therefore, this signal can be compressed in its particular

transform domain by discarding the smaller value coefficients, called transform coding.

Now, this compressed signal can be reconstructed from those fewer coefficients by taking the inverse transform. But there are three main drawbacks with transform coding which are:

- All the Nyquist samples are to be acquired even if the signal is sparse
- All the transform coefficients have to be calculated even if most of them are to be discarded.
- All the locations of the coefficients to be kept should be stored which is an overhead.

Therefore, the compression through transformed coding is always done as a postprocessing step. Recently a new data acquisition technique called compressed sensing
(CS) has emerged which made enormous progress and attention in various fields of
multidimensional signal processing, and many other areas. The CS theory has been
introduced by Donoho [4] and Candes [6] and has been successfully implemented by
Lustig et al [11] in MRI. The CS theory breaks the Nyquist criteria under some special
conditions [4, 8, 38] and enables the recovery of a sparse signal from far fewer
measurements of the Nyquist rate. Therefore, CS exploits the non-linear methods to
recover the original data from a small number of sparse coefficients [39, 40]. Thus, CS
makes the encoding process efficient by combining the acquisition and compression steps
and therefore avoids capturing all the unnecessary information, which is later to be
discarded. For the implementation of CS, the three fundamental conditions are that the
data must be sparse itself or in some transform domain, under-sampling must be done
randomly, and the reconstruction must be performed using some nonlinear techniques

[11, 39, 41, 42]. In CS the random under-sampling transforms the CS reconstruction problem to de-noising because random under-sampling generates noise-like effects rather than aliasing [11, 43, 44] as shown in Fig. 2-7.

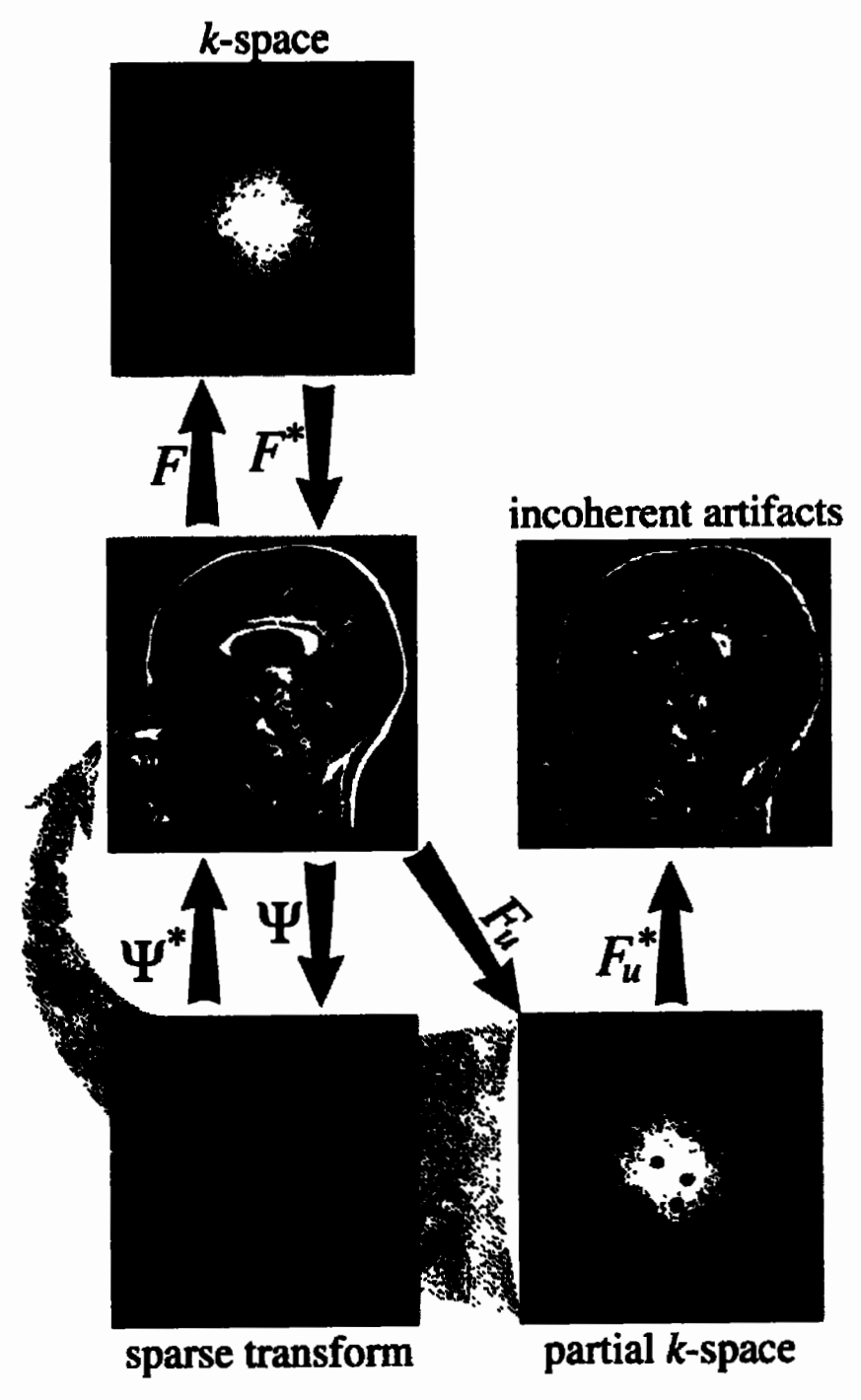


Fig. 2-7 CS Reconstruction Scheme [11].

Instead of using uniform under-sampling, CS exploits different random under-sampling techniques like Radial, Variable Density Under-Sampling (VRDU) [45], Spiral, etc. These under-sampling techniques have different artifacts in the reconstructed images. Fig. 2-8 shows some sampling strategies along with their effect on the reconstruction images.

It is shown that the low-resolution under-sampling causes blurring, Cartesian under-sampling generates image replicas, structured angular under-sampling generates more incoherent "streaking" artifacts, random under-sampling generates "cloud-like" artifacts, while Variable Density Under-Sampling (VRDU) produces noise-like aliasing. [46].

CS has been successfully applied to different biomedical imaging modalities to speed up the slow acquisition process. MRI is the most suitable candidate for the application of CS because of its inheritably slow data acquisition process and also MRI satisfies its basic requirements [9]. Thus, CSMRI has an edge to improve patient care by reducing MRI acquisition times by enabling higher resolution imaging in clinically acceptable scan times. With the edge of this reduced scan time, CSMRI has additional computational overhead compared to standard MRI where only inverse Fourier transform is sufficient [38].

The CSMRI trends can be broadly categorized as methods focused on improving the reconstruction strategies [47, 48], and parallel CSMRI techniques [25, 30, 49-54]. For successful CSMRI, the sparse regularization can be achieved in a specific transform domain [55, 56] such as the wavelet [11, 57], curvelet [58-60], or using some dictionary learning techniques [61-67]. The traditional CSMRI uses fixed sparsifying transforms like total variation (TV) [68], discrete cosine transforms (DCT) and discrete wavelet

transforms (DWT) [69]. Similarly, with the recent development, many CNN-based deep learning methods [70-76] have also evolved.

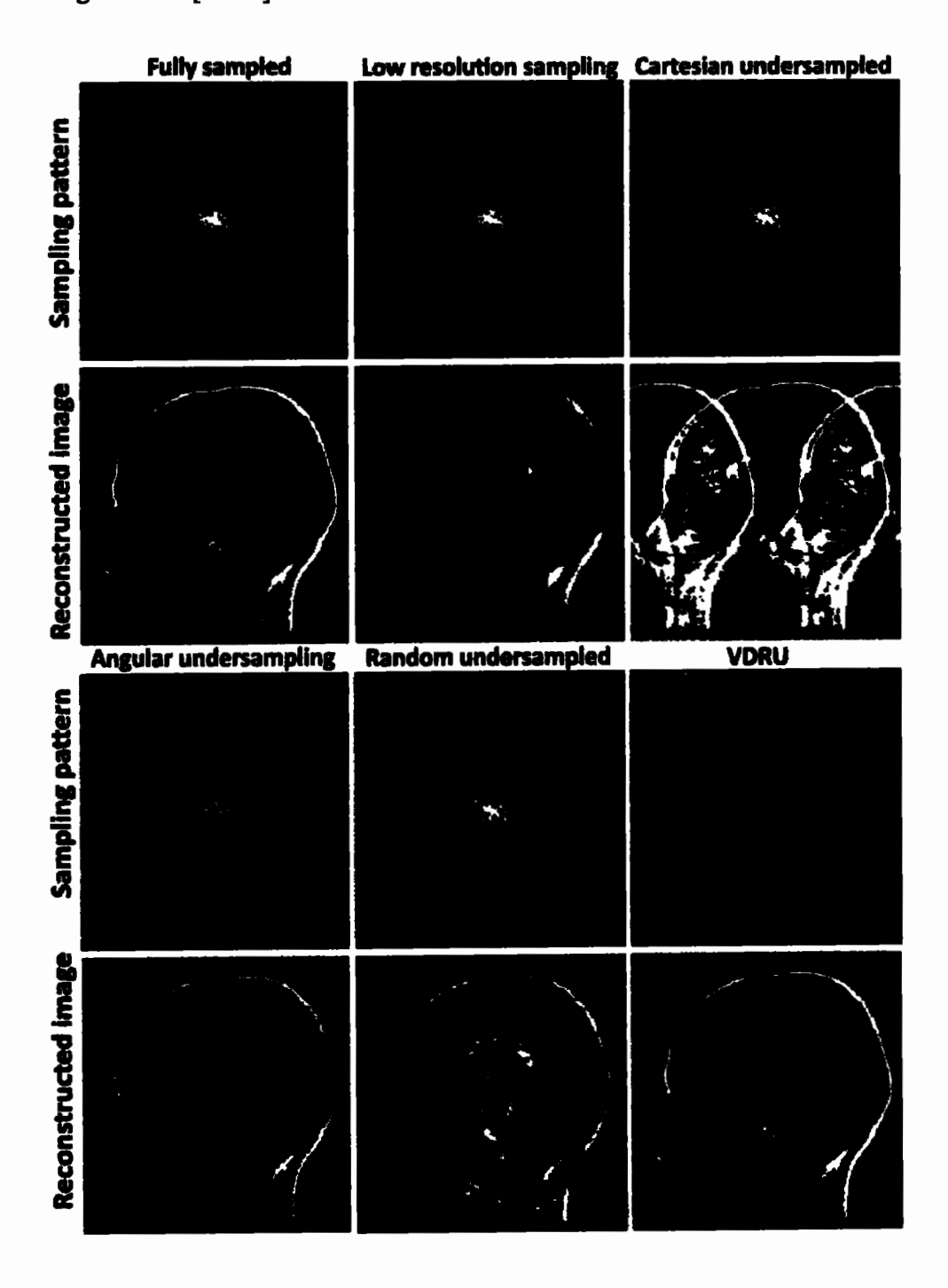


Fig. 2-8 Reconstructed MRI images produced from different under-sampling patterns in k-space. [46]

Unlike the single-step Fourier reconstruction of conventional MRI, CS MRI requires nonlinear iterative optimization algorithms that are repeated a number of times for the reconstruction of a single MR image [11].

Some commonly used non-linear reconstruction algorithms for CS are:

- Non-linear Conjugate Gradient (NCG) [77]
- Iterative Shrinkage-Thresholding Algorithm (ISTA) [78]
- Fast Iterative Shrinkage-Thresholding Algorithm (FISTA) [79, 80]
- Alternating directions of multiple multipliers (ADMM) [81]
- Bregman iterative algorithm [82, 83]
- Limited-memory Broyden-Fletcher-Goldfarb-Shanno (1-BFGS) [84]
- Projection Onto Convex Sets (POCS) [85, 86]

These algorithms vary in ease of implementation and computational complexity [87, 88]. In CSMRI all slices should be equally under-sampled and are then recovered using one of the non-linear reconstruction algorithms [2, 4, 89].

For an efficient reconstruction, the number of k-space samples should be roughly two to five times the number of sparse coefficients [11]. Thus, for a good CSMRI scan, at least 10% of the samples should be acquired from each slice for efficient reconstruction. In this thesis Non-Linear Conjugate Gradient (NCG) [77] technique is used as a CS reconstruction approach.

For clinical applications, CSMRI is just in its beginning to be offered as commercial product with the limitations of longer reconstruction times and some CS-related artifacts [90, 91].

#### **2.3.3 iCSMRI**

Interpolated Compressed Sensing MRI (iCSMRI) is an emerging technique to lower the under-sampling ratio of multi-slice CSMRI. It has been introduced by Pang et al. [15, 16] and has thus reduced the scan time beyond the CS limit.

In Multi-slice MRI there is a very narrow inter-slice gap and therefore has a very strong inter-slice correlation. This correlation has been exploited in iCSMRI to reduce the average samples per slice resulting in reduced scan time. Thus, the multi-slice MRI datasets are to be reconstructed from highly under-sampled k-space data initially acquired from the MRI scanners. There are three fundamental steps of iCSMRI for multi-slice datasets. The first step is the under-sampling, the next is an interpolation and the last step is the CS reconstruction. The complete three-step process of iCSMRI is shown in Fig.2-9.

#### 2.4 Literature Review

Interpolated Compressed Sensing MRI (iCSMRI), works in three steps; in the first step some of the CS samples in MRI acquisition are acquired and others and intentionally missed to reduce the average sampling rate. This under-sampling can be performed using different sampling patterns like Cartesian, Radial, Spiral, and their combinations [92-97]. In the second step, the intentionally missed samples are estimated using interpolation from the samples of the neighboring slices. The interpolation for the missing samples in the under-sampled slices can be accomplished using different interpolation techniques [15, 16, 98-103].

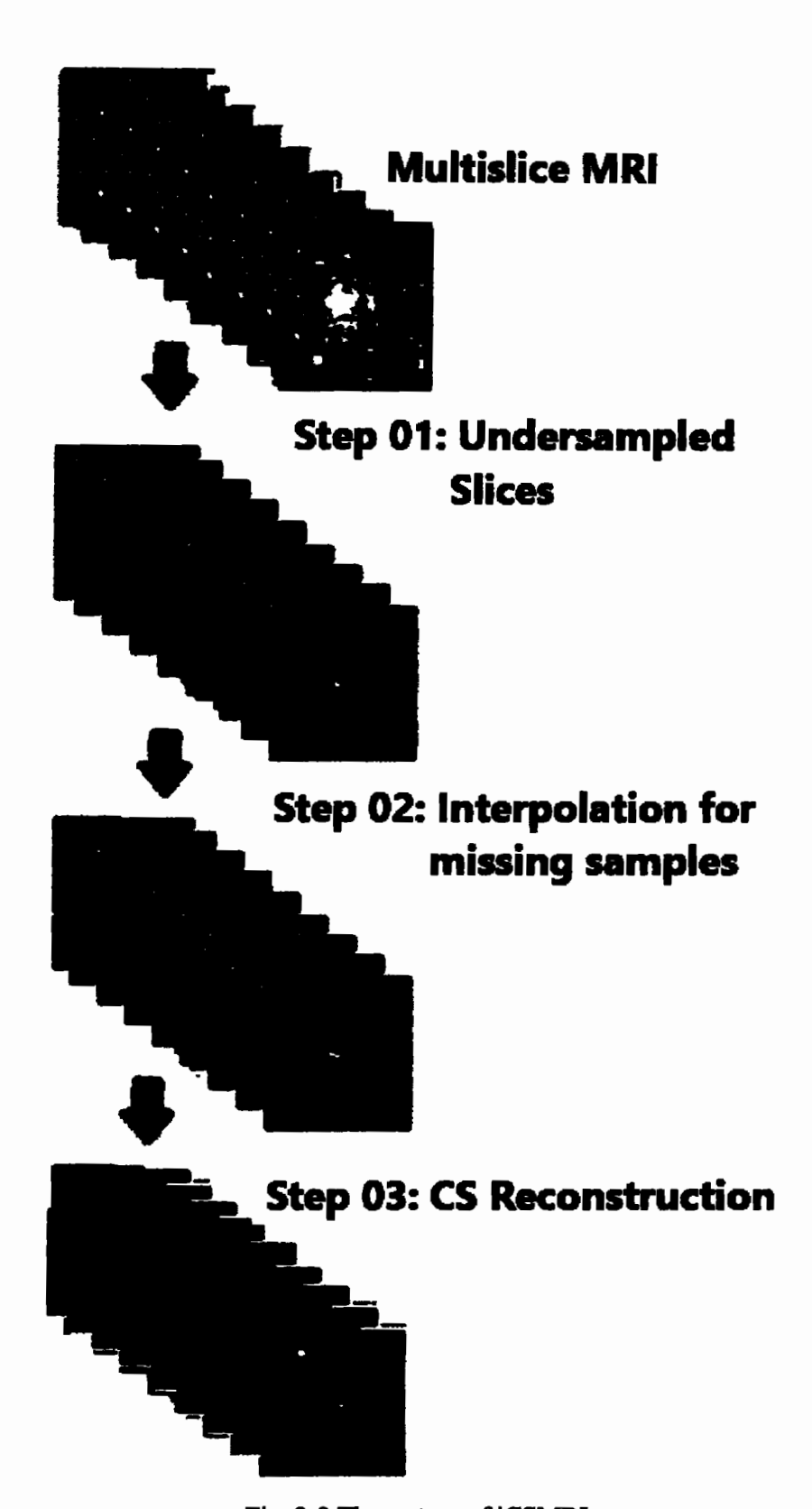


Fig. 2-9 Three steps of iCSMRI

The last step is the CS reconstruction which can be carried out using one of the CS reconstruction algorithms like Non-linear Conjugate Gradient (NCG) [11], Wavelet Tree Sparsity (WaTMRI) [104-106], Fast Composite Splitting Algorithm (FCSA) [107], and Iteratively weighted Wavelet Tree sparsity MRI (IWTMRI) [100]. The CS reconstruction techniques vary in computational complexity, convergence time, and reconstructed image quality.

The concept of iCS was introduced by Pang et al. [15, 16] in 2012. Pang [16], utilizes 9% average samples. He reduced the average sampling rate by acquiring some slices as lightly under-sampled (L slices) and others as highly under-sampled (H-slices). Their under-sampling pattern acquires adjacent slices with different under-sampling ratios and therefore has non-uniformity in their reconstruction results. Secondly, their interpolation technique is computationally inefficient along with inconsistency in slice-wise reconstructed image quality.

Hirabayashi et al. [108] use iCS by taking a different under-sampled slices sequence using fully sampled and CS slices (F and C slices). Although they have good quality reconstructed images, but their technique has rather increased the average under-sampling ratio and scan time.

The work of Pang [16] has later been explored by Datta and Deka [99, 100] but their under-sampling approaches do not produce clinically acceptable results by causing information loss in most (67%) of their reconstructed slices [109]. Secondly, their interpolation techniques are computationally inefficient with redundant Fourier steps. Although their results look visually better but the information content is not indigenous due to their non-uniform and a biased under-sampling scheme [100]. They used the same

under-sampling strategy in their work [100] as proposed by pang [16] but using a 1D Cartesian mask. Their adopted under-sampling pattern is shown in Fig. 2-10. They also explored iCS for pMRI in [30, 51].

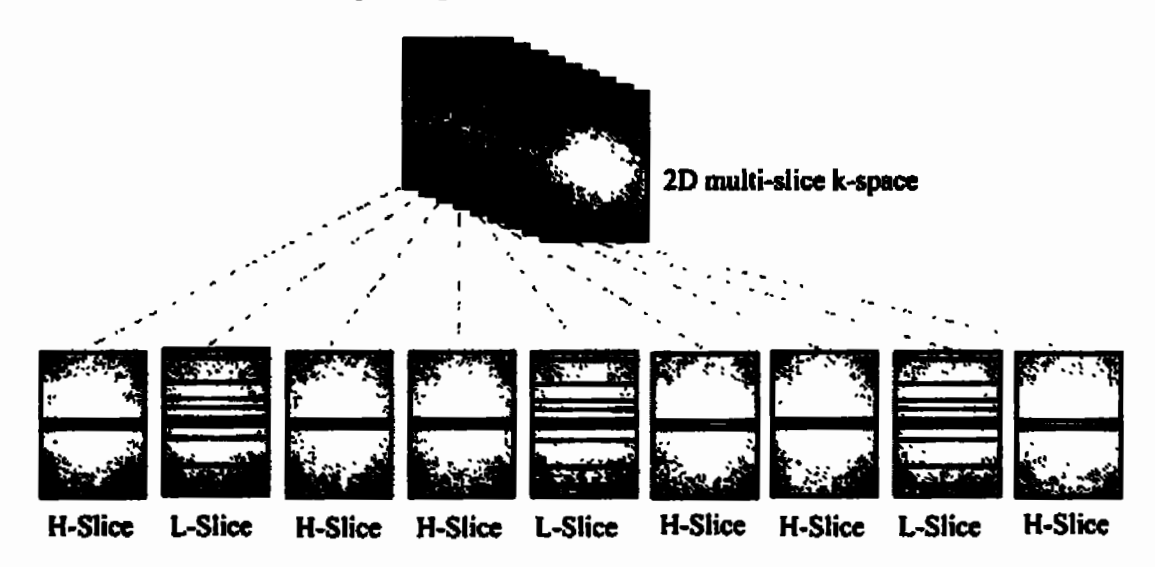


Fig. 2-10 Under-sampling of 2D multi-slice sequence using 1D-VRDU masks [100].

Datta and Deka [30, 51, 99, 100, 110, 111] further explored iCSMRI with different interpolation and reconstruction strategies. Although they reduced the computational cost of their interpolation algorithms [99, 100] but they neither work on reducing the average sampling ratios nor on the consistency of their slice-wise reconstruction results.

The sampling and interpolation strategy adopted in [16, 100] takes three consecutive slices with a specific under-sampling pattern of different sampling ratios and repeats that pattern after every three slices. Their under-sampling pattern of the three consecutive slices, which repeats after every three slices, is shown in Fig. 2-11. It is clear from the figure that, in three consecutive slices, the first one is highly under-sampled (H slice), the second is lightly under-sampled (L slice) and the third is again H slice, for both 1D and 2D-VRDU schemes. Each H and L slice has 1 % and 25% of the total samples

respectively. Therefore, the average sampling ratio for this scheme is 9%. The H slice missed samples are interpolated from the neighboring L slice to get H interpolated slice with 25 % samples. Finally, CS reconstruction is applied to all the H interpolated and L slices.

The main drawback of this non-uniform sampling strategy is that H slice 1% samples are insufficient to be called an original image after interpolation and reconstruction. Thus, in every three consecutive slices, the L slice will always dominate their two neighboring H slices. This results in almost the same imaging information in every three consecutive reconstructed slices and thus has information loss in two out of the three slices.

Pang et al. [16] have worked on 2D-VRDU whereas Datta and Deka [100] on 1D-VRDU. The interpolation technique of both the sampling schemes (1D and 2D) has complex computational steps of Fourier, Inverse Fourier, matrix division, and convolution resulting in increased computational cost along with inaccuracy in their reconstruction results. Different sampling strategies [89, 92, 94] have also been explored in iCS, but they neither reduced the scan time nor the average sampling ratio.

#### 2.5 Data Sets

Different data sets of knee and brain are used in this thesis. The knee data sets are taken from a free online database, http://mridata.org. This is a fully sampled data set acquired from a GE HD 3T scanner with 160×160x153.6 mm Field Of View (FOV), number of channels: 8, matrix size: 320x320 with 256 slices, slice thickness 0.6mm, zero inter-slice gaps, TR/TE: 1150/25 msec, flip angle 90, and bandwidth 50kHz. The brain data set is of a normal aging coronal plane with 123 slices, matrix size: 256x256, and is publicly available on the AANLIB database of Harvard medical school at http://www.med.harvard.edu/AANLIB/home.html [112].

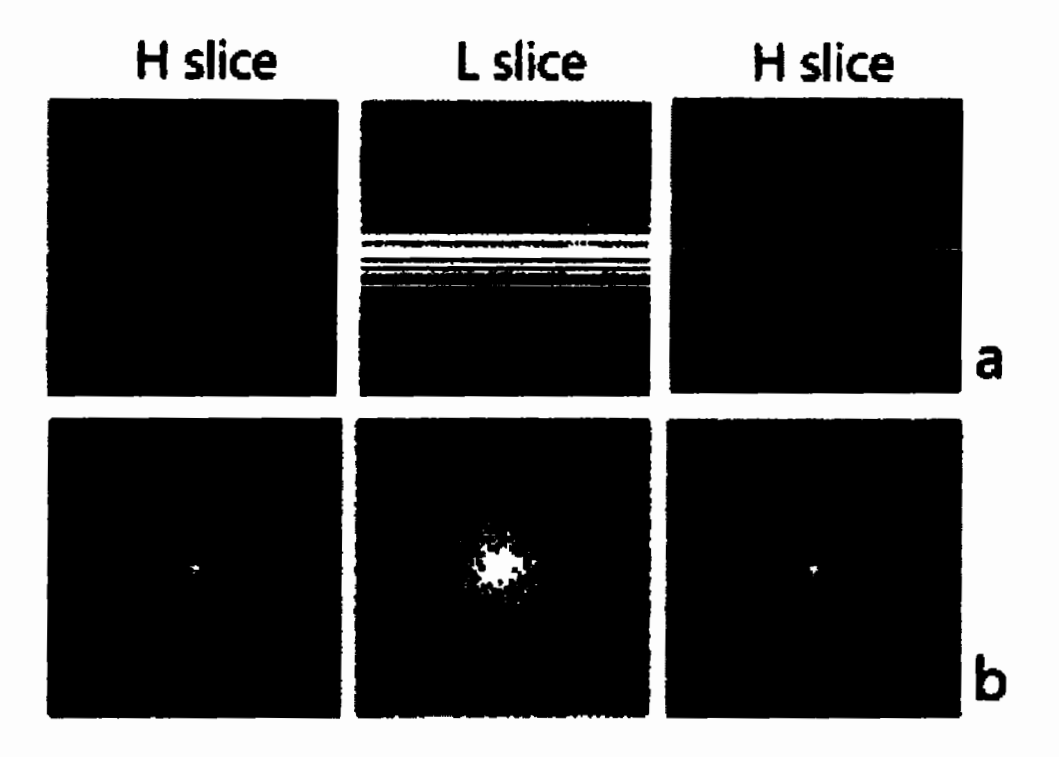


Fig. 2-11 (a) 1D (b) 2D-VRDU Sampling patterns for three consecutive slices used in [16, 100]

#### 2.6 Evaluation Criteria and Simulation Environment

To assess the quality of the reconstructed images two methods are used: subjective and objective. The subjective method is based on the perceptual assessment of radiologists about the attributes of the reconstructed data sets, while objective methods are based on computational models that can predict perceptual image quality.

#### 2.6.1 Subjective Assessment

For subjective assessment, we asked some expert radiologists to assess the reconstructed datasets. The rating is based on the overall quality and information content of the images.

#### 2.6.2 Objective Assessment

For Objective assessment two approaches are used, Full Reference (FR) and Non-Reference (NR). In the FR approach, the quality of the reconstructed images is evaluated

with the original images where for the NR approach, no original image is required. For the FR approach, five assessment parameters are used which are Structural Similarity Index Measurement (SSIM) [113], Feature Similarity Index Measurement (FSIM) [114] Mean Square Error (MSE) [115], Peak Signal to Noise Ratio (PSNR) [115], and correlation (CORR) [116]. For the NR approach, two assessment parameters are used which are Sharpness Index (SI) [117] and Perceptual Image Quality Evaluator (PIQE) [118].

**SSIM** and **FSIM** gives normalized mean values of structural similarity and feature similarity between the original and reconstructed images as represented in (2.1) and (2.2).

$$SSIM(x,y) = \frac{(2\mu_x\mu_y + c_1)(2\sigma_{xy} + c_2)}{(\mu_x^2 + \mu_y^2 + c_1)(\sigma_x^2 + \sigma_y^2 + c_2)}$$
(2.1)

Where x and y are the original and reconstructed images with size  $m \times n$ . Similarly  $\mu_x$  and  $\mu_y$  are the mean,  $\sigma_x^2$  and  $\sigma_y^2$  are the variances and  $\sigma_{xy}$  is the covariance of x and y. Similarly,  $c_1 = (k_1 L)^2$  and  $c_2 = (k_2 L)^2$  are the variables used to stabilize the division, L represents the dynamic range of the image and  $k_1$  and  $k_2$  are small constants.

$$FSIM(x,y) = \frac{\sum_{i,j} [S_{PC}.S_G].[max(PC_x,PC_y)]}{\sum_{i,j} max(PC_x,PC_y)}$$
(2.2)

Where  $PC_x$  and  $PC_y$  are the Phase Congruency of original and reconstructed images and  $S_{PC}$  is the similarity measure for  $PC_x$  and  $PC_y$ . Similarly,  $S_G$  is the similarity measure for Gradient Magnitude values for original and reconstructed images.

MSE is the most common FR estimator of image quality with values near to zero are better. The MSE between the original and reconstructed images can be calculated as in (2.3)

$$MSE = \frac{1}{mn} \sum_{i=0}^{m-1} \sum_{j=0}^{n-1} [x(i,j) - y(i,j)]^2$$
 (2.3)

**PSNR** is the ratio between the maximum possible power of the original image with **MSE** and because of the dynamic range of the signals it is calculated as the logarithm term of the decibel scale [119] as given in (2.4).

$$PSNR (in dB) = 10log_{10} \frac{(MAX_x)^2}{MSE}$$
 (2.4)

**CORR** between the original and reconstructed images is defined in (2.5), having a normalized value, and is better when close to one.

$$CORR = \frac{\sum_{i,j} \{ [x(i,j) - \mu_x] [y(i,j) - \mu_y] \}}{\sqrt{\{ \sum_{i,j} [x(i,j) - \mu_x]^2 \} \{ \sum_{i,j} [y(i,j) - \mu_y]^2 \}}}$$
(2.5)

SI is the NR, Image Quality (IQ) assessment parameter and is derived from the intensity distribution in an image, its mathematical description is given in (2.6)

$$SI(x) = -log_{10} \left[ \frac{\mu_{TV(x)} - TV(x)}{\sigma_{TV(x)}} \right]$$
 (2.6)

Where  $\mu_{TV(x)}$  and  $\sigma_{TV(x)}^2$  are the mean and variance of TV(x). TV(x) is the total variance of the input image as shown in (2.7).

$$||x||_{TV} = \sum_{i,j} \left[ (\nabla_1 x_{ij})^2 + (\nabla_2 x_{ij})^2 \right]$$
 (2.7)

**PIQE** is also a NR image quality score, as shown in (2.8), lies in the range (0-100) and is inversely related to the perceptual quality of an image, which means lower the value higher the quality of the image.

$$PIQE = \frac{\left(\sum_{k=1}^{N_{SA}} D_{sk}\right) + C_1}{N_{SA} + C_1}$$
 (2.8)

Where  $N_{SA}$  indicated the number of spatially active blocks in a given image,  $D_{sk}$  is the amount of distortion in a given block and  $C_1$  is a positive constant.

#### 2.6.3 Simulation Environment

The simulation results are obtained using MATLAB 2016-a, with a 2.6 GHz Intel Core i7 processor, a 64-bit operating system, and 16 GB RAM.

## 2.7 Summary

This chapter briefly discusses the conventional MRI acquisition process and how the slow acquisition process can be accelerated using CS theory. The related work of iCS in multi-slice MRI is also reviewed. Finally, the simulation environment, assessment parameters, and datasets used are discussed.

## Chapter 3

## Fast Interpolated Compressed Sensing Technique using 2D Sampling Scheme for Multi-Slice CSMRI Reconstruction.

#### 3.1 Introduction

In this chapter, a novel fast interpolated compressed sensing (FiCS) technique is discussed based on a 2D Variable Density Under-Sampling (VRDU) scheme [109]. The 2D-VRDU scheme has improved results because it takes maximum samples from the high-energy central part of the k-space slices and minimum samples from its periphery. The FiCS technique takes two consecutive under-sample slices and estimates the missing samples using the proposed interpolation approach. Compared to the previous methods [100], slices recovered with the FiCS technique have a maximum correlation with their corresponding original slices along with consistency in slice-wise image quality. The FiCS technique is evaluated by using both subjective and objective assessment techniques and compared with existing interpolation techniques [100] and CS.

#### 3.2 Related Work

The traditional MRI acquisition process is slow because of the number of samples it has to acquire to fulfill the Shannon-Nyquist theorem [1]. But CS [2, 10] breaks this criterion by reconstructing the same signal from even 10% of random Nyquist samples, provided that the basic conditions of CS are fulfilled. In Multi-slice MRI, there is a very narrow inter-slice gap and therefore has a very strong inter-slice correlation. This correlation has been used to reduce the average samples per slice. Pang et al. [15, 16] exploits this

correlation and introduced a new concept called interpolated Compressed Sensing (iCS) in multi-slice MRI. Pang [16], utilizes 9% average samples and has reduced the average under-sampling ratio. Later Datta and Deka [99, 100] further explored the work of Pang using the 1D-VRDU under-sampling scheme. The interpolation approaches of both the researchers are computationally inefficient with multiple redundant steps. Secondly, both adopted a biased under-sampling approach causing information loss in their reconstruction results [109]. Datta and Deka have also worked [30, 51, 110, 111] on reducing the computational cost of their initial work [99, 100] by increasing the undersampling ratios [111].

In interpolated Compressed Sensing MRI (iCSMRI), some of the CS samples of MRI are acquired while others and intentionally missed reducing the average sampling rate, next the missed samples are estimated from the samples of the neighboring slices which are later CS reconstructed. Datta in his recent work [100] claims improved results, therefore we have compared the novel FiCS technique with their work for both 1D and 2D sampling schemes. The main contributions of this chapter are a reduction in scan time by employing the highest under-sampling rates while improving image quality and consistency by applying a more uniform under-sampling strategy on every slice.

#### 3.3 The FiCS Technique

This section introduces a novel Fast interpolated Compressed Sensing (FiCS) technique using 2D-VRDU under-sampling and a fast interpolation scheme [109]. The FiCS technique reduces the average under-sampling ratio, thus decreasing the acquisition time. This technique also shows improved results with even 5% average samples thus reducing the under-sampling ratio and scan time. Secondly, the interpolation technique of FiCS is

computationally efficient with only a set difference and addition operation. The main advantage of the novel FiCS technique is that for reconstruction, consecutive undersampled slices retain maximum samples of the original slices and rest from the neighboring slices. Thus, the resulting reconstructed images have a maximum correlation with the original images. In the previous iCS techniques [16, 100] most of the slices are more correlated to their neighboring slices, rather than their original ones. The novel FiCS algorithm works in three steps, (i) under-sampling, (ii) interpolation, and (iii) CS reconstruction. Each step is discussed separately in subsections.

#### 3.3.1 2D-VRDU Under-Sampling Scheme

The original k-space or Fourier data of the multi-slice MRI sequence has maximum energy points at the center which resembles a 2D-VRDU pattern, as shown in Fig. 3-1. Therefore, the same 2D under-sampling pattern is adopted in FiCS because it can efficiently under-sample the original k-space data of a multi-slice MRI sequence with a much lower under-sampling ratio. It is also clear from the figure that the 2D-VRDU mask takes maximum samples from the k-space center and minimum from its periphery.

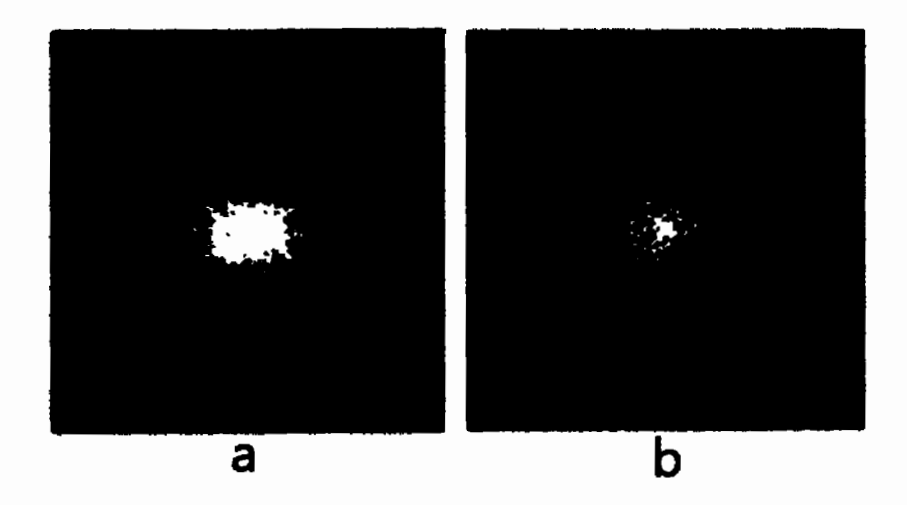


Fig. 3-1 (a) Full k-space data and (b) under-sampled k-space data acquired using a 2D-VRDU mask

The under-sampling strategy of FiCS takes only 5%, 2D-VRDU samples, from each slice of a multi-slice MRI sequence, and therefore its average under-sampling ratio is also 5%. First, two such masks with 5%, samples are generated using 2D Gaussian PDF. Then these masks are used for under-sampling of two consecutive slices and repeated after every two slices for the whole multi-slice MRI sequence. Two such masks are shown in Fig. 3-2. A detailed examination of the figure reveals that the 2D-VRDU pattern always takes different sampling locations with the same sampling ratios.

Two fully sampled original multi-slice MRI data sets are used to evaluate FiCS, but before applying the novel FiCS technique, the multi-slice MRI sequence is first undersampled into k-space data. For the under-sampling of an  $i^{th}$  slice  $S_i$ , first a down-sampling Fourier operator  $F_u$  of the 2D-VRDU sampling pattern is generated. Then  $F_u$  is applied on  $S_i$ , resulting in an under-sampled slice  $U_i$ , in k-space as represented in (3.1).

$$\mathbf{U_i} = \mathbf{F_u} * \mathbf{S_i} \tag{3.1}$$

This step is repeated for each slice of the multi-slice sequence using the 2D-VRDU under-sampling patterns of Fig. 3-2 for two consecutive slices and repeated for the whole dataset.

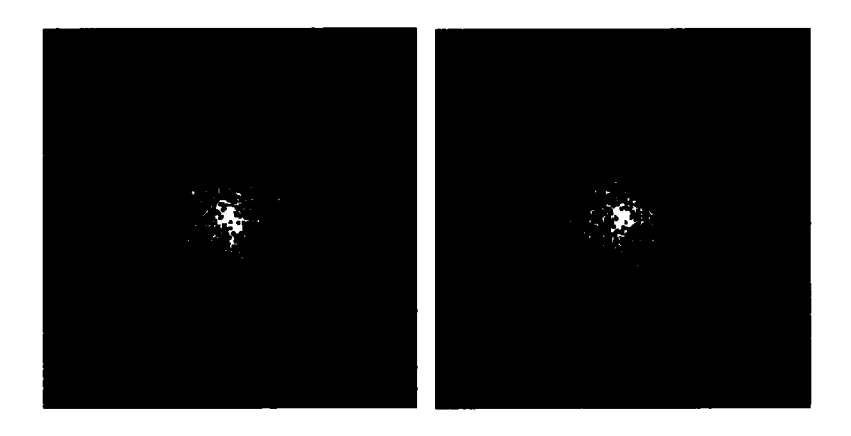


Fig. 3-2 2D-VRDU Sampling pattern for two consecutive slices

As clear from Fig. 3-2, both 2D-VRDU masks have the same sampling pattern but different sampling locations. A detailed examination of both the under-sampling patterns reveals that any two such generated masks will always have 72% samples on different locations and the rest 28% on identical locations. The sampling points on different locations will be exploited for the novel interpolation scheme of FiCS in the next step.

#### 3.3.2 Novel Fast Interpolation Scheme

The novel fast interpolation scheme of the FiCS technique estimates the missing samples in each under-sampled slice  $U_1$  of the multi-slice MRI sequence using only set difference and addition operation. The set difference is an operation to find those samples which have been missed out, while the set addition operation embeds those missed samples in the target slice.

This scheme works by taking two consecutive slices, in which the first one is called the Left slice (L slice) and the second one is called the Target slice (T slice). The T slice will always be interpolated from its corresponding L slice. The novel interpolation scheme of FiCS has two steps. The first step is the set difference between the L and T slices as shown in (3.2), where the set difference is actually finding those pixels of L sliced which was missed from the T slice as presented in Fig. 3-3. This resultant difference between the two slices is called T<sub>new</sub>, containing the new sampling information.

$$T_{new} = L \ominus T \tag{3.2}$$

Where the ⊖ sign shows a set difference operator. Both L and T slices have 5% 2D-VRDU samples, therefore their set difference T<sub>new</sub>, will have 3.6% samples. Actually, in every two consecutive slices with 5% 2D-VRDU samples, there are always 1.4% samples

on the same locations while the rest 3.6% on different locations and this is the reason that  $T_{new}$ , will have 3.6% samples.

In the second step these 3.6% samples of  $T_{new}$  are combined with 5% samples of T slice resulting in 8.6% samples in the interpolated T slice called  $T_{int}$  as shown in (3.3). The samples of the two slices are combined using a set addition operation represented by the  $\oplus$  sign.

$$T_{int} = T_{new} \oplus T \tag{3.3}$$

This two-step interpolation technique is applied on all the slices of under-sampled multi-slice MRI sequence, considering every slice as T and its preceding as L slice, to get interpolated slices, T<sub>int</sub>. The complete two-step interpolation approach of the novel interpolation technique of FiCS is shown in Fig. 3-3. For the current clinical scanners, the same sampling strategy has also been implemented using 1D-VRDU masks.

Hence comparing the computational complexity of the proposed interpolation strategy with the most recent techniques [16, 99, 100], it is shown in Fig. 3-3 that the proposed interpolation scheme only involves a set difference and addition operation. This set difference and addition operation is only finding the missed samples and then embedding it in the target slices. Thus the complex computations of Fourier, Inverse Fourier, convolution, and matrix division that are the essential steps of the previously proposed techniques [16, 99, 100].] are replaced. Therefore the computational complexity of the novel interpolation algorithm has been reduced to O(n), compared to  $O(n^2)$  in [16] and  $O(n \log n)$  in [100]

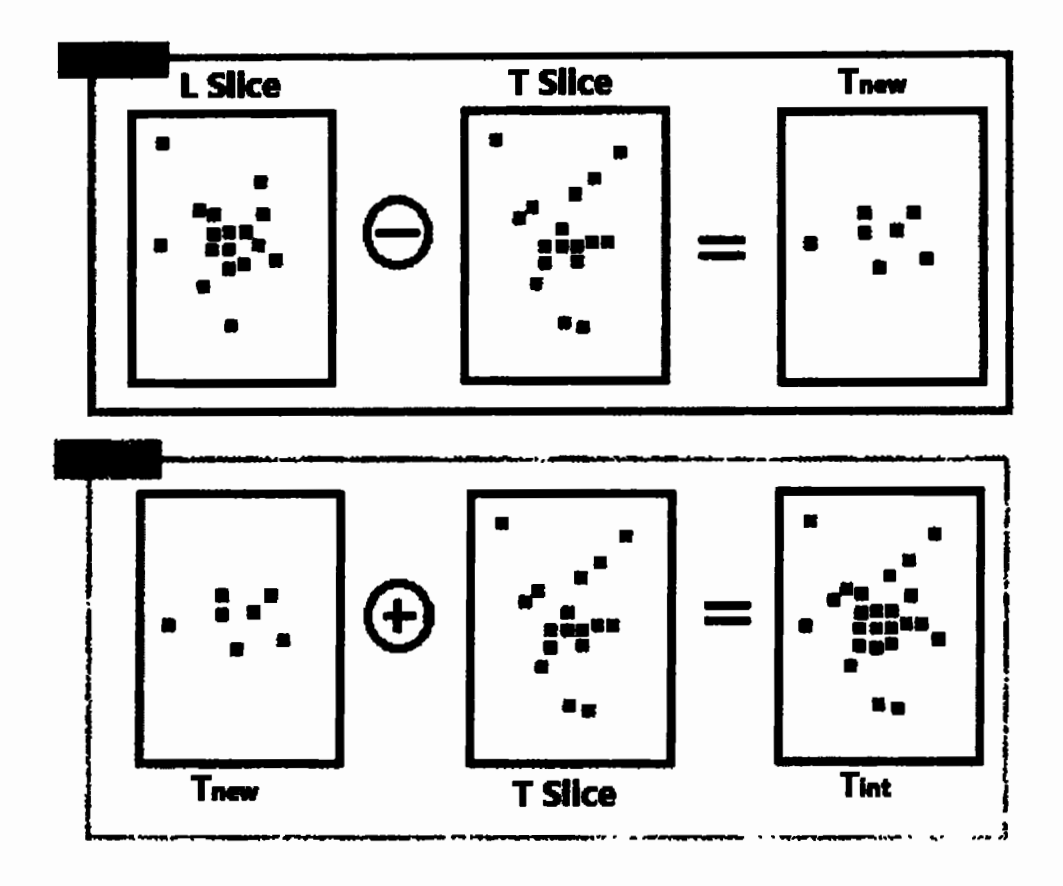


Fig. 3-3 The novel fast interpolation technique

#### 3.3.3 CS Reconstruction

After interpolation, the 3rd and final step is to apply CS reconstruction on all the interpolated slices, to get the CS reconstructed images. The CS reconstruction algorithm uses a non-linear conjugate gradient (NCG) with  $\ell_1$ -norm and Total Variance (TV) [11] as shown in (3.4).

$$\hat{x} = \underset{x}{arg} \ \underset{x}{min} \ \|F_{u}x - y\|_{2}^{2} + \lambda_{1} \|\Psi x\|_{1} + \lambda_{2} \|x\|_{TV} \eqno(3.4)$$

Thus for a given k-space measurement y and a down-sampled Fourier operator  $F_u$ , the function reconstructs the image x that minimizes the cost function with the given  $\ell_1$ -norm and TV constraints, where  $\Psi$  represents the wavelet operator. The objective

function is  $\ell_1$ -norm which is defined in (3.5) and minimizing  $\|\Psi\mathbf{x}\|_1$  promotes sparsity. Similarly, the constraint  $\|\mathbf{F_u}\mathbf{x} - \mathbf{y}\|_2^2$  enforces data consistency. Where  $\lambda_1$  and  $\lambda_2$  are the thresholding parameters for  $\ell_1$  wavelet penalty and TV penalty respectively. The TV is defined discretely in (3.5).

$$\|\mathbf{x}\|_1 = \sum_i |\mathbf{x}_i| \tag{3.5}$$

$$\|\mathbf{x}\|_{TV} = \sum_{i,j} \left[ (\nabla_i \mathbf{x}_{ij})^2 + (\nabla_2 \mathbf{x}_{ij})^2 \right]$$
 (3.6)

Where  $\nabla_1$  and  $\nabla_2$  denote the forward finite difference operators on the first and second coordinates respectively. The complete process of the novel FiCS technique is shown in Fig. 3-4.

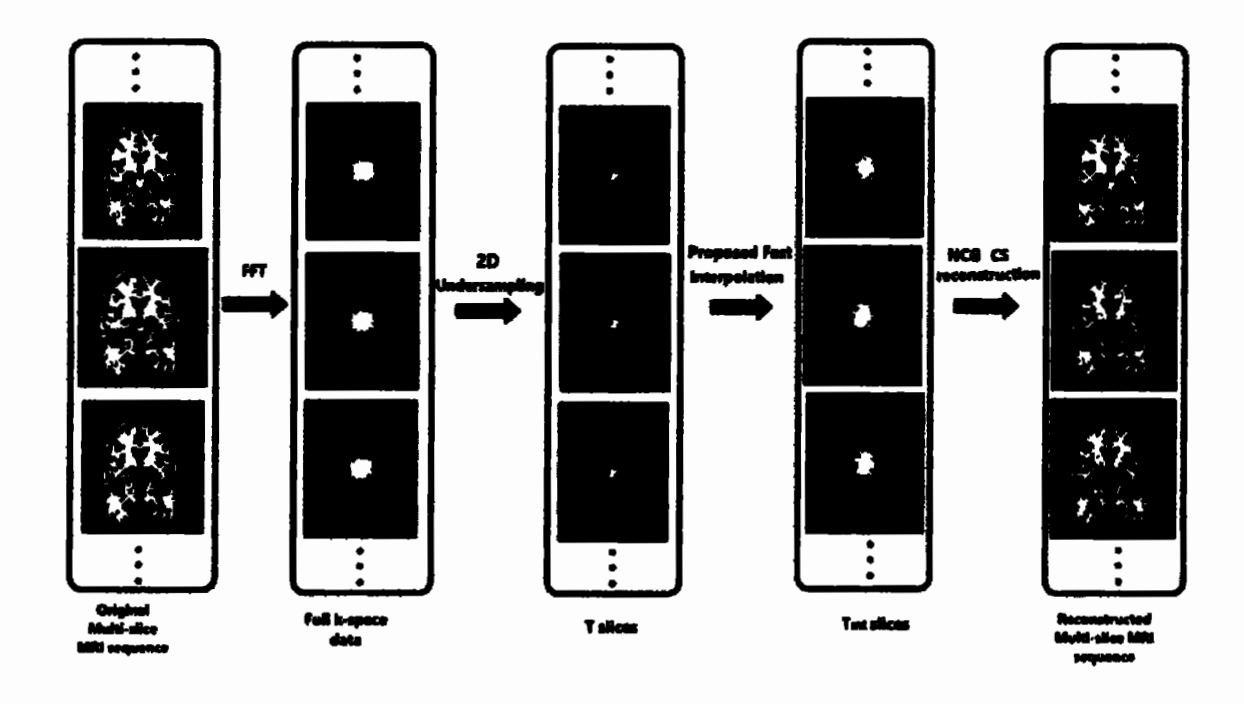


Fig. 3-4 The Novel FiCS Technique

#### 3.4 Simulation and Results

The FiCS technique is evaluated in three steps. In the first step, the 2D-VRDU undersampling scheme of FiCS is evaluated. Secondly, the novel interpolation approach of FiCS is evaluated, and finally, the overall behavior of FiCS is analyzed. All the three evaluations are discussed as under:

#### 3.4.1 Evaluation of the Under-Sampling Scheme

Like CS, the under-sampling strategy of FiCS equally under samples all the slices of the multi-slice MRI sequence. The main edge of this uniform under-sampling using the 2D-VRDU approach for the novel FiCS technique is that during interpolation most of the samples are retained from the original slices.

The benefit of the 2D-VRDU sampling strategy to acquire the under-sampled T slices is that after interpolation every T<sub>int</sub> slice will have 60% samples from T slice and the rest 40% from its L slice. In the previous techniques [16, 100] each interpolated slice had only 4% samples from its original under-sampled slice and the rest 96% from its neighboring slice. Thus their result is that every three consecutive reconstructed images represent the same information as shown in Fig. 3-5 (b1-b3 and c1-c3). A Comparison of three consecutive original images with reconstructed images using iCS-1D and iCS-2D is shown in Fig. 3-5, while Fig. 3-6 shows a comparison with FiCS-1D and FiCS-2D.

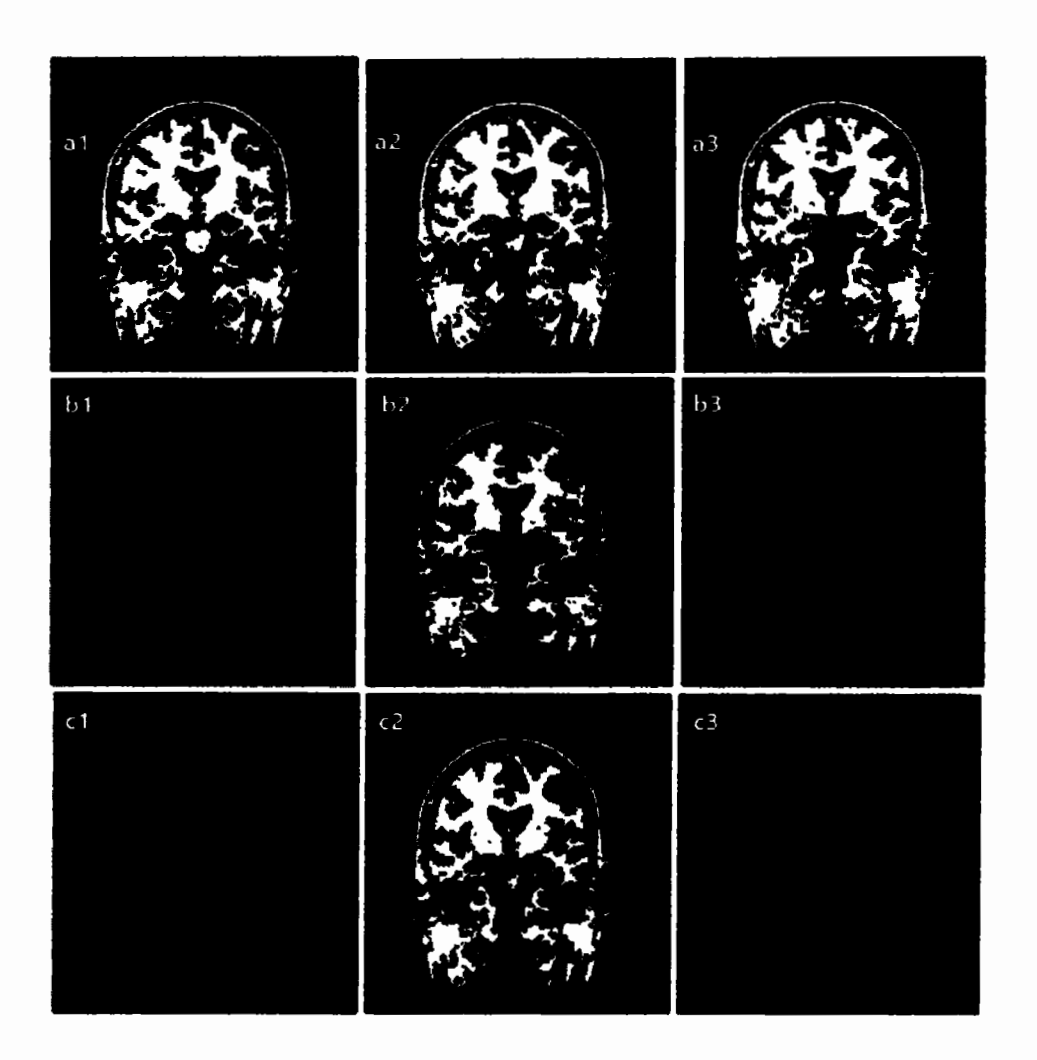


Fig. 3-5 Three consecutive (a) original and reconstructed images using (b) iCS-1D and (c) iCS-2D. New information is pointed by the arrow in a3 which is missed by iCS in both b3 and c3. The three consecutive slices of iCS (b1-b3 and c1-c3) show similar information to the central slice (b2 and c2) and are the same as in the original centered slice (a2). Secondly, iCS also shows large contrast variation among adjacent slices.

It is clear from Fig. 3-6 that each reconstructed slice using FiCS has preserved the original information of their corresponding original slices. While in iCS two of the three consecutive slices have missed their original information and represented the information of their neighboring centered slices. In short, the three consecutive slices of iCS are the same in terms of the information content while our FiCS technique has retained the information of the respective original slices.

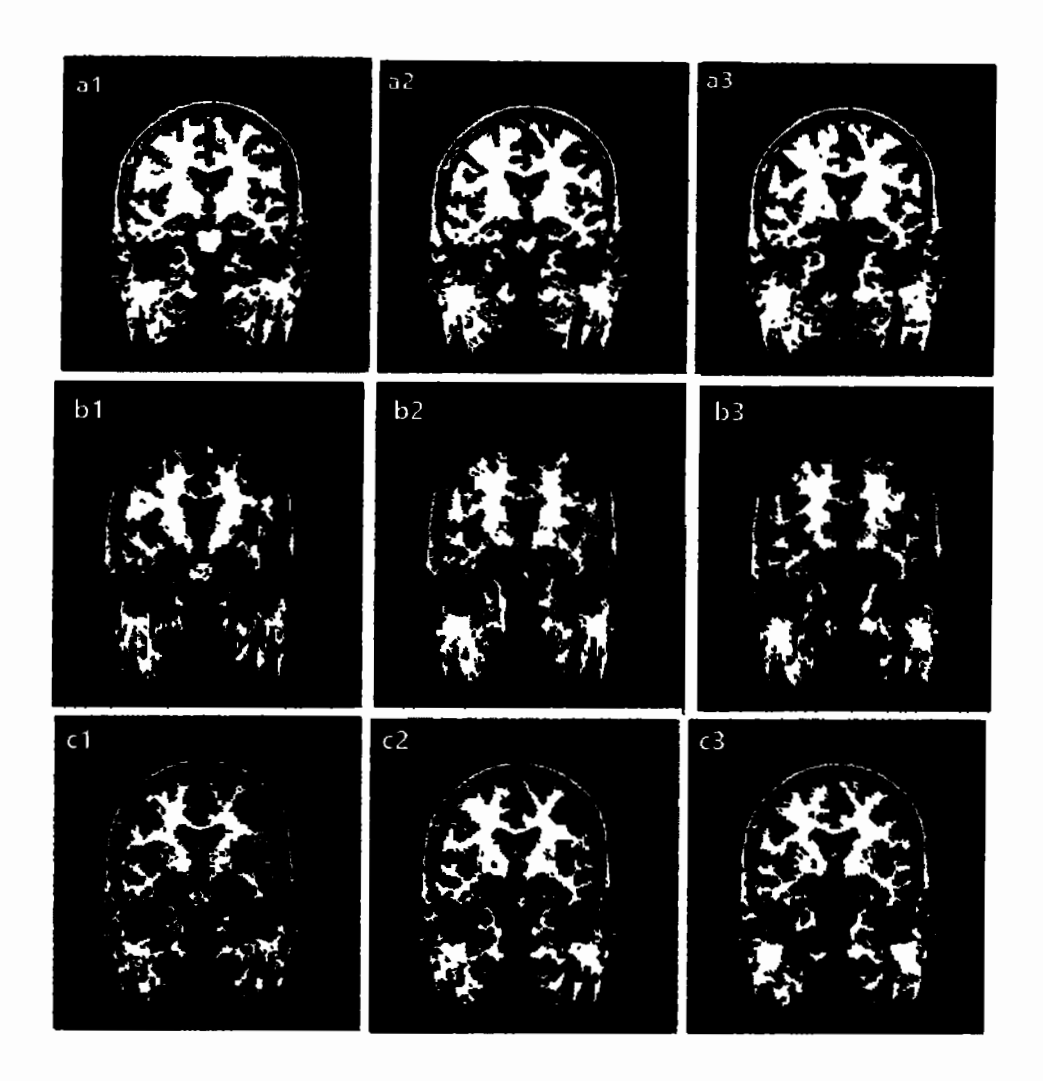


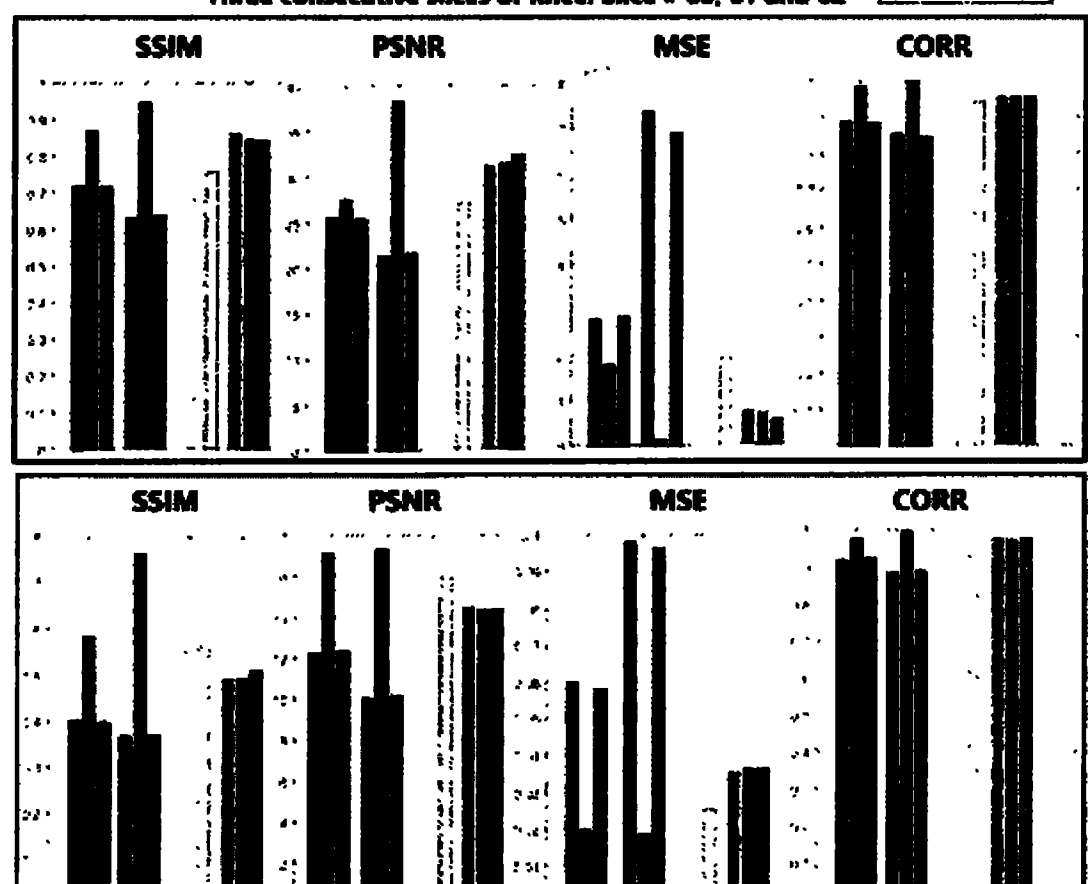
Fig. 3-6 Three consecutive (a) original and reconstructed images using (b) FiCS-1D and (c) FiCS-2D. New information is pointed by the arrow in a3 which was missed by iCS, while FiCS has retained that information in both 1D (b3) and 2D (c3). Similarly, FiCS also shows no contrast variation among adjacent slices while preserving the original information of their corresponding original slices.

Hence the reconstructed images of FiCS have maximum information of the original images along with consistency in slice-wise image quality, as shown in Fig. 3-6.

Assessment of three consecutive slices of both knee and brain data sets, using the four parameters, are shown in Fig. 3-7. This assessment is performed on iCS-1D, iCS-2D, FiCS-1D, and FiCS-2D using the same 9% average samples.



Three consecutive slices of Knee: Slice # 60, 61 and 62



Three consecutive slices of Brain: Slice # 94, 95 and 96

Fig. 3-7 Slice-wise assessment of three consecutive slices on both knee and brain data sets. iCS-1D and iCS-2D show huge variations in values while the novel FiCS technique has consistent values in both 1D and 2D like CS and is better than CS.

As shown in the three consecutive reconstructed images of Fig. 3-6 (b1-b3 and c1-c3), iCS shows wide variation in terms of image quality and contrast. The same variation is verified through their assessment in Fig. 3.7, which shows huge variations in values.

The assessment of FiCS, in Fig. 3-7, shows no such abrupt changes in values of three consecutive slices, and the same is verified from Fig. 3-6 (b1-b3 and c1-c3). The centered

slice in iCS Fig. 3-5 (b2 and c2) looks good and has improved assessment on all parameters, as shown in Fig. 3-7 because it has 25% of the original samples while the novel FiCS technique has only 9% of it. But this uneven distribution of the undersampling ratios in iCS results in every three consecutive slices being the same in terms of the imaging information. Thus, iCS shows non-consistent results both qualitatively and quantitatively whereas FiCS shows consistent results.

#### 3.4.2 Evaluation of the Fast Interpolation Scheme of FiCS

The novel Fast interpolation scheme (FiCS) is evaluated by comparing the assessment parameters of FiCS with recent iCS [100] and CS [11] techniques for both 1D and 2D-VRDU masks. Fig. 3-8 shows the evaluation of all four assessment parameters using 9% average sampling ratios.

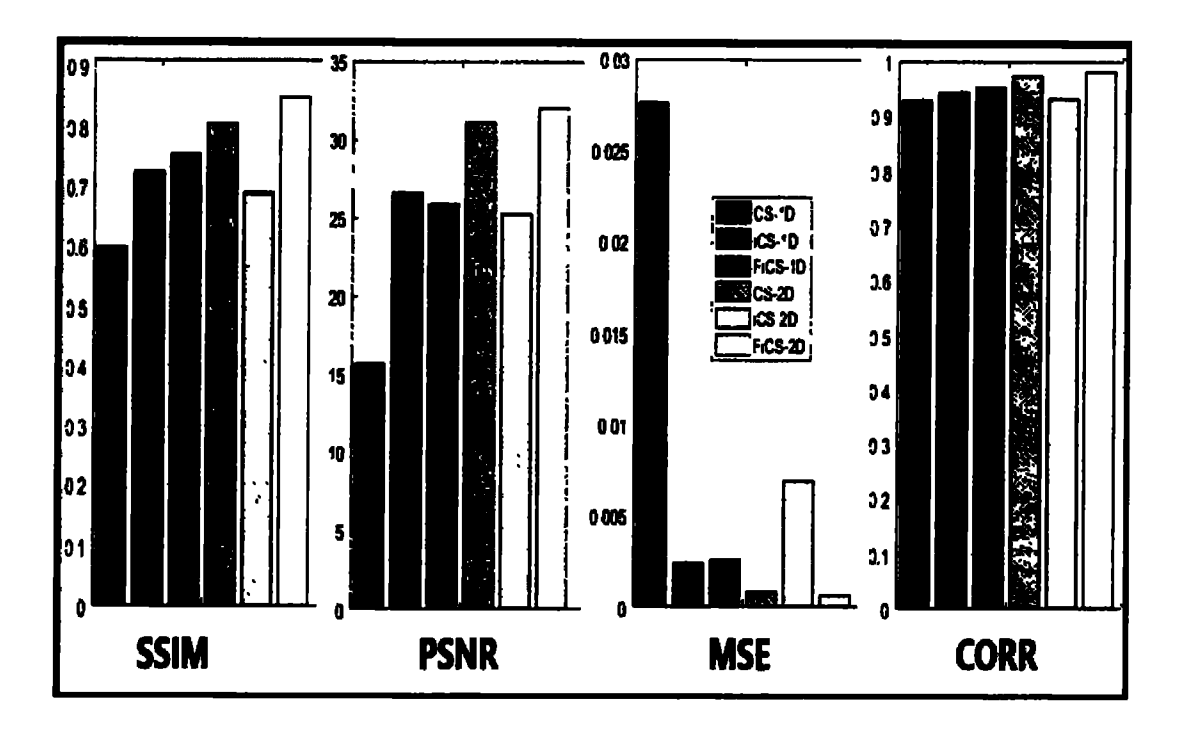


Fig. 3-8 Comparing CS-1D, iCS-1D, FiCS-1D, CS-2D, iCS 2D, and FiCS-2D with 9% average sampling ratio. The assessment is done on 9 consecutive slices (slice number 74-82) and averaged using four assessment parameters on knee dataset. Thus FiCS-2D outperforms all, on all the assessment parameters.

For a fair comparison, the assessment has been done on 9 consecutive slices and averaged. It is clear from the graph that although iCS technique with a 1D-VRDU mask performed better than CS, as claimed by its authors [100]. But when the same is implemented with a 2D-VRDU mask it performs worse even from CS.

2D-VRDU mask is most capable to acquire the k-space data of a multi-slice MRI sequence, because of its resemblance with the original k-space data. Therefore, a good iCS technique performs better using 2D-VRDU masks.

The novel FiCS-2D outperforms all the other techniques on all four assessment parameters. Although FiCS-1D also performs far better than iCS-1D on individual consecutive slices as shown in Fig. 3-7 but due to the uneven distribution of sampling ratios in iCS their average assessment of 9 consecutive slices is almost the same as FiCS-1D.

For fair comparison selected zoomed parts of the original images of both knee and brain are also compared with the reconstructed images using CS, iCS, and FiCS. The original image has 100% samples while the reconstructed images have 9% average samples as shown in Fig. 3-7. It is clear from the figure that our novel FiCS technique has more clear results, compared to all other techniques. It is to be clarified that the reconstructed images of iCS (c, f and i, l) look sharper because it has been reconstructed using 25% samples, in which 1% samples are taken from the original slice and the rest 24% from the neighboring slice. Therefore, although their images look sharper, but the information is not original. Secondly, the redundant Fourier steps in the interpolation of iCS [100] cause large contrast variation in their adjacent slices. Thus these extra Fourier steps not only

make their algorithm computationally complex but also cause huge contrast variations in consecutive reconstructed slices as shown in Fig. 3-7

Most importantly the computational complexity of the novel interpolation algorithm of FiCS is reduced to O(n), compared to O(n log n) of iCS [100]. The processing time of the novel fast interpolation technique is up to five times faster compared to the current interpolation technique [100]

The novel FiCS technique has not only improved performance with the same average sampling ratio (9%) but also outperforms with 7% and with even 5% sampling ratios as shown in Table 3-1. Similarly, the reconstructed images using 7% and 5% are also better than iCS with even half the sampling rate as shown in Fig. 3-7.

Table 3-1 Comparison of iCS with the novel FiCS technique using 9%, 7%, and 5% under-sampling ratios

Average assessment of 9 consecutive slices of Knee Dataset, [74-82]						
S. No	Assessment Parameter	iCS-1D-9%	iCS-2D-9%	FiCS-9%	FiCS-7%	FiCS-5%
1	SSIM	0.7434	0.67581	0.8551	0.831	0.7626
2	PSNR	26.5709	25.2133	32.021	30.71	29.4
3	MSE	0.00239	0.00688	0.0007	0.0009	0.0012
4	CORR	0.94428	0.93285	0.981	0.976	0.9654

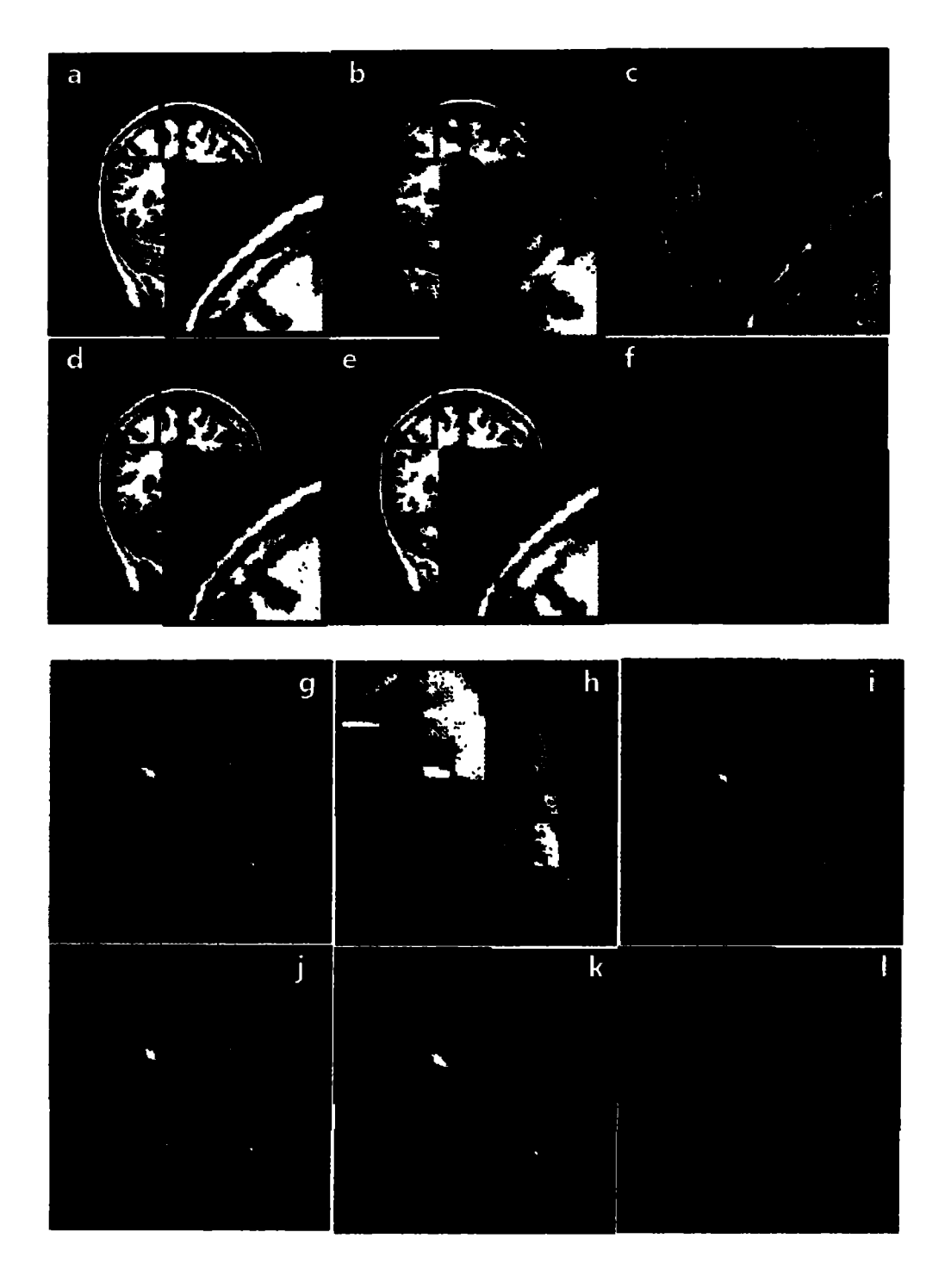


Fig. 3-9 Comparison of (a) Original brain Image with Reconstructed images using (b) CS-1D, (c) iCS-1D, (e) CS-2D, (f) iCS-2D and (d) FiCS-2D with 9% average sampling ratio. Similarly, comparison of (g) Original knee Image with Reconstructed images using (h) CS-1D, (i) iCS-1D, (k) CS-2D, (l) iCS-2D and (j) FiCS-2D with 9% average sampling ratio. The reconstructed image using the novel FiCS technique has better quality compared to other techniques.

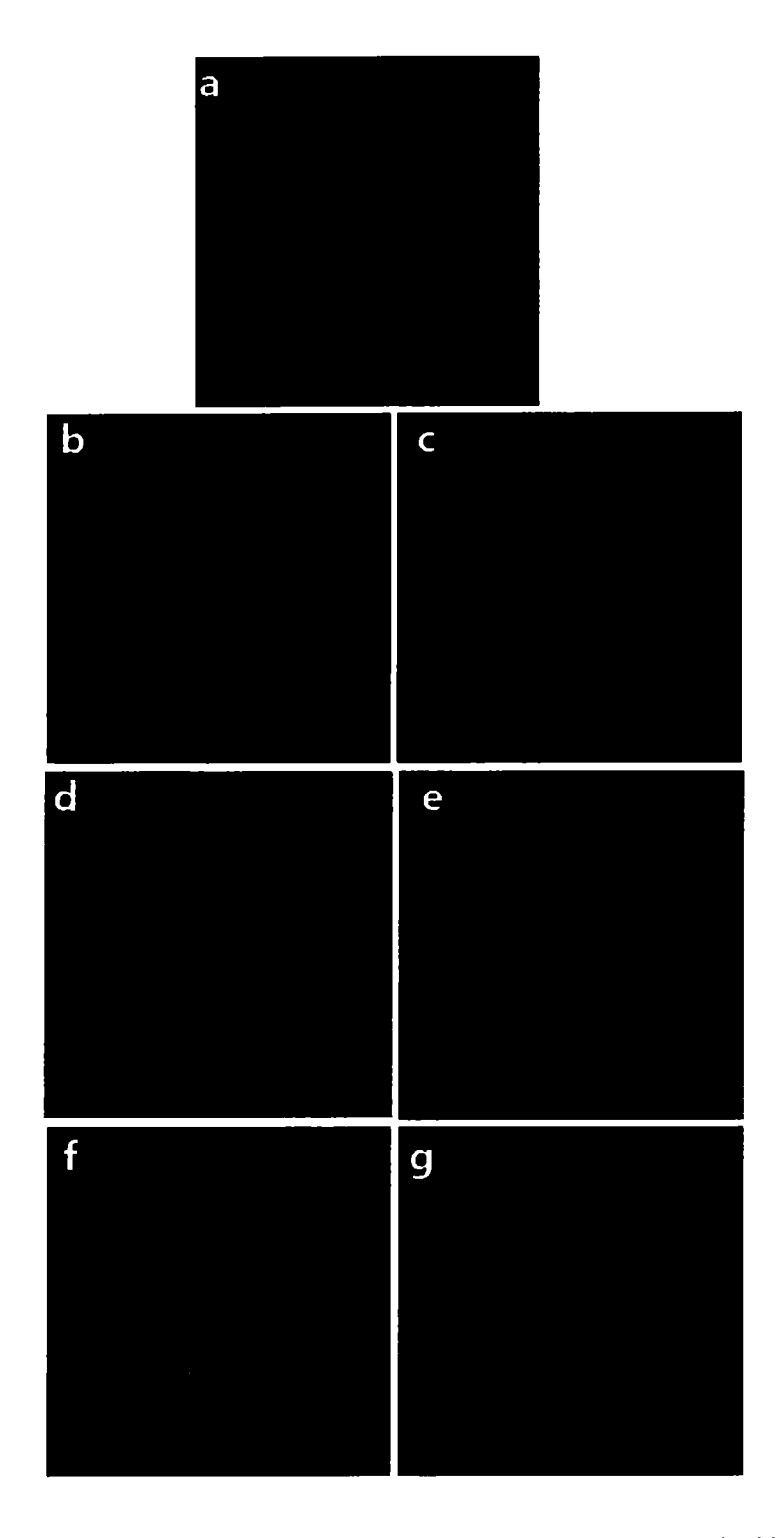


Fig. 3-10 Comparison of (a) Original image with (b) iCS-1D-9%, (c) iCS-2D-9%, (d) FiCS-1D-9%, (e) FiCS-2D-9%, (f) FiCS-2D-7% and (g) FiCS-2D-5%. The novel FiCS shows better results with even 5% under-sampling ratio.

#### 3.4.3 Evaluation of FiCS.

The novel FiCS technique is evaluated on centered 150 slices of knee data set (slice # 51 to 200) as shown in Fig. 3-11. It can be seen in the graphs that iCS-1D and 2D have huge fluctuation throughout the data set while FiCS follows a uniform pattern like CS, with improved results. The fluctuations in the graphs of iCS are such that it has peaks on the centered 25% slices and depressions on 1% (25% after interpolation) slices. While FiCS has no such biasing in sampling like CS and therefore has uniformity in their results.

The FiCS technique is implemented using both 1D and 2D-VRDU masks. Although, the 1D-VRDU mask is more realistic from the current hardware point of view but the 2D-VRDU is best suitable to represent the original k-space data of multi-slice MRI. The 2D under-sampling patterns are not commonly available on clinical scanners at present [89] and as with any novel technique within MRI practical implementation requires pulse programming access. There are now several research groups that have implemented pulse programs that can perform prospective under-sampling of 2D masks on clinical platforms. For 2D multi-slice MRI, under-sampling in the frequency-encode direction does not reduce acquisition time as the readout direction is acquired very quickly compared to the phase-encode direction.

#### 3.5 Summary

The FiCS technique not only preserves the original information in every reconstructed slice but also gives consistency in the slice-wise image quality. This technique also reduces the scan time by reducing the under-sampling ratio to almost half, compared to iCS [100], with an even improved image.

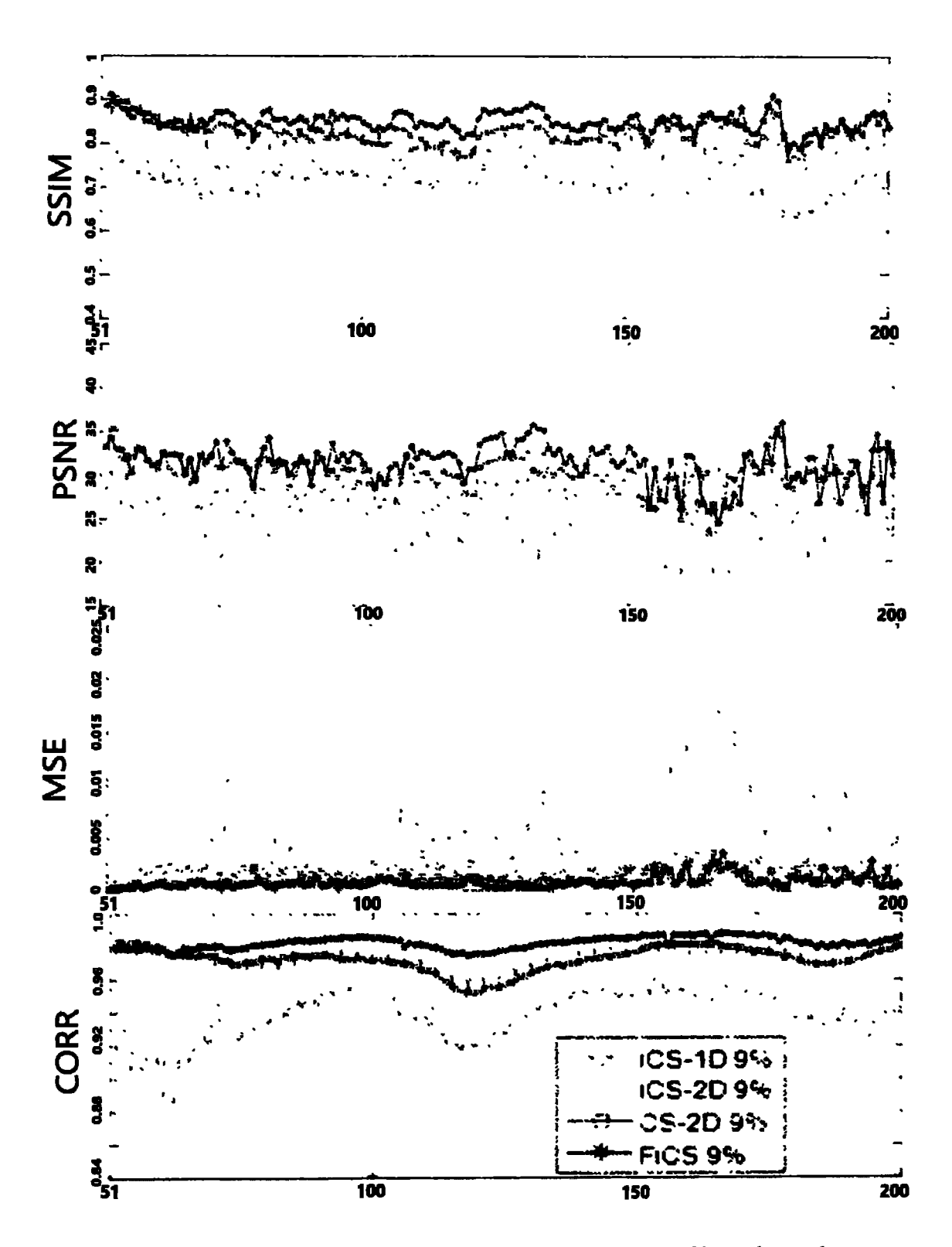


Fig. 3-11 Evaluation of the novel FiCS-2D technique on 150 slices of knee dataset by comparing it with iCS-1D, iCS-2D, and CS-2D using 9% average sampling ratios. It is clear from the graphs that FiCS-2D has a consistent graph like CS with improved results while iCS-1D and iCS-2D show huge fluctuations in values.

The uniformity in the 5% under-sampling ratio for all the slices causes lesser partial volume loss in the reconstructed images of FiCS as compared to iCS. FiCS also beats previous interpolation techniques in terms of computational complexity and processing time. Thus, the fast interpolation strategy along with 2D-VRDU under-sampling not only simplifies the novel FiCS technique but also improves the results both qualitatively and quantitatively.

## Chapter 4

# Efficient Interpolated Compressed Sensing Technique using Radial Under-Sampling for Multi-Slice CSMRI

## Reconstruction

#### 4.1 Introduction

In this chapter, an improved Efficient interpolated Compressed Sensing (EiCS) technique is discussed using different Radial under-sampling schemes [120]. Compared to the preceding two-step interpolation approach of FiCS [109], EiCS [120] uses three consecutive slices to estimate the missing samples of the central target slice from its two neighboring slices. Seven different evaluation metrics are used to analyze the performance of the EiCS technique and compared with the latest interpolation techniques and CS.

#### 4.2 Related Work

Compressed Sensing (CS) theory has enabled to accelerate the MRI acquisition process using some non-linear reconstruction techniques from even 10% of the Nyquist samples. In recent years interpolated compressed sensing (iCS) has further reduced the scan time, as compared to CS, by exploiting the strong inter-slice correlation of multi-slice MRI.

In Chapter 04, The FiCS [109] technique based on a 2D-VRDU under-sampling scheme has been discussed. FiCS shows more clinically acceptable results with less partial

volume loss, lower average under-sampling ratio, and by using a computational efficient interpolation technique. The interpolation approach of FiCS is a simple two-step process utilizing two consecutive slices to estimate the missing samples of each target slice (T slice) from its corresponding left slice (L slice). FiCS has reduced the average undersampling ratio to 5%, compared to the previous iCS techniques which have a minimum of 9% average samples. The results of FiCS also show improvement in terms of information content and image quality with even half of the sampling ratio compared to their previous interpolation techniques. Moreover, the interpolation technique of FiCS is very computationally efficient with just a set addition and difference operations. But the basic drawback of FiCS is that their under-sampling strategy does not apply to current clinical scanners and their images lack sharpness.

In this chapter, a new EiCS technique [120] based on different Radial under-sampling patterns is discussed. The novel EiCS technique is implemented using both Uniform-Angle (UA) and Golden-Angle (GA) Radial sampling patterns, using an even lower sampling ratio.

The radial under-sampling strategy reduces the under-sampling ratio to even 3%. Secondly, the novel three-step interpolation approach of EiCS ensures that each interpolated slice gets maximum samples from its respective target slice and the rest from its neighboring two slices, to have enough samples to be reconstructed as a sharper and improved image.

### 4.3 Non-Uniform Sampling

CS has been implemented using both Cartesian and Non-Cartesian under-sampling schemes [22, 93, 121]. Non-Cartesian sampling in k-space has appeared in many medical imaging modalities including MRI.

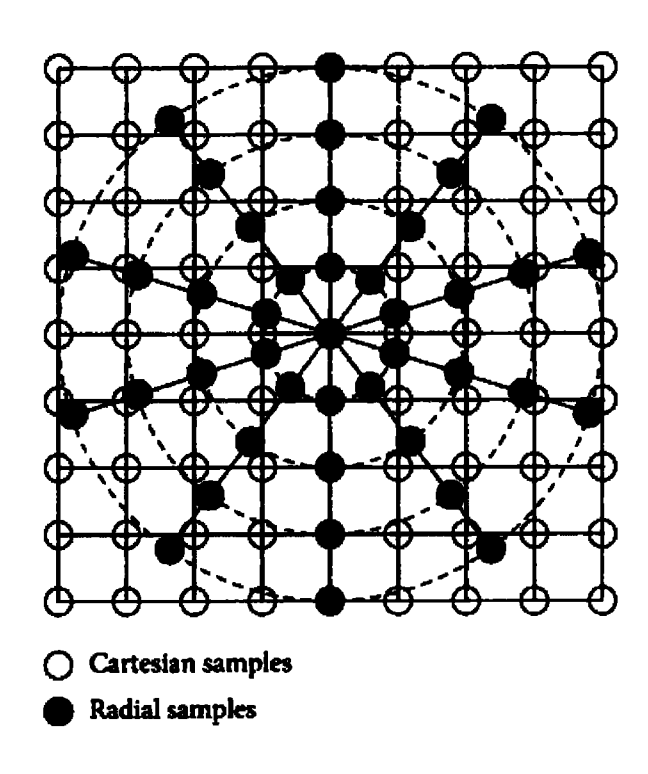


Fig. 4-1 Gridding Radial samples on the Cartesian grid [122]

Radial sampling has evolved since the beginning of MRI, with the limitation that its non-uniformly spaced samples of the spatial frequency domain, are to be projected on uniformly spaced samples in the image domain [123]. Fig. 4-1 shows some polar Radial samples which are to be projected on a Cartesian grid. The value of each Cartesian sample is to be determined from the samples of the adjacent Radial samples through gridding reconstruction [124] which uses Non-Uniform FFT (NUFFT) [123] and a Density Compensation Function (DCF). The DCF helps to mitigate the artifacts caused by the overrepresentation of some spatial frequencies in non-Cartesian acquisitions.

Similarly for converting uniformly sampled Cartesian image data into non-uniform kspace data inverse gridding is used [123].

Image reconstruction using Radial under-sampling has rapidly evolved as it allows reduced scan time with increased spatial resolution. The iterative reconstruction of CS from an under-sampled radially encoded MRI dataset is helpful for artifact-free images [93, 121, 122, 125-127]. These artifacts are directly related to the number of samples available for reconstruction. Thus, if we first estimate the missing samples in the highly under-sampled radially encoded multi-slice MRI datasets, before CS reconstruction, one can get an alias-free reconstructed image from just a fraction of the total samples.

A single multi-slice MRI scan acquires hundreds of slices. Therefore their consecutive slices have a very strong inter-slice correlation, because of having very narrow inter-slice gaps [15]. In recent years many researchers have exploited this correlation of multi-slice MRI for further reduction of the scan time, through interpolation. This new concept is termed as interpolated compressed sensing (iCS) in the literature [15, 16]. Through iCS, the average sampling ratio of CSMRI has been reduced even beyond the CS limit. Interpolated Compressed Sensing mainly works in three steps (i) under-sampling the multi-slice MRI data (ii) interpolation and (iii) CS reconstruction. For the first step, the desired under-sampling is done using a much lower under-sampling ratio compared to CS. In iCS under-sampling, some of the CS samples are missed intentionally to reduce the average sampling ratio and scan time. The random under-sampling of iCS can be accomplished using one of the many under-sampling approaches like Cartesian, Radial, spiral, and their combinations [92-94, 128]. Fig. 4-2 shows the original k-space of Multi-slice MRI and some different under-sampling approaches that can be used in CSMRI. The second step of iCS approximates the missed samples of the highly under-sample

slices from the samples of their neighboring slices [15, 16, 98, 101]. The aim of this interpolation [15, 16, 98-100] is to get CS slices. Finally, in the third step, CS reconstruction techniques [11, 93, 100, 104-107, 129, 130] are applied to the interpolated slices to get reconstructed multi-slice MRI datasets.

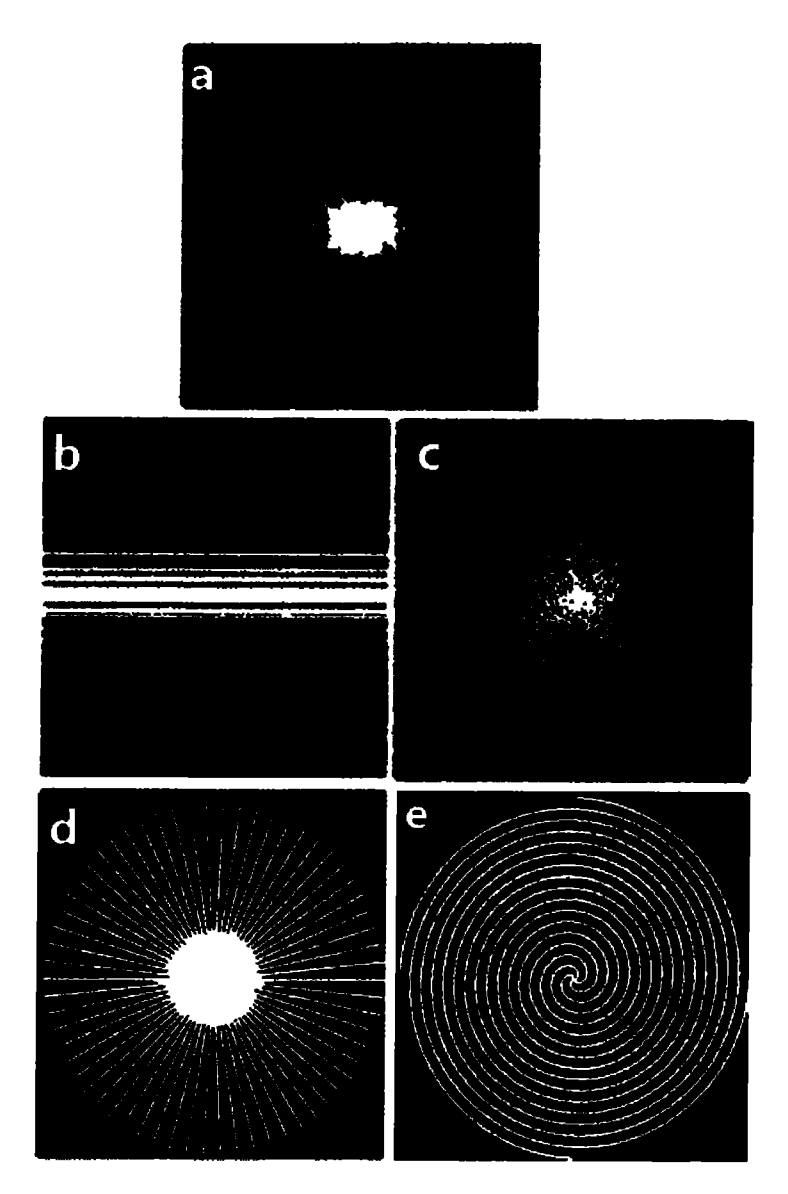


Fig. 4-2 (a) Original k-space and under-sampled k-space slices using (b) 1D-VRDU (c) 2D-VRDU (d) Radial and (e) Spiral mask.

### 4.4 The EiCS Technique

The proposed novel EiCS Technique [120] has three important steps. Every step is elaborated separately in the following subsections.

#### 4.4.1 Radial Under-Sampling Scheme

The fully sampled k-space multi-slice MRI data greatly resembles 2D-VRDU and Radial masks, as shown in Fig. 4-2. The Radial under-sampling approach is more suitable as it is practical from the present hardware point of view compared to the 2D-VRDU undersampling schemes. Most importantly, the Radial masks oversample the central region using intersecting spokes and thus detect and correct any movement in the k-space center for changes in between views. Thus, the motion artifacts in Radial under-sampling are averaged out because of the inherent oversampling of the k-space center. Therefore the reconstructed images using the Radial masks are lesser motion sensitive with higher SNR [121], compared to the 1D and 2D-VRDU schemes.

In Uniform-Angle (UA) Radial, all spokes are uniformly spaced while in Golden-Angle (GA) Radial every two spokes are spaced none uniformly depending upon the GA ratio as shown in Fig. 4-3. The GA ratio  $(180^{\circ}/((1+\sqrt{5})/2)\approx 111.246^{\circ})$  of Radial sampling acquires the spokes such that they are self-interleaving and no spoke is acquired twice [131]. The number of spokes that are needed to meet the Nyquist sampling criteria is 402 uniformly spaced spokes, with 256 samples on each spoke for a 256x256 pixel image [125, 132]. Therefore, for acquiring 3%, 5%, 7%, and 9% of the samples we must acquire 12, 20, 28, and 36 spokes which are used for the EiCS scheme.

When the Radial data are acquired using the GA ratio [131] the k-space data are under-

sampled using high temporal incoherence [94]. Therefore, the sampling patterns explored in this chapter are UA and GA-Radial as shown in Fig. 4-3.

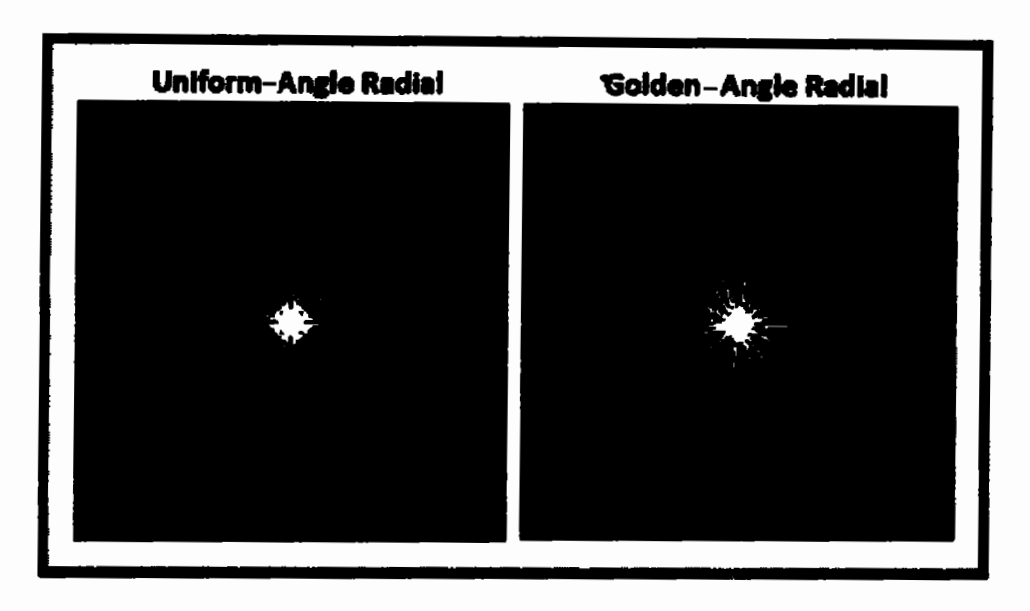


Fig. 4-3 Two different Radial under-sampling approaches used in EiCS technique

Unlike 1D and 2D-VRDU, the Radial samples are acquired on a polar grid. Therefore, the distance between the sampling points of the neighboring spokes is non-uniform. This distance is smaller in the k-space center and larger in the periphery. Thus the Radial readouts require re-gridding from the polar k-space data into the pixel domain through a Density Compensation Function (DCF) and Non-Uniform FFT (NUFFT) [123].

The under-sampling approach adopted with the novel interpolation technique of EiCS takes only 3%, Radial samples, from every slice of the multi-slice MRI sequence. The Radial under-sampling scheme is slice-wise uniform like CS, which means every slice is under-sampled with the same under-sampling ratio but using different non-overlapping spokes. Thus using different spokes in the neighboring consecutive slices will allow us to interpolate the samples in our target slices.

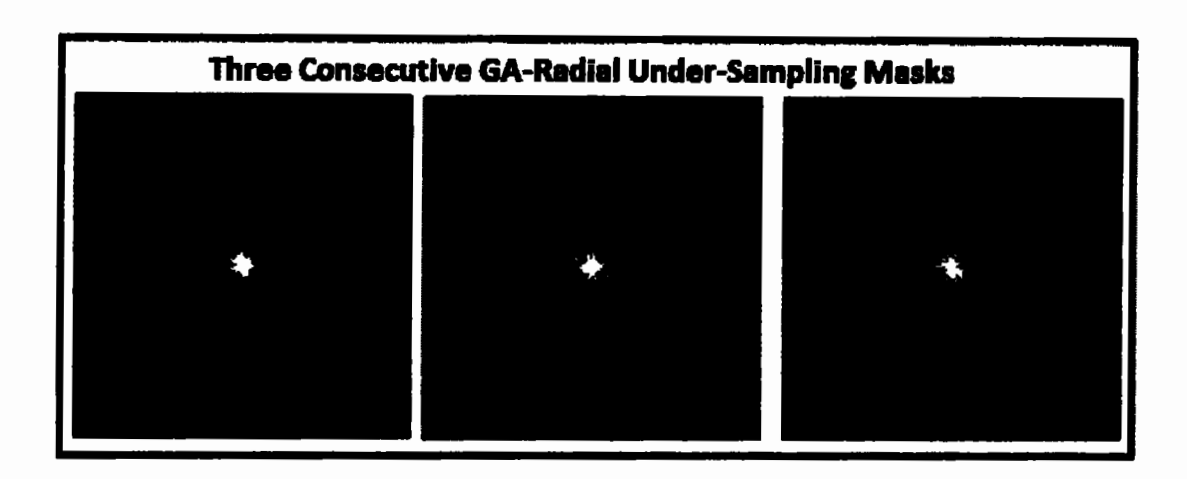


Fig. 4-4 Three consecutive Radial under-sampling masks with non-overlapping spokes

In the novel EiCS scheme, first, three different under-sampled Radial masks with the same sampling ratios are generated, as shown in Fig. 4-4. These masks are different in the sense that any two of them are having their spokes on different locations which is the fundamental key toward our novel interpolation approach.

The masks shown in Fig. 4-4 are used to under-sample three consecutive slices and repeated after every three slices for the whole multi-slice MRI sequence. Thus enabling every slice to be interpolated from its neighboring two slices. Let the three masks shown in Fig. 4-4 be termed as R<sub>1</sub>, R<sub>2</sub> and R<sub>3</sub> which are the three desired non-overlapping under-sampling Radial masks. The three consecutive under-sampling Radial masks are such that they have the same number of spokes but have different sampling locations, except its center where it will overlap, as shown in Fig. 4-4.

Two fully sampled, original multi-slice MRI data sets of the knee are used for EiCS. But first, the multi-slice MRI datasets are under-sampled into k-space data and then the novel interpolation approach of the EiCS technique is applied. For the under-sampling of three consecutive slices  $S_i$ ,  $S_{i+1}$  and  $S_{i+2}$ , first three down-sampling NUFFT operators of the

Radial sampling patterns are generated. The three down-sampling NUFFT operators are termed as NUFFT<sub>1</sub>, NUFFT<sub>2</sub> and NUFFT<sub>3</sub>. Where, each NUFFT operator is generated using its respective Radial under-sampling mask, and a DCF. To interpolate the k-space data from the non-Cartesian trajectories, the NUFFT by J. Fessler [133] and the NUFFT wrapper by M. Lustig [11] are implemented, which are available online [12, 13]. The NUFFT operators are then applied on three consecutive slices, resulting in an undersampled k-space slice sequence as represented in (4.1) -(4.3).

$$U_1 = NUFFT_1 * S_1 \tag{4.1}$$

$$U_{i+1} = NUFFT_2 * S_{i+1}$$
 (4.2)

$$U_{i+2} = NUFFT_3 * S_{i+2}$$
 (4.3)

Where  $U_i$ ,  $U_{i+1}$  and  $U_{i+2}$  represents the three consecutive under-sampled slices. This under-sampling step for three consecutive slices is repeated after every three slices for the whole multi-slice MRI dataset. Thus resulting in an under-sampled dataset in which every three consecutive slices have the same sampling patterns and under-sampling ratios but different sampling locations because of using different non-overlapping spokes, as shown in Fig. 4-4. All the samples that are on different locations can be exploited for the novel interpolation technique of EiCS in the next step.

## 4.4.2 The Novel Efficient Interpolation Scheme

The novel efficient interpolation scheme of EiCS approximates the missing sampling points from each under-sampled slice using their two neighboring slices. This approach works by considering any three consecutive down-sampled slices, out of which the central one is termed as the Target slice (T slice) which has to be interpolated from its Left (L) and Right (R) slices.

The novel interpolation technique of EiCS has three steps. The first step is to find the set difference between the L and T slice as represented in (4.4).

$$L_{\mathsf{Tnew}} = L \ominus \mathsf{T} \tag{4.4}$$

The resultant set difference is called  $L_{Tnew}$ , having the new information of the L slice with respect to the T slice. Where the  $\Theta$  sign represents the set difference operator. Secondly, the same step of L slice is repeated with the R slice, getting  $R_{Tnew}$  slice as shown in (4.5).

$$\mathbf{R}_{\mathsf{Tnew}} = \mathbf{R} \ominus \mathbf{T} \tag{4.5}$$

Where  $R_{Tnew}$  contains the new sampling information in R slice with respect to T slice. In the third and last step, the T slice samples are combined with the samples of  $L_{Tnew}$  and  $R_{Tnew}$  to get the interpolated T slice termed as  $T_{int}$  as represented in (4.6), where the  $\oplus$  sign is the set addition operator.

$$T_{int} = L_{Tnew} \oplus T \oplus R_{Tnew}$$
 (4.6)

This three-step interpolation technique of EiCS is applied on each slice of the undersampled multi-slice MRI sequence, considering every slice as a T slice and its two neighboring as L and R slices, to acquire an interpolated slice, T<sub>int</sub>. The three-step process of the efficient interpolation technique is represented in Fig. 4-5.

#### 4.4.3 CS Reconstruction

After the interpolation step, the interpolated multi-slice datasets have almost three times the samples initially under-sampled or acquired. The third and final step of EiCS is the CS reconstruction which gives the reconstructed images.

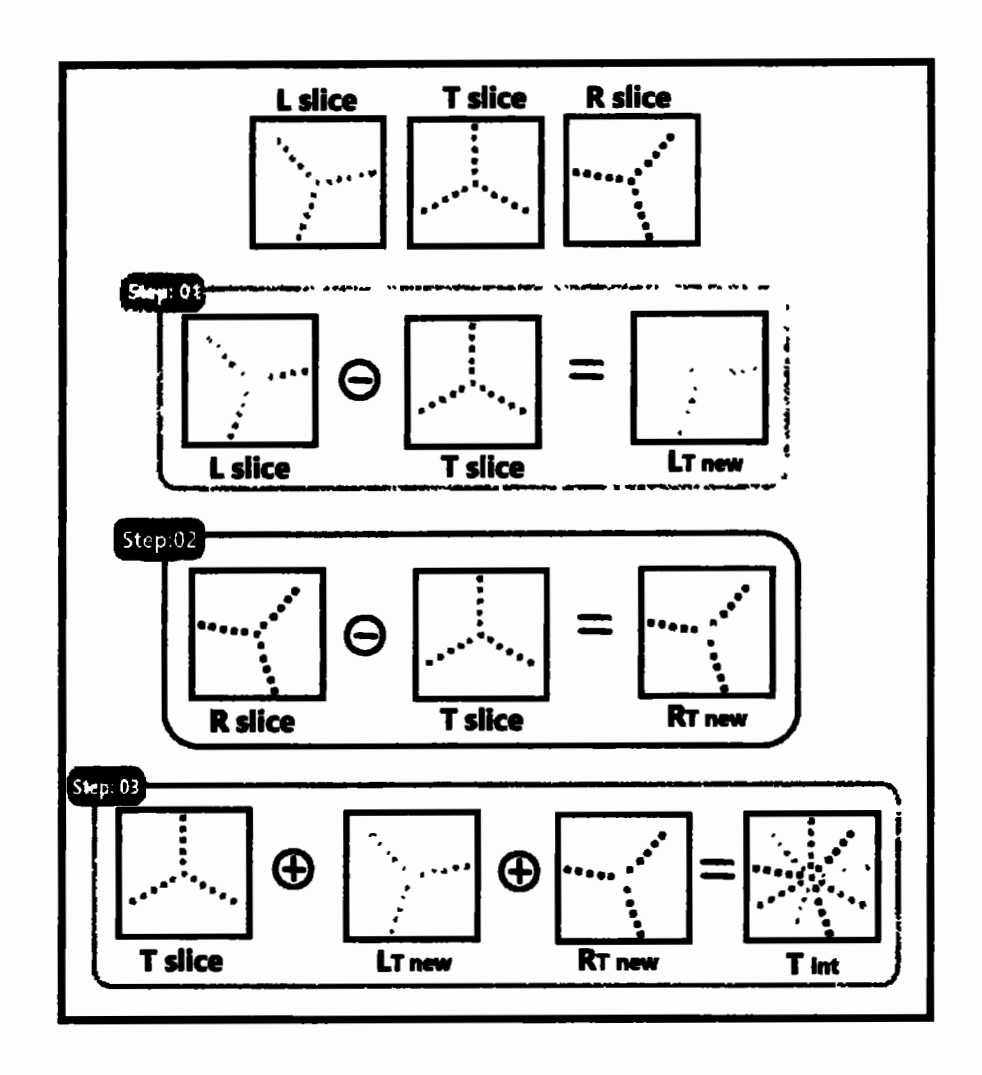


Fig. 4-5 The three-step efficient interpolation technique

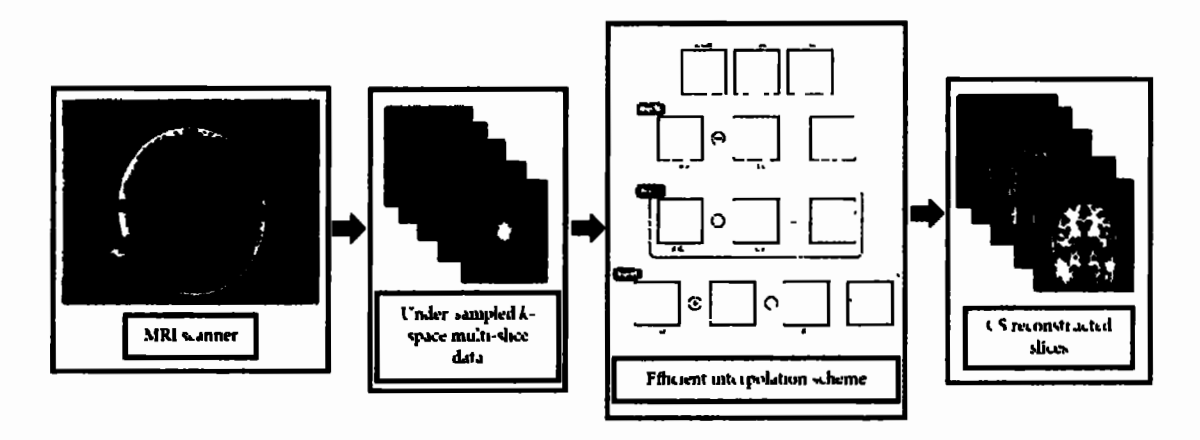


Fig. 4-6 The novel EiCS Technique

The CS reconstruction technique used for EiCS is the same as in FiCS which is the non-linear conjugate gradient (NCG) with  $\ell_1$ -norm and Total Variance (TV) [11] as discussed in the previous chapter. The complete EiCS technique is expressed in Fig. 4-6.

## 4.5 Simulation and Results

Seven different evaluation metrics are used to analyze the performance of the EiCS technique [120] such as structural similarity index measurement (SSIM), feature similarity index measurement (FSIM), mean square error (MSE), peak signal to noise ratio (PSNR), correlation (CORR), sharpness index (SI), and Perceptual Image Quality Evaluator (PIQE) and compared with latest interpolation techniques and CS. The EiCS technique is evaluated in four steps. In the first step, the Radial under-sampling scheme of EiCS is evaluated. Secondly, the novel interpolation approach of EiCS is evaluated. In the third step, the overall behavior of EiCS is analyzed and finally, the EiCS technique is evaluated for an increased inter-slice gap dataset. Different knee datasets are used in the evaluation of the novel EiCS technique which has already been discussed in Chapter 02. These knee datasets are fully sampled and are to be under-sampled using the different Radial under-sampling approaches discussed previously.

#### 4.5.1 Evaluation of the Radial Under-Sampling Scheme

Like FiCS, and CS the Radial under-sampling strategy of EiCS equally under-samples the k-space multi-slice MRI sequence but uses a much lower under-sampling ratio.

Table 4-1 shows a comparison of the Radial under-sampling schemes with the 2D-VRDU under-sampling scheme of FiCS [109], 1D-VRDU scheme of iCS [100], and CS[11]. The assessment has been performed using all the seven assessment parameters for three successive slices and averaged.

Table 4-1 Comparison of the Radial under-sampling schemes with 1D-VRDU and 2D-VRDU schemes. The assessment has been done on 3 consecutive slices and averaged (slice 165-167 of knee dataset)

Under-Sampling scheme		1D-VRDU		2D-VRDU		UA-Radial		GA-Radial	
S. No	Assessment Parameter	CS-9%	iCS- 9%	CS-5%	FiCS- 5%	CS-5%	FiCS- 5%	CS-5%	FiCS-5%
1	SSIM	0.5596	0.7226	0.7834	0.8008	0.7995	0.8388	0.7669	0.8339
2	FSIM	0.9387	0.9733	0.9713	0.9463	0.9201	0.95933	0.9150	0.9516
3	MSE	0.0398	0.0058	0.0056	0.0023	0.0008	0.00047	0.0010	0.00052
4	PSNR	14.002	23.779	22.636	26.367	30.738	33.221	29.797	32.778
5	CORR	0.9317	0.9522	0.9762	0.9647	0.9476	0.9703	0.9358	0.9671
6	SI	48.88	501.64	374.46	275.61	175.06	267.63	46.07	276.44
7	PIQE	65.791	30.915	62.121	73.850	72.577	54.582	79.574	65.978

It is clarified from the comparison of the different sampling strategies in the table that the Radial under-sampling scheme has more improved results, for both Uniform-Angle (UA) and Golden-Angle (GA) strategies, compared to the 1D and 2D-VRDU schemes. The Radial under-sampling strategy has also an edge in that it is more practical from the current hardware point of view.

#### 4.5.2 Evaluation of the Novel Efficient Interpolation Scheme

The novel three-step interpolation scheme of EiCS [120] is evaluated by comparing its reconstructed images with that of iCS [100], FiCS [109], and CS [11]. Fig. 4-7 shows a comparison of the original image with the reconstructed images using different interpolation techniques along with different under-sampling ratios. It is clear from the figure that although iCS shows visually improved results but represents information of the neighboring slices due to their biased under-sampling scheme [109]. FiCS using 2D-VRDU under-sampling shows improved results and has no loss of information but their sampling pattern is non-realistic with some blurred edges. CS reconstruction is also performed using the Radial under-sampling pattern, but their images look even more blurry with some streaking artifacts. The reconstructed images of the Radial under-sampling pattern show improved results for both FiCS and EiCS techniques. But EiCS, due to its three-slice interpolation approach has better results compared to FiCS, using the same Radial under-sampling strategy. This proves that the three-step EiCS technique is better compared to its preceding two-step FiCS approach.

The edge information pointed by the red arrow in Fig. 4-7 shows that although FiCS-Radial has improved results but for 3% under-samples ratio it has a blurring effect, while EiCS has no blurring effect with sharper and clear details. FiCS 2D-VRDU also shows better results but its under-sampling approach is non-realistic with some blurred edges. In short, EiCS has got the benefits of all the other techniques as its reconstructed images have no blurring effect with sharper details and original information and with a more realistic under-sampling approach using only 3% samples.

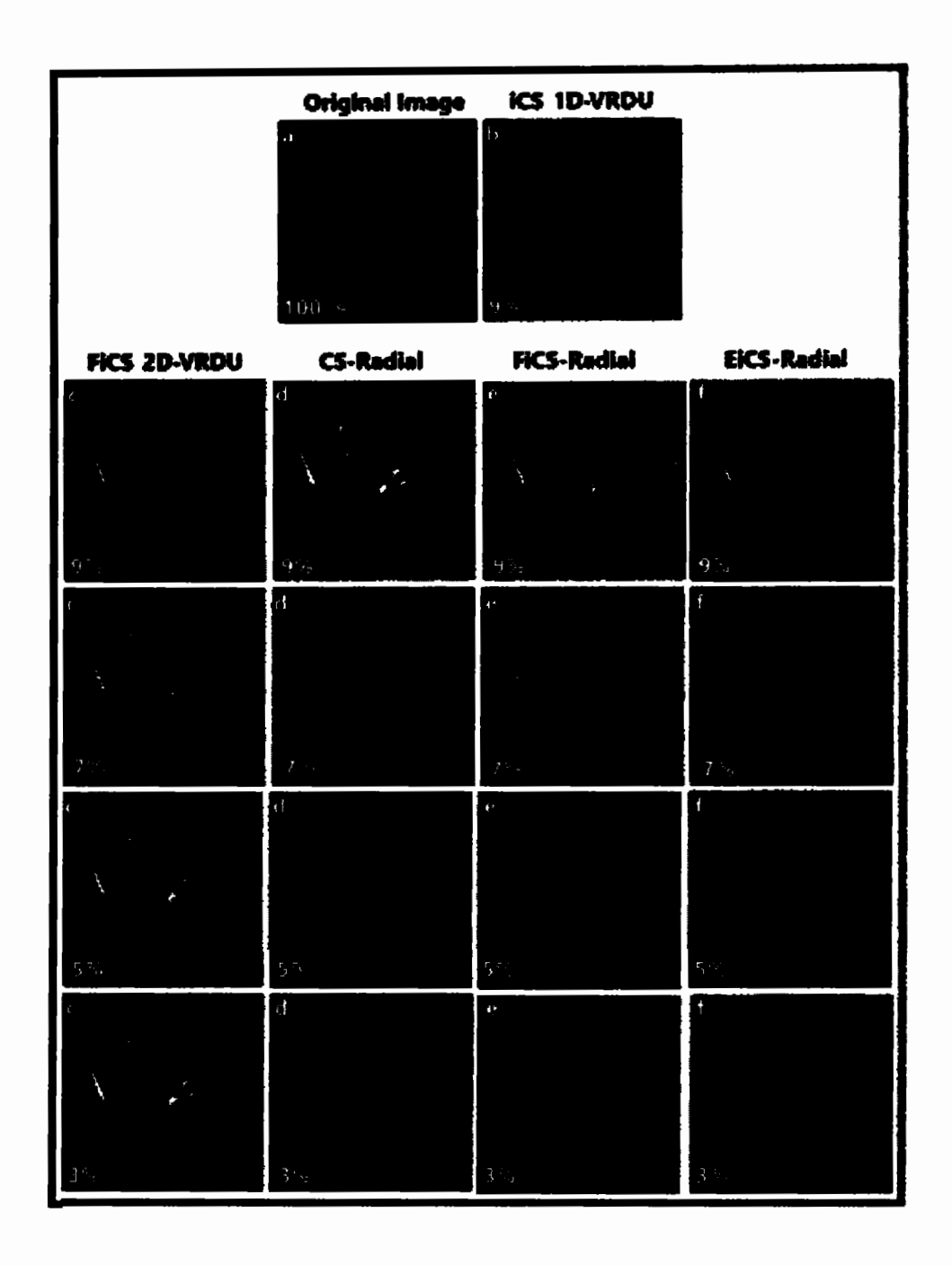


Fig. 4-7 Comparison of (a) Original Image with (b-f) reconstructed images using different reconstruction strategies and under-sampling ratios. (b) iCS reconstructed image has sharper details but with loss of information (c) FiCS 2D-VRDU has preserved the original information but has a blurring effect which becomes more prominent when the under-sampling ratio is reduced (d) CS reconstruction using the Radial under-sampling also shows severe degradation when the under-sampling ratio reduces (e) FiCS-Radial and (f) EiCS-Radial has improved results compared to CS-Radial but the sharpness degrades for (e) FiCS with 3% samples while (f) EiCS has improved results with clear and sharp details as pointed by the red arrow

In the EiCS technique, the acquired under-sampled T slices when interpolated as Tint have 34% samples from T slices and 33% from each of the L and R slices. In FiCS [109] every T<sub>int</sub> slice has 60% samples from T slice and the rest 40% from its respective L slice. In FiCS although a greater percentage of samples were taken from the original slices but because of their two-step interpolation approach, when the sampling ratio further reduces, the interpolated slices have insufficient samples to be reconstructed as a clear and sharper image. In iCS [16, 100] each interpolated slice has only 4% samples from its original under-sampled slice and the remaining 96% from its corresponding neighboring slices. The reconstructed images of iCS show sharp details due to more samples in their interpolated slices but with the limitation that their resultant three consecutive reconstructed images show repeated information because of their biased under-sampling strategy, as discussed in [109]. Although the 1D under-sampling scheme of iCS is also practical from the current hardware point of view but has a three times higher under-sampling ratio along with a biased under-sampling strategy. Table 4-2 summarizes the total percentage of the original and interpolated samples for different reconstruction techniques.

Table 4-2 Comparison of %age number of samples of different interpolation techniques and CS

S.No.	Reconstruc tion Techniques	Samples Taken from Original Slices (%)	Samples Interpolated from Neighboring Slices (%)	Total Samples for Reconstruction With 9% Average Sampling	
1	CS	100 %	0 %	9 %	
2	iCS	4 %	96 % from L slice	25 %	
3	FiCS	60 %	40 % from L slice	16 %	
4	<b>EiCS</b> 34 %		33 % from L slice 33 % from H slice	26 %	

It is clear from the table that the Radial under-sampling strategy has the lowest percentage of samples from the neighboring slices, and still has the highest percentage of interpolated samples, which gives us the benefit that information content is original and the reconstructed images are sharper.

The novel Efficient interpolation scheme of EiCS [120] is also evaluated by comparing the seven assessment parameters of EiCS with iCS [100] and CS [11]. For a fairer comparison, FiCS using the Radial under-sampling strategy is also performed. The EiCS technique shows not only improved performance with the same average under-sampling ratio (5%) of FiCS but also outperforms with even a 3% sampling ratio as shown in Table 4-3. The assessment has been done on 3 consecutive slices and averaged. Table 4-3 represents a detailed evaluation where Fig. 4-8 shows a brief summary of it.

The graphs of Fig. 4-8 clearly show that FiCS-Radial has improved performance with even 3% samples which proves that the Radial under-sampling strategy is better than 2D-VRDU. Secondly, the novel EiCS-Radial outperforms FiCS-Radial which proves that the three-step interpolation technique of EiCS is better than the two-step approach of FiCS. EiCS-Radial is also better than iCS-1D VRDU with even one-third of the samples but in three out of the seven assessment parameters (FSIM, SI, and PIQE) iCS looks better. The reason is that firstly, iCS has 9% samples and, secondly, iCS has a biased under-sampling strategy, by taking 96% of samples from neighboring slices. Therefore, although iCS shows better feature similarity, sharpness, and perceptual image quality but represents neighboring slice information. Thus EiCS-Radial beats all other techniques by taking only 3% samples.

Table 4-3 Comparison of the novel EiCS technique with CS, FiCS, and iCS for different under-sampling ratios

Average Under-	Interpolati on Technique	Under- Sampling Technique	Assessment Parameters							
Sampling Ratio			SSIM	FSIM	MSE	PSNR	CORR	SI	PIQE	
3%	EiCS	GA-Radial	0.82	0.94	0.0005	32.68	0.966	305.4	66.5	
		UA-Radial	0.82	0.95	0.0005	32.75	0.967	251.0	56.8	
	FiCS	GA-Radial	0.80	0.93	0.0007	31.39	0.954	183.7	77.5	
		UA-Radial	0.81	0.94	0.0006	32.00	0.960	229.1	70.3	
	CS	GA-Radial	0.69	0.87	0.0017	27.66	0.895	19.44	87.3	
		UA-Radial	0.70	0.87	0.0017	27.53	0.888	20.60	80.9	
	EiCS	GA-Radial	0.84	0.96	0.0004	33.91	0.974	338.0	50.9	
5%		UA-Radial	0.84	0.96	0.0003	34.23	0.976	476.9	45.3	
	FiCS	GA-Radial	0.83	0.95	0.0005	32.77	0.967	276.4	65.9	
		UA-Radial	0.83	0.95	0.0004	33.22	0.970	267.6	54.5	
	CS	GA-Radial	0.76	0.91	0.0010	29.79	0.935	46.07	79.5	
		UA-Radial	0.79	0.92	0.0008	30.73	0.947	175.0	72.5	
	EiCS	GA-Radial	0.86	0.97	0.0003	34.80	0.979	442.7	50.8	
		UA-Radial	0.85	0.97	0.0003	34.65	0.978	462.5	49.1	
79/	FiCS	GA-Radial	0.86	0.96	0.0003	34.05	0.975	516.6	61.7	
7%		UA-Radial	0.86	0.97	0.0003	34.20	0.976	449.1	54.5	
	CS	GA-Radial	0.83	0.94	0.0006	32.17	0.963	220.6	76.4	
		UA-Radial	0.83	0.94	0.0005	32.53	0.965	303.4	68.6	
9%	iCS	1D-VRDU	0.72	0.97	0.0058	23.77	0.952	501.6	30.9	

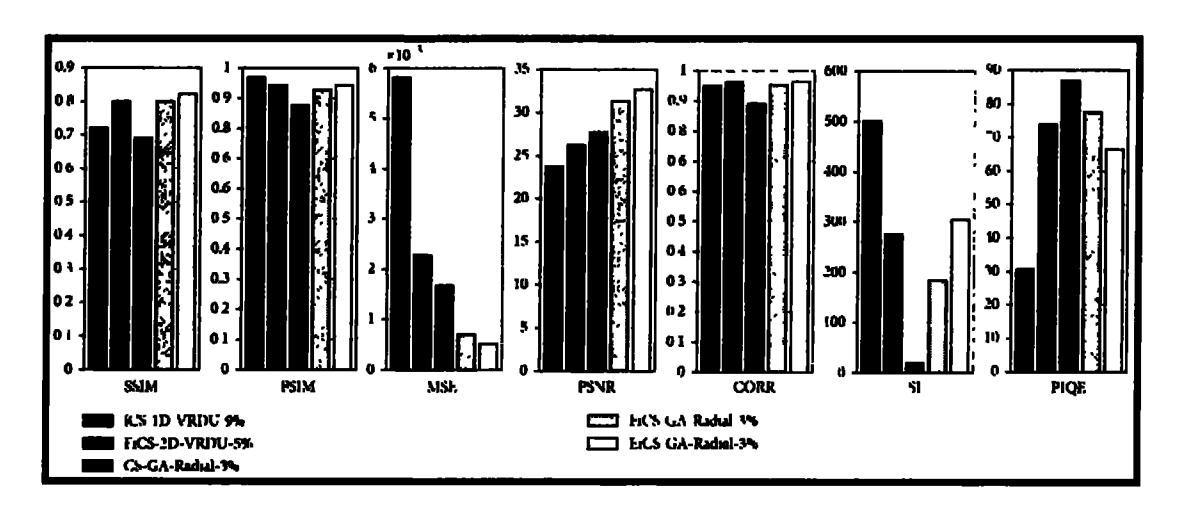


Fig. 4-8 Comparison of the novel EiCS averaged assessment parameters with iCS, FiCS, and CS. iCS 1D-VRDU has 9%, FiCS 2D-VRDU has 5% while CS-Radial, FiCS-Radial, and EiCS-Radial have 3% samples. Thus, the novel EiCS-Radial technique outperforms all with even 3% average samples

Fig. 4-9 represents a comparison of the original image with that of the reconstructed images using FiCS 2D-VRDU, FiCS-Radial, and EiCS-Radial with 3% samples by considering a zoomed edge. It is clear from the figure that EiCS-Radial is better than both FiCS 2D-VRDU, and FiCS-Radial by showing clearer and sharper results.

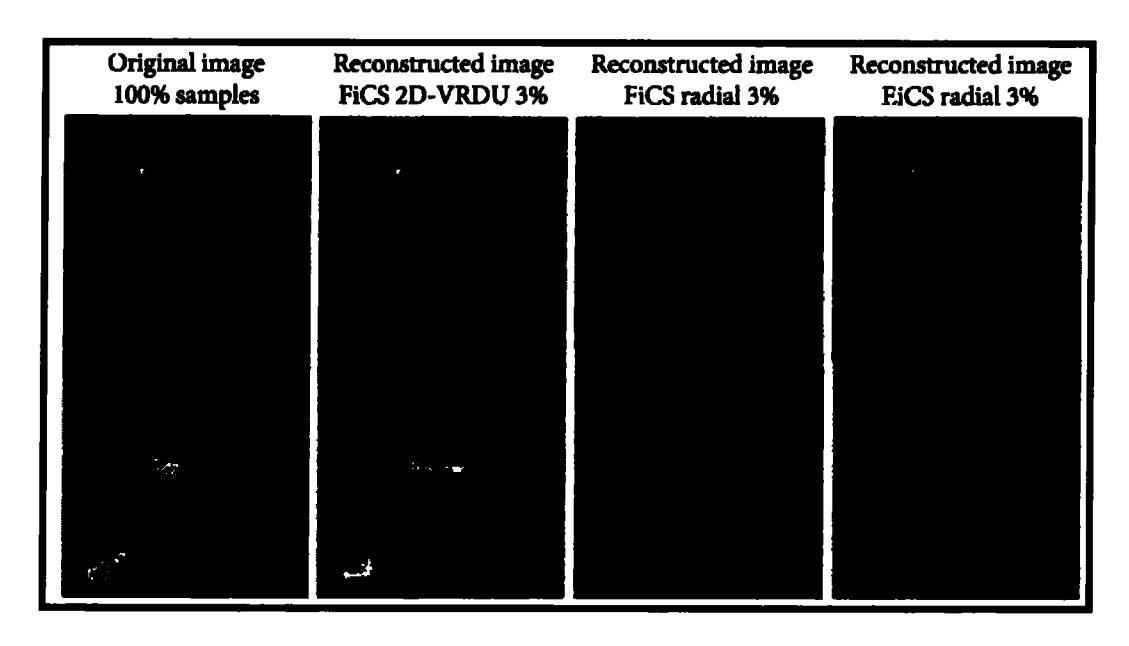


Fig. 4-9 Comparison of the original image with reconstructed images using FiCS 2D-VRDU 3%, FiCS-Radial 3%, and EiCS-Radial 3%. It is clear from the comparison of the selected zoomed portions that the EiCS technique outperforms FiCS by retaining sharper details.

## 4.5.3 Evaluation of the EiCS technique

The detailed evaluation of the novel EiCS technique [120] is done on centered 150 slices of knee data set (slice # 51 to 200) as shown in Fig. 4-10. The evaluation is done using GA-Radial under-sampling pattern for all the seven assessment parameters. It is clear from the figure that when we increase the under-sampling ratio the performance improves but while increasing the sampling ratio from 7% to 9%, the total number of interpolated samples saturates and is over-sufficient for CS reconstruction. Thus, as clear from the figure, when the sampling ratio increases from 7% to 9% the EiCS technique shows lesser improvement. This is because the three-step EiCS technique collects sufficient samples from reduced under-sampling ratios that give improved results, with even 3% samples. Secondly, Fig. 4-10 shows that EiCS has consistency in its results like FiCS where iCS shows inconsistent results as discussed in [109].

## 4.5.4 Evaluation of EiCS for Increased Inter-Slice Gap

The novel EiCS technique also outperforms for increased inter-slice gap datasets. The zero inter-slice gap means, considering all the slices of the original dataset. One and two inter-slice gaps mean skipping one and two slices from consecutive slices while taking two slices. Increasing the gap helps to further reduce the average under-sampling ratio from 3% to 1.5% and 1%. Skipping one and two slices means that we are considering 128 and 85 slices from the 256-slice knee dataset.

Fig. 4-11 shows the evaluation of CS, FiCS, and on Radial sampling for 3%, 5%, and 7% under-sampling ratios with zero, one, and two inter-slice gaps. It is clear from the graphs of Fig. 4-11 that both FiCS and EiCS have improved performance compared to CS for even increased inter-slice gaps.

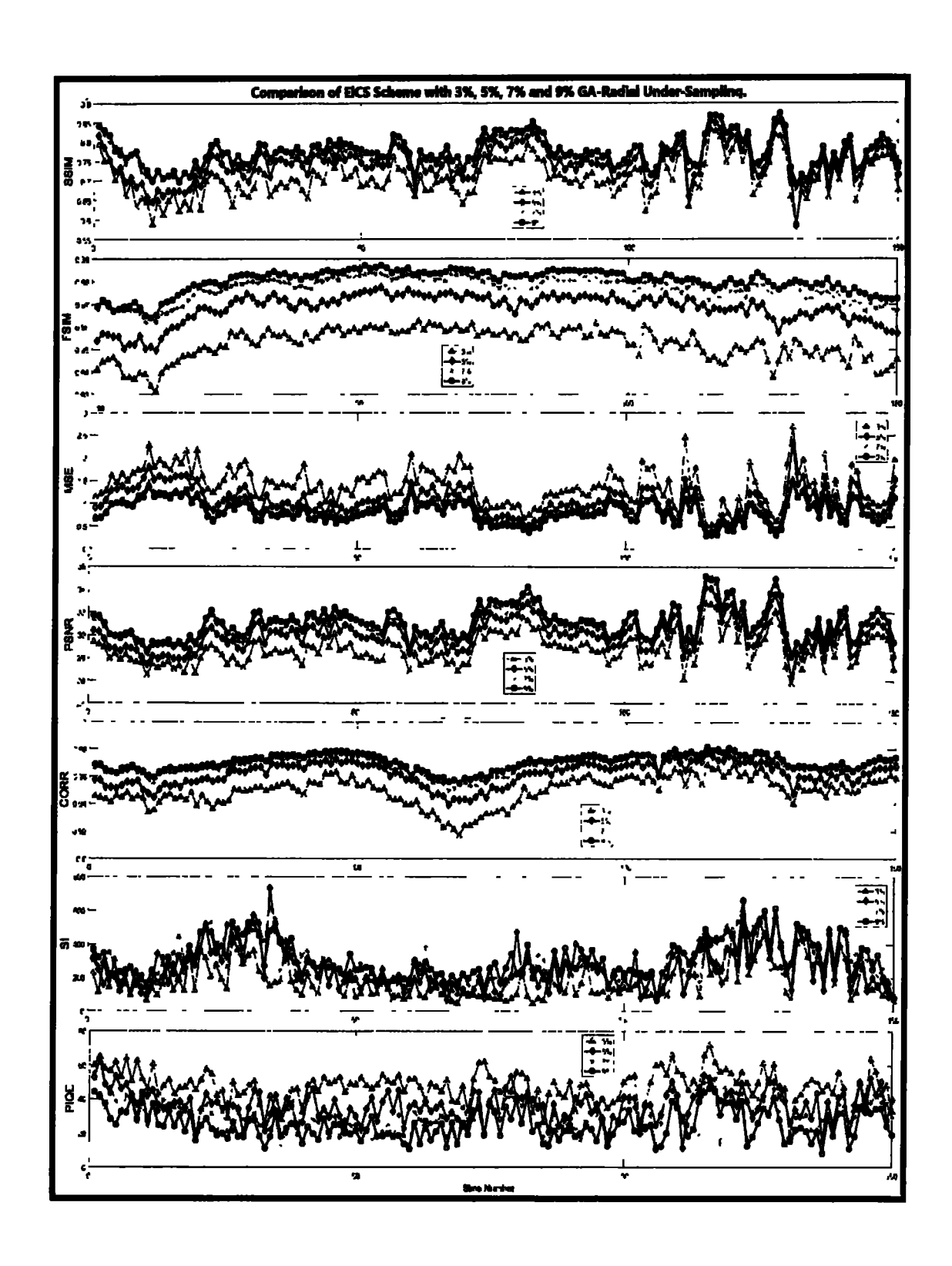


Fig. 4-10 Evaluation of EiCS using the seven assessment parameters with GA-Radial under-sampling for 3%, 5%, 7%, and 9% samples. The evaluation has been done on 150 centered slices of the knee dataset and compared slice-wise.

While comparing the performance of FiCS and EiCS, for higher inter-slice gaps, EiCS is better for lower under-sampling ratios but for 7% and higher ratios, FiCS is better on some assessment parameters. The reason is that for lower under-sampling ratios when the inter-slice gap is increased, EiCS, because of its three slices approach, collects sufficient samples for improved reconstruction. Therefore, for higher under-sampling ratios when we increase the gap, FiCS performs better because of having sufficient samples using its two-slice approach, while for lower under-sampling ratios EiCS is better.

## 4.6Summary

In this chapter, for the first time, the implementation of iCS has been discussed using Radial under-sampling schemes. The Radial sampling pattern used in the novel EiCS techniques is more realistic from the current hardware point of view compared to the 2D-VRDU sampling pattern adopted in FiCS. Secondly, the Radial sampling strategy is also lesser motion-sensitive compared to other sampling schemes. Thus, EiCS exploits different Radial under-sampling patterns using its three-step interpolation approach to get interpolated slices with the maximum number of samples using the lowest undersampling ratios while ensuring sharper reconstructed images. The EiCS technique not only preserves the original information in every slice but also gives consistency in the slice-wise image quality along with sharper IQ. Thus, EiCS neither show blurring like FiCS nor any information loss like iCS with improved results on seven different assessment parameters.

The EiCS technique can also be successfully applied to Dynamic MRI datasets to get even more benefits from the Radial under-sampling schemes because it can efficiently

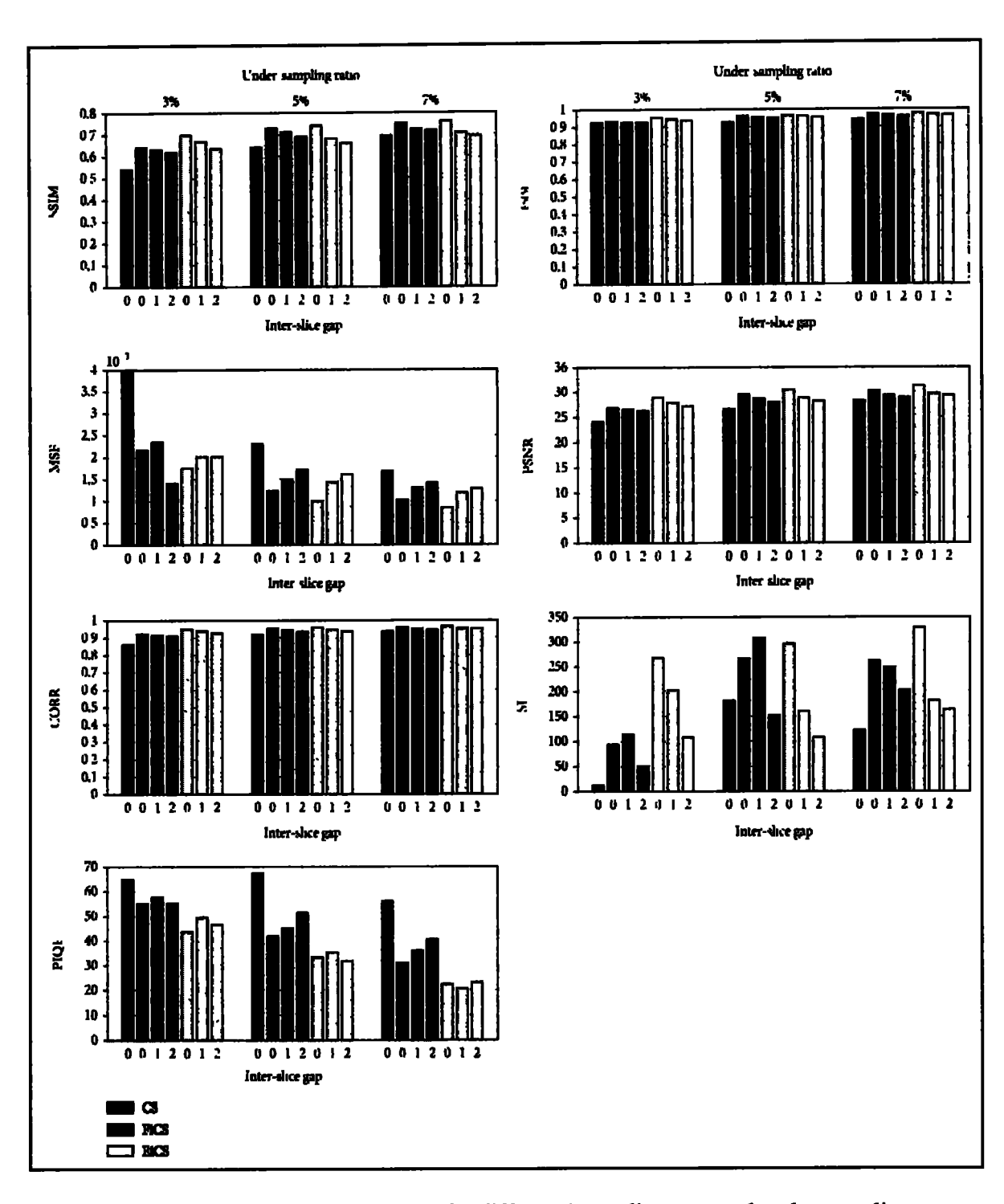


Fig. 4-11 Comparison of FiCS and EiCS for different inter-slice gaps and under-sampling ratios

handle motion artifacts. This technique can also be combined with the latest CS reconstruction algorithms for more prominent results with reduced reconstruction time.

The improved novel interpolation technique adopted in EiCS is computationally efficient with only a set difference and addition operations like FiCS. Thus the computational complexity of the interpolation algorithm of EiCS [120] is O(n) like FiCS [109], compared to O(n log n) of iCS [100]. EiCS also show better results with even increased inter-slice gap datasets.

## Chapter 5

# Gaussian-Radial Under-Sampling Based CSMRI Reconstruction using a Modified FiCS Approach

## 5.1 Introduction

In this chapter, a modified FiCS (Mod-FiCS) technique is discussed using the Gaussian-Radial under-sampling scheme. The Gaussian-Radial under-sampling approach adopted by Mod-FiCS has an edge that it neither shows any streaking artifacts like Radial nor blurred edges like Gaussian. The modified interpolation approach used in Mod-FiCS technique uses three consecutive slices like EiCS to estimate the missing samples of the central target slice. The simulation result shows that the Mod-FiCS technique has improvement both quantitatively and qualitatively compared to the previous techniques.

#### 5.2 Related Work

Compressed Sensing (CS) has efficiently accelerated the MRI acquisition process by employing different reconstruction strategies using a fraction of the Nyquist samples. This scan time has been further reduced using a new technique called interpolated compressed sensing (iCS) by exploiting the strong inter-slice correlation of multi-slice MRI. In Chapter 03 a novel FiCS technique is discussed based on the 2D-VRDU undersampling scheme. The FiCS technique [109] has improved results along with reduced

scan time and consistency in slice-wise image quality and information content, but due to the Gaussian under-sampling approach, it shows some blurred edges.

Chapter 04 discusses a novel EiCS technique based on different Radial under-sampling schemes. The EiCS technique [120] shows improved results compared to both iCS and FiCS with sharper details. Unlike the Gaussian masks of FiCS, which require an FFT operator, the Radial masks of EiCS need NUFFT along with DCF as discussed in Chapter 04.

The under-sampling using Radial masks only reduces the number of acquired spokes and does not lessen the number of samples on each spoke. Secondly, the Radial undersampling causes some streaking artifacts. Thus, the Radial mask when combined with 2D Gaussian is an optimum choice for under-sampling by having the benefits of both the Radial and 2D-Gaussian schemes.

The combination of 2D-VRDU and Radial under-sampling schemes is termed as Gaussian-Radial as shown in Fig. 5-1. This under-sampling approach has an edge that it causes no streaking artifacts like Radial, no blurred edges like Gaussian, and with a min number of samples. The Gaussian-Radial under-sampling pattern is explored for both Uniform-Angle (UA) and Golden-Angle (GA) Radial as shown in Fig. 5-1.

## 5.3The Mod-FiCS Technique

The Mod-FiCS technique is based on Gaussian-Radial under-sampling scheme. The Gaussian-Radial under-sampling strategy uses the same under-sampling ratio of FiCS [109] but by employing three consecutive slices like EiCS [120]. Thus, the missing

samples of each under-sampled slice are estimated from their neighboring two slices to collect enough samples to be reconstructed as a sharper and improved image[134].

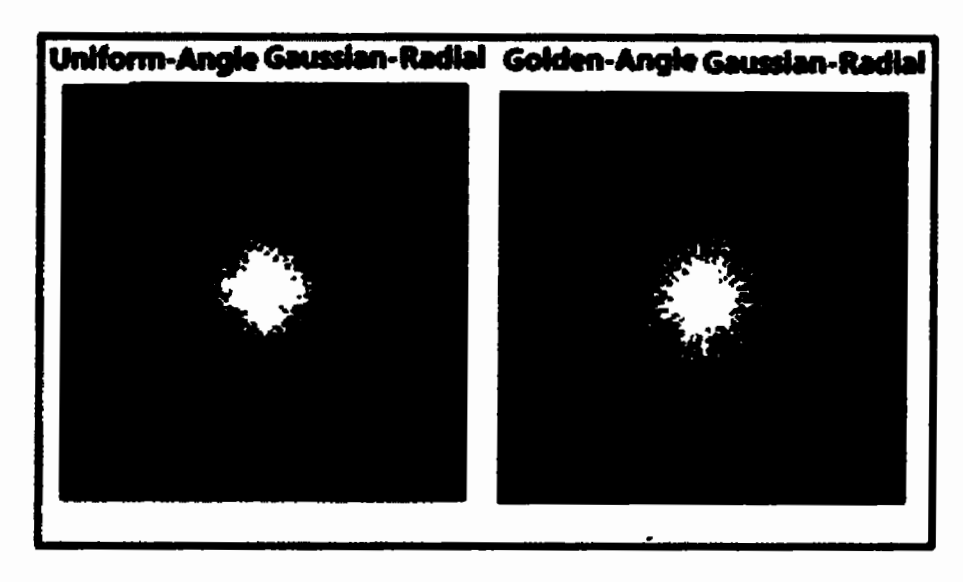


Fig. 5-1 UA and GA Gaussian-Radial sampling approach

## 5.3.1 Gaussian-Radial Under-Sampling

The Mod-FiCS technique takes any three consecutive Gaussian-Radial under-sampled slices to calculate the missing samples in the central target slice. While combining the Radial mask with Gaussian two approaches can be adopted. For the first approach, every three consecutive masks have all Gaussian sampling points on different and non-overlapping spokes, while in the second approach, any three consecutive masks have all the Gaussian sampling points on the same spokes. In the first approach, the desired masks for three consecutive slices are generated using different non-overlapping Radial spokes with Gaussian points. These Gaussian-Radial patterns are generated using (1) -(3).

$$M_{11} = R_1 * G (1)$$

$$\mathbf{M}_{12} = \mathbf{R}_2 * \mathbf{G} \tag{2}$$

$$\mathbf{M}_{13} = \mathbf{R}_3 * \mathbf{G} \tag{3}$$

Where, R<sub>1</sub>, R<sub>2</sub> and R<sub>3</sub> are the three different Radial masks with non-overlapping and same number of spokes and G is a Gaussian mask. Thus, M<sub>11</sub>, M<sub>12</sub> and M<sub>13</sub> are the three consecutive down-sampling Gaussian-Radial masks for Approach-I. In the second approach, the three consecutive under-sampling masks use the same Radial spokes but with different Gaussian sampling points as represented in (4) -(6).

$$\mathbf{M}_{21} = \mathbf{R} * \mathbf{G}_1 \tag{4}$$

$$\mathbf{M}_{22} = \mathbf{R} * \mathbf{G}_2 \tag{5}$$

$$\mathbf{M}_{23} = \mathbf{R} * \mathbf{G}_3 \tag{6}$$

Where,  $M_{21}$ ,  $M_{22}$  and  $M_{23}$  are the three consecutive Gaussian-Radial masks for Approach-II. These masks are generated using, three different Gaussian patterns  $G_1$ ,  $G_2$ ,  $G_3$  and R represents the Radial mask. Thus we have two different approaches for the under-sampling of Mod-FiCS as shown in Fig. 5-2.

For the under-sampling of three consecutive slices  $S_1$ ,  $S_{i+1}$  and  $S_{i+2}$ , first the Fourier operators of the desired Gaussian-Radial under-sampling patterns are generated. The down-sampling Fourier operators are termed as  $F_1$ ,  $F_2$ , and  $F_3$ . These Fourier operators are then applied on three consecutive slices, resulting in under-sampled slices in k-space as represented in (7) -(9).

$$U_i = F_1 * S_i \tag{7}$$

$$U_{i+1} = F_2 * S_{i+1} \tag{8}$$

$$U_{i+2} = F_3 * S_{i+2} \tag{9}$$

Where  $U_i$ ,  $U_{i+1}$  and  $U_{i+2}$  represents the three consecutive under-sampled slices in k-space. This under-sampling step of three consecutive slices is repeated after every three slices for the whole multi-slice MRI dataset.

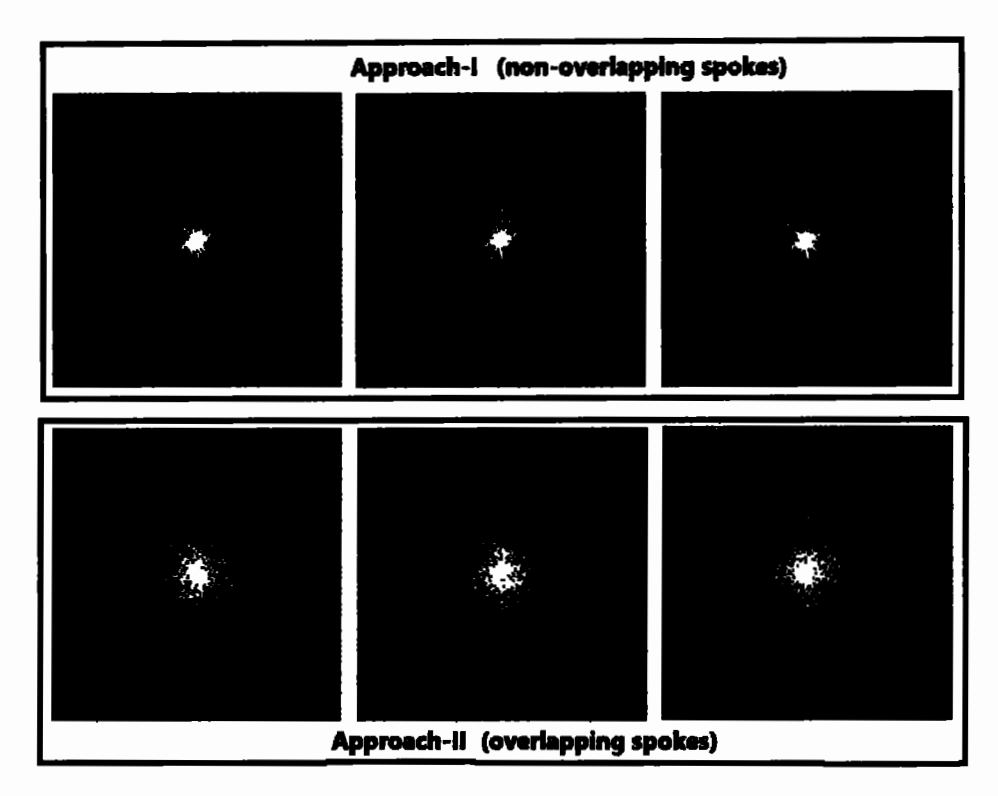


Fig. 5-2 Three Consecutive Gaussian-Radial under-sampling masks using both approaches

Thus the result will be an under-sampled dataset in which every three consecutive slices have the same sampling patterns but different sampling locations as shown in Fig. 5-2. The sampling points on different locations using one of the two approaches will be used for the interpolation step.

## 5.3.2 Modified Interpolation Scheme

For the interpolation step of Mod-FiCS, any three consecutive slices like EiCS and termed it as Left (L), Target (T), and Right (R) slices. For interpolation first, the set difference between the L and T slice called  $L_{Tnew}$  is generated. Where,  $L_{Tnew}$  has the new sampling information of the L slice with respect to the T slice. Next, the same step of L slice is repeated with the R slice, getting  $R_{Tnew}$  slice. Then  $R_{Tnew}$  and  $L_{Tnew}$  are compared to get  $R_{TLnew}$ , which are the new sampling information of R slice with respect

to both T and L slices. Lastly, the samples of the T slice are combined with the samples of  $L_{Tnew}$  and  $R_{TLnew}$  to get the interpolated T slice called  $T_{int}$ . The three-step interpolation approach of Mod-FiCS is represented in (10)-(13) and shown in Fig. 5-3.

$$\mathbf{L}_{\mathsf{Tnew}} = \mathbf{L} \ominus \mathbf{T} \tag{10}$$

$$R_{\mathsf{Tnew}} = R \ominus \mathsf{T} \tag{11}$$

$$R_{TLnew} = R_{Tnew} \ominus L_{Tnew} \tag{12}$$

$$T_{int} = L_{Tnew} \oplus T \oplus R_{TLnew}$$
 (13)

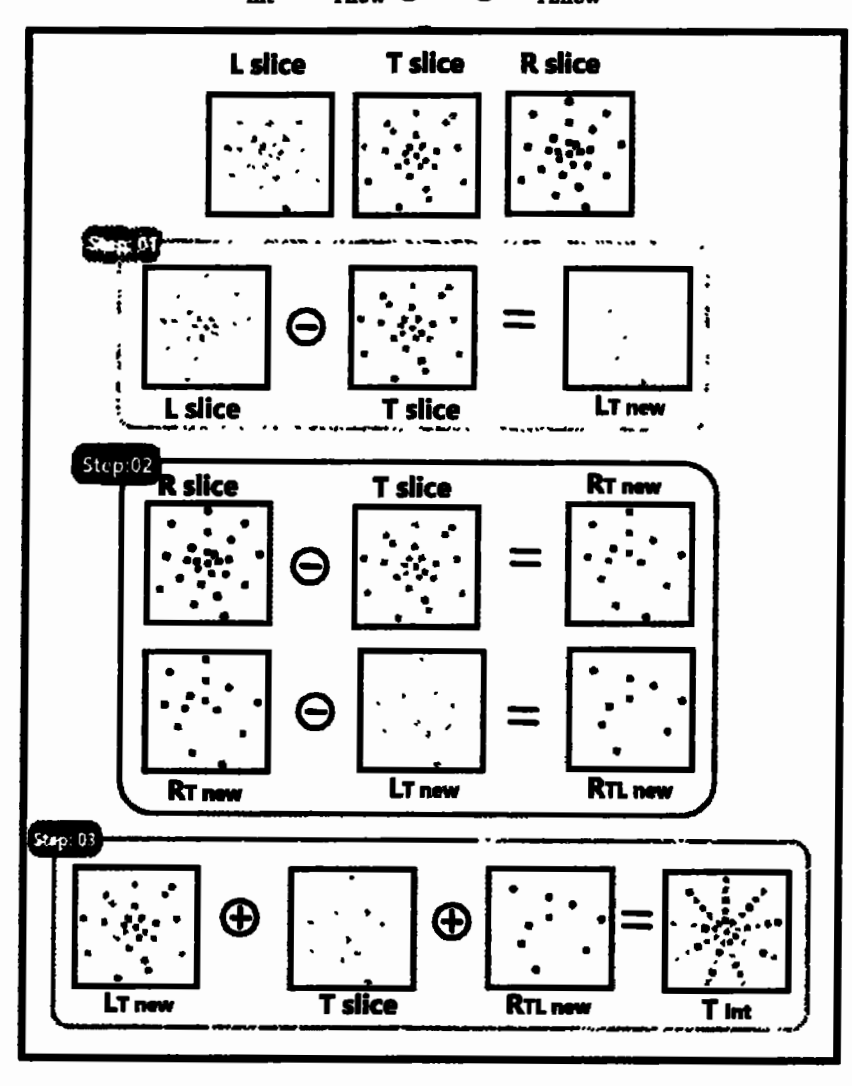


Fig. 5-3 The novel interpolation technique

This three-step interpolation technique is applied on each slice of the under-sampled multi-slice MRI sequence. Where, every slice is considered as T and its two neighboring as L and R, to get an interpolated slice as T<sub>int</sub>. The interpolated slices collect almost the same number of samples and have the same sampling patterns for both under-sampling approaches. The only difference is that in the first approach each under-sampled slice has one-third of the spokes with three times samples on each spoke compared to the second approach in which there are three times of the spokes with only one-third of the samples on each spoke.

Once the interpolation step is completed the interpolated slices are identical irrespective of which interpolation approach is adopted, even with the same number of samples on it. After interpolation, the interpolated multi-slice datasets have almost three times the samples initially under-sampled or acquired. Fig. 5-4 shows the resultant interpolated slices using both approaches, showing almost identical results.

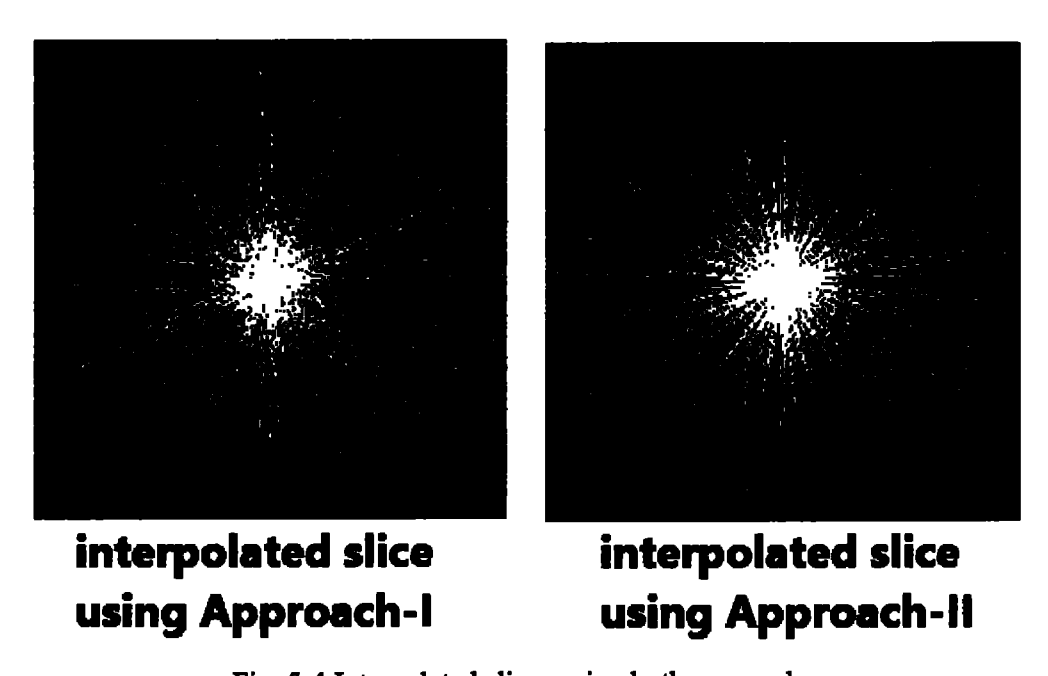


Fig. 5-4 Interpolated slices using both approaches

In Approach-I all the non-overlapping spokes of the three neighboring slices combines while in Approach-II the gapes in the same spokes are filled during interpolation. That is why the interpolation result of both approaches looks identical as shown in Fig. 5-4.

## **5.3.3 CS Reconstruction**

After interpolation, the NCG CS reconstruction is applied to all the interpolated slices. The CS reconstruction step is the same as used for FiCS [109] and EiCS [120] in the previous chapters.

## 5.4Simulation and results

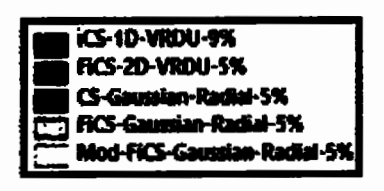
The evaluation of the Mod-FiCS technique has been performed on two different fully sampled knee data sets. To evaluate the quality of the reconstructed images six evaluation metrics are used which are SSIM, FSIM, MSE, PSNR, CORR, and SI. Their mathematical expressions are already discussed in Chapter 2.

The Mod-FiCS technique is evaluated using all the six assessment parameters and compared with recent interpolation techniques [100, 109] and CS [11]. Table 5-1 shows a comparison of the novel Mod-FiCS technique with FiCS [109] and CS [11] using both UA and GA Gaussian-Radial under-sampling schemes using both the under-sampling approaches. The results of FiCS using 2D-VRDU [109] and iCS using 1D-VRDU [100] have also been included for comparison. This assessment has been performed using 9 consecutive slices and averaged.

Table 5-1 Comparison of the novel Mod-FiCS technique with FiCS and CS using different under-sampling schemes

Averaged assessment of 9 consecutive slices (slice 91-99 of knee dataset)								
Assessment Parameters Sampling Scheme		SSIM	FSIM	MSE	PSNR	CORR	SI	
								42 1727°
1D-VRDU	ICS-9%	0.76	0.97	0.001	27.86	0.961	364.8	
AD LIDDU	CS-5%	0.73	0.94	0.002	25.63	0.941	123.5	
2D-VRDU	FICS-5%	0.78	0.96	0.001	29.22	0.96	180.6	
	CS-5%	0.71	0.93	0.001	27.46	0.95	55.5	
UA Gaussian-Radial with Non-Overlapping Spokes	FICS-5%	0.79	0.96	0.0009	30.25	0.973	166.9	
Mon-Over tapping Spoacs	Mod-FICS-5%	0.82	0.97	0.0007	31.2	0 97	193.9	
	CS-5%	0.78	0.95	0.001	29.31	0.967	135.5	
UA Gaussian-Radial with Overlapping Spokes	FICS-5%	0.82	0.97	0.0007	31.38	0.979	200.4	
Over unblung phones	Mod-FiCS-5%	0.82	0.97	0.0006	31.9	0.97	173.8	
	CS-5%	0.76	0.94	0.001	28.93	0.957	83.3	
GA Gaussian-Radial with Non-Overlapping Spokes	FICS-5%	0.82	0.97	0.0007	31.27	0.978	185.3	
140m-Over ishbing aboves	Mod-FICS-5%	0.84	0.97	0.0006	32.2	0.98	220.7	
	CS-5%	0.79	0.95	0 001	30.03	0.968	132.9	
GA Gaussian-Radial with Overlapping Spokes	FICS-5%	0.82	0.97	0.0007	31.53	0.979	195.8	
Over inhhim Shores	Mod-FiCS-5%	0.84	0.98	0.0006	32	0.98	229.3	

It is clear from the table that the Mod-FiCS technique outperforms all using GA Gaussian-Radial under-sampling schemes using both the overlapping and non-overlapping spokes. The assessment of Table 5-1 has been summarized in Fig. 5-5 showing iCS [100] and FiCS [109] using 1D and 2D-VRDU as originally proposed in their works while CS, FiCS, and Mod-FiCS using GA Gaussian-Radial under-sampling schemes.



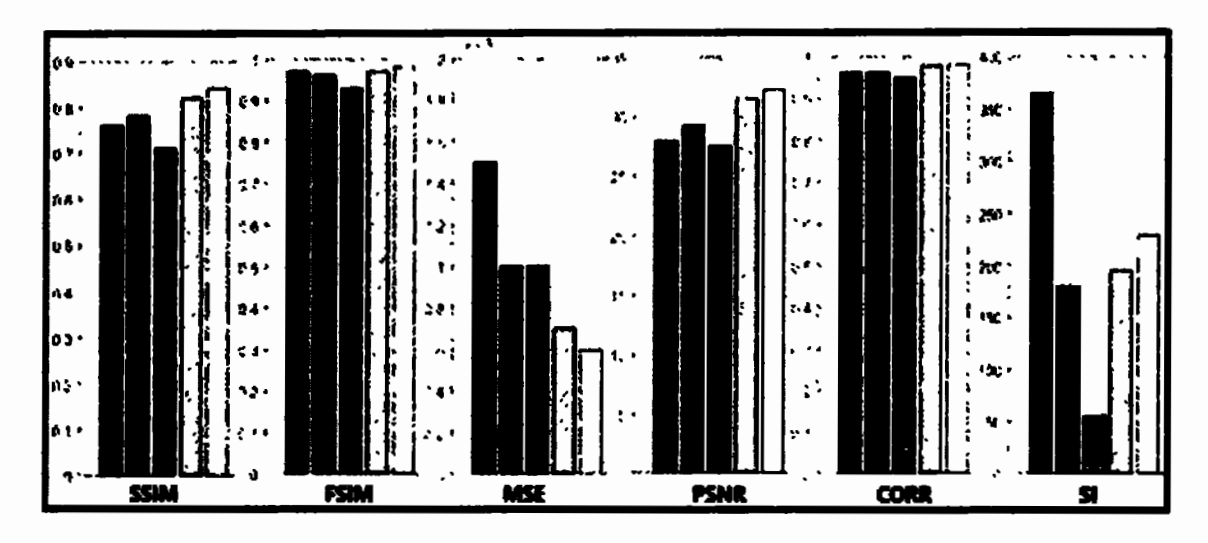


Fig. 5-5 Average assessment of iCS, FiCS and Mod-FiCS

It is clear from the figure that the Mod-FiCS technique outperforms all except for the Sharpness Index of iCS and the reason is that iCS has a biased under-sampling scheme and uses 9% average samples.

Fig. 5-6 shows a comparison of the reconstructed images of both FiCS and Mod-FiCS using the same under-sampling ratios. The zoomed edges are also compared along with the original image. It is clear from the figure that the Mod-FiCS technique has sharper and clearer results.

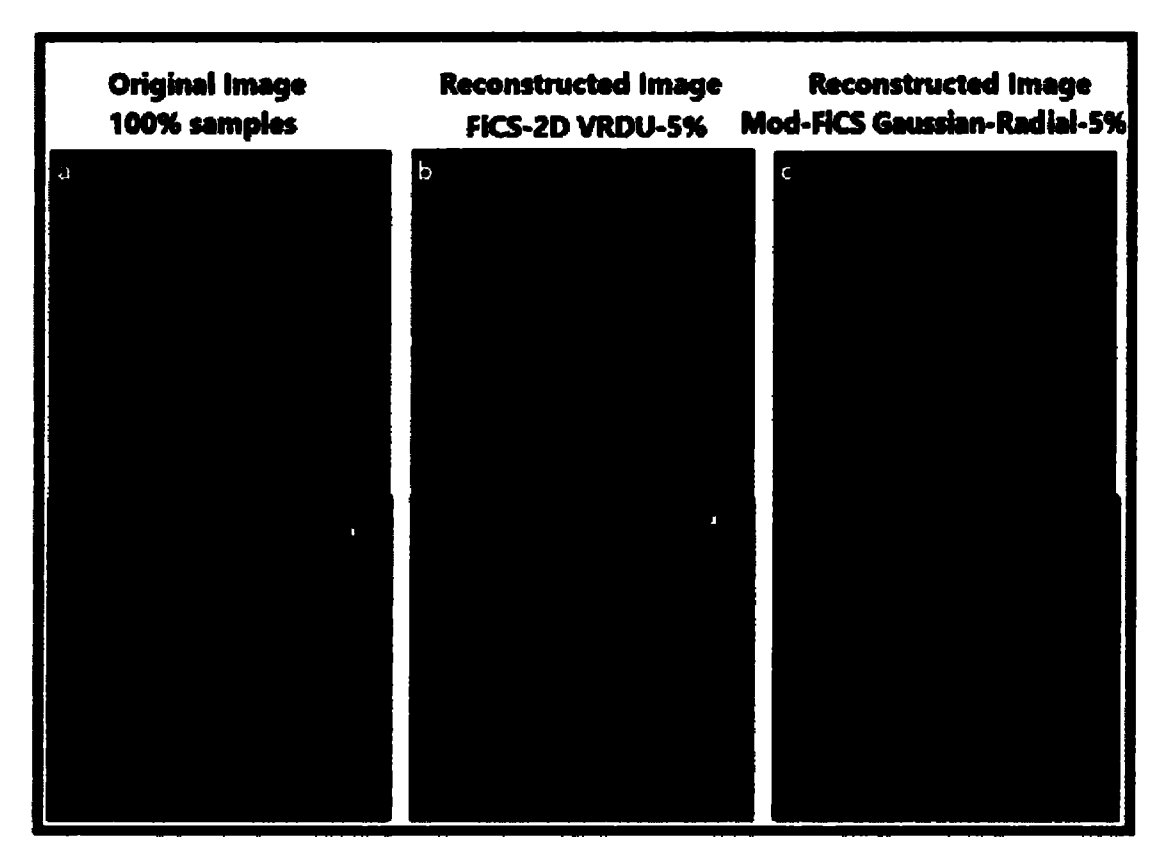


Fig. 5-6 Comparison of the reconstruction results of FiCS and Mod-FiCS with the original image. It is clear from the figure that Mod-FiCS has sharper and clear results compared to the FiCS technique.

## 5.5 Summary

The Mod-FiCS technique outperforms FiCS, iCS, and CS on all six assessment parameters. The under-sampling scheme of this technique combines the 2D-VRDU and Radial schemes of both FiCS and EiCS as a Gaussian-Radial under-sampling approach. Therefore the Mod-FiCS technique neither shows any streaking artifacts like Radial nor any blurred edges like Gaussian. This technique has the same computational cost as FiCS and EiCS but with more improved results.

# Chapter 6

## **Conclusion and Future Work**

This chapter concludes the research work of the dissertation along with some discussions about the future directions of the work presented in this thesis.

## **6.1 Thesis Conclusion**

Compressed Sensing (CS) has enabled to accelerate the acquisition time of multi-slice MRI using some non-linear reconstruction techniques from even one-tenth of the random Nyquist samples. This scan time has been further reduced through iCS by exploiting the strong inter-slice correlation of multi-slice MRI, from an even lower under-sampling ratio compared to CS. In this thesis, a number of efficient iCSMRI reconstruction techniques are proposed based on highly under-sampled data and the most efficient and novel interpolation approaches.

In this thesis, first a novel FiCS technique [109] is discussed which is implemented using both 1D and 2D-VRDU schemes. The novel interpolation approach of FiCS uses 5% average samples. Although, the 1D-VRDU mask is more realistic from the current hardware point of view but 2D-VRDU is best suitable to represent the original k-space data of multi-slice MRI. The FiCS technique reduces the average under-sampling ratio to almost half, compared to the previous techniques, with even improved image quality and information content. The FiCS also beats previous interpolation techniques in terms of computational complexity and processing time.

The EiCS technique [120] discussed in this thesis uses different Radial under-sampling patterns along with a new interpolation approach. The EiCS technique has an edge that its Radial under-sampling approach is more practical from the current hardware point of view along with lesser motion sensitivity compared to the 2D-VRDU under-sampling approach adopted in FiCS. EiCS exploits the Radial under-sampling pattern in its three-step interpolation process to get interpolated slices with the maximum number of samples and by using a lower under-sampling ratio compared to FiCS, with even sharper reconstructed images, no blurred edges, and improved qualitative and quantitative assessment.

The Mod-FiCS technique introduced in this thesis uses Gaussian-Radial under-sampling approach and outperforms FiCS, iCS, and CS on all the assessment parameters. Similarly, the reconstruction images of Mod-FiCS are also sharper and clear compared to the rest of all. The Mod-FiCS has the same computational cost and under-sampling ratio as FiCS and EiCS with even improved results.

The new sampling and fast interpolation strategies of FiCS, EiCS, and Mod-FiCS have not only simplified the interpolation approach but also preserves the original information resulting in improved results both qualitatively and quantitatively. These techniques not only preserve the original information in every slice but also give consistency in the slicewise image quality. The improved interpolation technique adopted in FiCS, EiCS, and Mod-FiCS is computationally efficient with only a set difference and addition operations. Thus, the computational complexity of these techniques is O(n) which is much lower than its preceding iCS techniques and therefore has reduced the processing time up to five times.

#### **6.2 Directions for Future Work**

Based on the novel interpolation ideas and iCS techniques presented in this thesis there are several future directions, some of which are discussed below:

- The proposed techniques have been implemented using static multi-slice datasets.
  These techniques can also be extended to dynamic MRI datasets to accelerate the acquisition process with improved image quality and motion robustness, with respiration and without respiratory motion.
- The computational efficiency achieved using the proposed techniques can also be extended to the pMRI for high spatial and temporal resolution.
- The Gaussian-Radial under-sampling scheme has been generated using the FFT approach which can be improved by implementing it using the NUFFT method.
- The proposed iCS techniques can also be implemented to recover the CS video frames, as the consecutive video frames are also highly correlated like multi-slice MRI datasets.
- The NCG, CS reconstruction technique can also be upgraded for even more improved results and reduced computational load.
- The Golden-Angle (GA) Radial under-sampling approach increases the computational cost through the NUFFT operation, in the forward as well as in the backward direction during each iteration. This issue can be resolved using some parallel computational techniques.
- The primary focus of this thesis is to reduce the scan time of multi-slice CSMRI
   by acquiring the highest under-sampled slices and reconstructing the original datasets.

 The computational time can be reduced through parallel programming concepts along with GPU which will make it feasible for clinical applications.

## REFERENCES

- [1] H. Nyquist, "Certain topics in telegraph transmission theory," Transactions of the American Institute of Electrical Engineers, vol. 47, pp. 617-644, 1928.
- [2] M. Lustig, J. M. Santos, J.-H. Lee, D. L. Donoho, and J. M. Pauly, "Application of compressed sensing for rapid MR imaging," SPARS, (Rennes, France), 2005.
- [3] M. Zaitsev, J. Maclaren, and M. Herbst, "Motion artifacts in MRI: a complex problem with many partial solutions," *Journal of Magnetic Resonance Imaging*, vol. 42, pp. 887-901, 2015.
- [4] D. L. Donoho, "Compressed sensing," *IEEE Transactions on information theory*, vol. 52, pp. 1289-1306, 2006.
- [5] Y. Tsaig and D. L. Donoho, "Extensions of compressed sensing," Signal processing, vol. 86, pp. 549-571, 2006.
- [6] E. J. Candes, J. K. Romberg, and T. Tao, "Stable signal recovery from incomplete and inaccurate measurements," Communications on Pure and Applied

  Mathematics: A Journal Issued by the Courant Institute of Mathematical

  Sciences, vol. 59, pp. 1207-1223, 2006.
- [7] E. J. Candes, M. B. Wakin, and S. P. Boyd, "Enhancing sparsity by reweighted & 1 minimization," *Journal of Fourier analysis and applications*, vol. 14, pp. 877-905, 2008.
- [8] R. G. Baraniuk, E. Candes, R. Nowak, and M. Vetterli, "Compressive sampling [from the guest editors]," *IEEE Signal Processing Magazine*, vol. 25, pp. 12-13, 2008.

- [9] Y. C. Eldar and G. Kutyniok, Compressed sensing: theory and applications:Cambridge University Press, 2012.
- [10] M. Lustig, D. L. Donoho, J. M. Santos, and J. M. Pauly, "Compressed sensing MRI," *IEEE signal processing magazine*, vol. 25, p. 72, 2008.
- [11] M. Lustig, D. Donoho, and J. M. Pauly, "Sparse MRI: The application of compressed sensing for rapid MR imaging," Magnetic Resonance in Medicine: An Official Journal of the International Society for Magnetic Resonance in Medicine, vol. 58, pp. 1182-1195, 2007.
- [12] J. Fessler. *Image reconstruction toolbox*. Available: http://web.eecs.umich.edu/~fessler/code/index.html
- [13] M. Lustig, "SparseMRI V0.2."
- [14] J. A. Shah, "Applications of Compressed Sensing to Biomedical Imaging," Doctoral dissertation, Department of Electronic Engineering Faculty of Engineering and Technology International Islamic University, Islamabad, Pakistan, 2015.
- [15] Y. Pang and X. Zhang, "Interpolated compressed sensing MR image reconstruction using neighboring slice k-space data," in *Proceedings of the 20th Annual Meeting of ISMRM, Melbourne, Australia*, 2012, p. 2275.
- [16] Y. Pang and X. Zhang, "Interpolated compressed sensing for 2D multiple slice fast MR imaging," *PloS one*, vol. 8, p. e56098, 2013.
- [17] K. Revett, "An introduction to magnetic resonance imaging: from image acquisition to clinical diagnosis," in *Innovations in intelligent image analysis*, ed: Springer, 2011, pp. 127-161.

- [18] V. S. Khoo, D. P. Dearnaley, D. J. Finnigan, A. Padhani, S. F. Tanner, and M. O. Leach, "Magnetic resonance imaging (MRI): considerations and applications in radiotherapy treatment planning," *Radiotherapy and Oncology*, vol. 42, pp. 1-15, 1997.
- [19] S. G. Waxman, Correlative neuroanatomy: Appleton & Lange, 1999.
- [20] E. M. Haacke, R. W. Brown, M. R. Thompson, and R. Venkatesan, *Magnetic resonance imaging: physical principles and sequence design* vol. 82: Wiley-liss New York:, 1999.
- [21] T. W. Cabral, M. Khosravy, F. M. Dias, H. L. M. Monteiro, M. A. A. Lima, L. R.
   M. Silva, et al., "Compressive sensing in medical signal processing and imaging systems," in Sensors for Health Monitoring, ed: Elsevier, 2019, pp. 69-92.
- [22] M. Lustig, D. Donoho, J. Santos, and J. Pauly, "Compressed sensing MRI: a look at how CS can improve on current imaging techniques. IEEE Signal Process Mag. 2008; 25: 72–82," ed, 2007.
- [23] D. W. McRobbie, E. A. Moore, M. J. Graves, and M. R. Prince, MRI from Picture to Proton: Cambridge university press, 2017.
- [24] P. Paolantonio, R. Ferrari, F. Vecchietti, S. Cucchiara, and A. Laghi, "Current status of MR imaging in the evaluation of IBD in a pediatric population of patients," *European journal of radiology*, vol. 69, pp. 418-424, 2009.
- [25] J. Hamilton, D. Franson, and N. Seiberlich, "Recent advances in parallel imaging for MRI," Progress in nuclear magnetic resonance spectroscopy, vol. 101, pp. 71-95, 2017.

- [26] A. Deshmane, V. Gulani, M. A. Griswold, and N. Seiberlich, "Parallel MR imaging," Journal of Magnetic Resonance Imaging, vol. 36, pp. 55-72, 2012.
- [27] R. Ahmad, H. H. Hu, R. Krishnamurthy, and R. Krishnamurthy, "Reducing sedation for pediatric body MRI using accelerated and abbreviated imaging protocols," *Pediatric radiology*, vol. 48, pp. 37-49, 2018.
- [28] J. W. Schnaiter, F. Roemer, A. McKenna-Kuettner, H.-J. Patzak, M. S. May, R. Janka, et al., "Diagnostic accuracy of an MRI protocol of the knee accelerated through parallel imaging in correlation to arthroscopy," in RöFo-Fortschritte auf dem Gebiet der Röntgenstrahlen und der bildgebenden Verfahren, 2018, pp. 265-272.
- [29] B. Liu, Y. M. Zou, and L. Ying, "SparseSENSE: application of compressed sensing in parallel MRI," in 2008 International Conference on Information Technology and Applications in Biomedicine, 2008, pp. 127-130.
- [30] B. Deka and S. Datta, "Calibrationless joint compressed sensing reconstruction for rapid parallel MRI," *Biomedical Signal Processing and Control*, vol. 58, p. 101871, 2020.
- [31] M. Bilal, J. A. Shah, I. M. Qureshi, and K. Kadir, "Respiratory motion correction for compressively sampled free breathing cardiac MRI using smooth-norm approximation," *International journal of biomedical imaging*, vol. 2018, 2018.
- [32] M. Bilal, H. Anis, N. Khan, I. Qureshi, J. Shah, and K. A. Kadir, "Reduction of Motion Artifacts in the Recovery of Undersampled DCE MR Images Using Data Binning and L," *BioMed research international*, vol. 2019, 2019.

- [33] K. P. Pruessmann, M. Weiger, M. B. Scheidegger, and P. Boesiger, "SENSE: sensitivity encoding for fast MRI," *Magnetic Resonance in Medicine: An Official Journal of the International Society for Magnetic Resonance in Medicine*, vol. 42, pp. 952-962, 1999.
- [34] M. A. Griswold, P. M. Jakob, R. M. Heidemann, M. Nittka, V. Jellus, J. Wang, et al., "Generalized autocalibrating partially parallel acquisitions (GRAPPA),"

  Magnetic Resonance in Medicine: An Official Journal of the International Society for Magnetic Resonance in Medicine, vol. 47, pp. 1202-1210, 2002.
- [35] M. Lustig and J. M. Pauly, "SPIRiT: iterative self-consistent parallel imaging reconstruction from arbitrary k-space," *Magnetic resonance in medicine*, vol. 64, pp. 457-471, 2010.
- [36] E. J. Candes and J. K. Romberg, "Signal recovery from random projections," in Computational Imaging III, 2005, pp. 76-86.
- [37] S. Mallat, A wavelet tour of signal processing: Elsevier, 1999.
- [38] E. Candes, J. Romberg, and T. Tao, "Robust uncertainty principles: Exact signal reconstruction from highly incomplete frequency information," arXiv preprint math/0409186, 2004.
- [39] E. J. Candès and M. B. Wakin, "An introduction to compressive sampling [a sensing/sampling paradigm that goes against the common knowledge in data acquisition]," *IEEE signal processing magazine*, vol. 25, pp. 21-30, 2008.
- [40] J. Romberg, "Imaging via compressive sampling," *IEEE Signal Processing Magazine*, vol. 25, pp. 14-20, 2008.

- [41] M. Akçakaya, S. Nam, P. Hu, M. H. Moghari, L. H. Ngo, V. Tarokh, et al., "Compressed sensing with wavelet domain dependencies for coronary MRI: a retrospective study," *IEEE Transactions on Medical Imaging*, vol. 30, pp. 1090-1099, 2010.
- [42] J. P. Haldar, D. Hernando, and Z.-P. Liang, "Compressed-sensing MRI with random encoding," *IEEE transactions on Medical Imaging*. vol. 30, pp. 893-903, 2010.
- [43] M. Elad and M. Aharon, "Image denoising via sparse and redundant representations over learned dictionaries," *IEEE Transactions on Image processing*, vol. 15, pp. 3736-3745, 2006.
- [44] M. Manimala, C. D. Naidu, and M. G. Prasad, "Sparse MR Image Reconstruction Considering Rician Noise Models: A CNN Approach," Wireless personal communications, vol. 116, pp. 491-511, 2021.
- [45] C. M. Tsai and D. G. Nishimura, "Reduced aliasing artifacts using variable-density k-space sampling trajectories," Magnetic Resonance in Medicine: An Official Journal of the International Society for Magnetic Resonance in Medicine, vol. 43, pp. 452-458, 2000.
- [46] M. Lustig, D. Donoho, and J. M. Pauly, "Sparse MRI: The application of compressed sensing for rapid MR imaging," *Magnetic resonance in medicine*, vol. 58, pp. 1182-1195, 2007.
- [47] J. Shah, I. Qureshi, J. Proano, and Y. Deng, "Compressively sampled MR image reconstruction using hyperbolic tangent-based soft-thresholding," *Applied Magnetic Resonance*, vol. 46, pp. 837-851, 2015.

- [48] J. Shah, I. Qureshi, Y. Deng, and K. Kadir, "Reconstruction of sparse signals and compressively sampled images based on smooth 1 1-norm approximation,"

  Journal of Signal Processing Systems, vol. 88, pp. 333-344, 2017.
- [49] M. Sandilya and S. Nirmala, "Compressed sensing trends in magnetic resonance imaging," Engineering science and technology, an international journal, vol. 20, pp. 1342-1352, 2017.
- [50] R. Otazo, D. Kim, L. Axel, and D. K. Sodickson, "Combination of compressed sensing and parallel imaging for highly accelerated first-pass cardiac perfusion MRI," *Magnetic resonance in medicine*, vol. 64, pp. 767-776, 2010.
- [51] S. Datta and B. Deka, "Interpolated Compressed Sensing for Calibrationless

  Parallel MRI Reconstruction," in 2019 National Conference on Communications

  (NCC), 2019, pp. 1-6.
- [52] S. Vasanawala, M. Murphy, M. T. Alley, P. Lai, K. Keutzer, J. M. Pauly, et al., "Practical parallel imaging compressed sensing MRI: Summary of two years of experience in accelerating body MRI of pediatric patients," in 2011 ieee international symposium on biomedical imaging: From nano to macro, 2011, pp. 1039-1043.
- [53] A. M. MURPHYM, "Fast□ SPIRiT compressed sensing parallel imaging MRI:

  Scalableparallelimplementation and clinically feasible runtime," IEEE

  Transactions on Med. Imaging, vol. 31, p. 1250, 2012.
- [54] M. Dieckmeyer, A. G. Roy, J. Senapati, C. Wachinger, L. Grundl, J. Döpfert, et al., "Effect of MRI acquisition acceleration via compressed sensing and parallel

- imaging on brain volumetry," Magnetic Resonance Materials in Physics, Biology and Medicine, pp. 1-11, 2021.
- [55] X. Qu, X. Cao, D. Guo, C. Hu, and Z. Chen, "Combined sparsifying transforms for compressed sensing MRI," *Electronics letters*, vol. 46, pp. 121-123, 2010.
- [56] Z. Chen, C. Huang, and S. Lin, "A new sparse representation framework for compressed sensing MRI," Knowledge-Based Systems, vol. 188, p. 104969, 2020.
- [57] M. Ragab, O. A. Omer, and H. S. Hussien, "Compressive sensing MRI using dual tree complex wavelet transform with wavelet tree sparsity," in 2017 34th National Radio Science Conference (NRSC), 2017, pp. 481-486.
- [58] J. Ma, "Improved iterative curvelet thresholding for compressed sensing and measurement," *IEEE Transactions on Instrumentation and Measurement*, vol. 60, pp. 126-136, 2010.
- [59] A. P. Yazdanpanah and E. E. Regentova, "Compressed sensing mri using curvelet sparsity and nonlocal total variation: Cs-nltv," *Electronic Imaging*, vol. 2017, pp. 5-9, 2017.
- [60] J. Ma and G. Plonka, "The curvelet transform," IEEE signal processing magazine, vol. 27, pp. 118-133, 2010.
- [61] G. Wang, "A perspective on deep imaging," *Ieee Access*, vol. 4, pp. 8914-8924,2016.
- [62] S. Yu, H. Dong, G. Yang, G. Slabaugh, P. L. Dragotti, X. Ye, et al., "Deep dealiasing for fast compressive sensing mri," arXiv preprint arXiv:1705.07137, 2017.

- [63] G. Yang, S. Yu, H. Dong, G. Slabaugh, P. L. Dragotti, X. Ye, et al., "DAGAN: Deep de-aliasing generative adversarial networks for fast compressed sensing MRI reconstruction," *IEEE transactions on medical imaging*, vol. 37, pp. 1310-1321, 2017.
- [64] J. Schlemper, G. Yang, P. Ferreira, A. Scott, L.-A. McGill, Z. Khalique, et al., "Stochastic deep compressive sensing for the reconstruction of diffusion tensor cardiac MRI," in *International conference on medical image computing and* computer-assisted intervention, 2018, pp. 295-303.
- [65] S. Ikram, S. Zubair, J. A. Shah, I. M. Qureshi, A. Wahid, and A. U. Khan, "Enhancing MR Image Reconstruction Using Block Dictionary Learning," *IEEE Access*, vol. 7, pp. 158434-158444, 2019.
- [66] S. Ikram, J. A. Shah, S. Zubair, I. M. Qureshi, and M. Bilal, "Improved reconstruction of MR scanned images by using a dictionary learning scheme," Sensors, vol. 19, p. 1918, 2019.
- [67] S. Ravishankar and Y. Bresler, "MR image reconstruction from highly undersampled k-space data by dictionary learning," *IEEE transactions on medical imaging*, vol. 30, pp. 1028-1041, 2010.
- [68] J. Yang, Y. Zhang, and W. Yin, "A fast alternating direction method for TVL1-L2 signal reconstruction from partial Fourier data," *IEEE Journal of Selected Topics in Signal Processing*, vol. 4, pp. 288-297, 2010.
- [69] Z. Lai, X. Qu, Y. Liu, D. Guo, J. Ye, Z. Zhan, et al., "Image reconstruction of compressed sensing MRI using graph-based redundant wavelet transform," Medical image analysis, vol. 27, pp. 93-104, 2016.

- [70] W. Zeng, J. Peng, S. Wang, and Q. Liu, "A comparative study of CNN-based super-resolution methods in MRI reconstruction and its beyond," Signal Processing: Image Communication, vol. 81, p. 115701, 2020.
- [71] J. Zhu, G. Yang, and P. Lio, "How can we make gan perform better in single medical image super-resolution? a lesion focused multi-scale approach," in 2019 IEEE 16th International Symposium on Biomedical Imaging (ISBI 2019), 2019, pp. 1669-1673.
- [72] J. Zhu, G. Yang, and P. Lio, "Lesion focused super-resolution," in Medical Imaging 2019: Image Processing, 2019, p. 109491L.
- [73] D. Zhao, F. Zhao, and Y. Gan, "Reference-Driven Compressed Sensing MR Image Reconstruction Using Deep Convolutional Neural Networks without Pre-Training," Sensors, vol. 20, p. 308, 2020.
- [74] F. Hashimoto, K. Ote, T. Oida, A. Teramoto, and Y. Ouchi, "Compressed-sensing magnetic resonance image reconstruction using an iterative convolutional neural network approach," *Applied Sciences*, vol. 10, p. 1902, 2020.
- [75] A. Wahid, J. A. Shah, A. U. Khan, M. Ahmed, and H. Razali, "Multi-Layer Basis Pursuit for Compressed Sensing MR Image Reconstruction," *IEEE Access*, vol. 8, pp. 186222-186232, 2020.
- [76] Y. Li, J. Li, F. Ma, S. Du, and Y. Liu, "High quality and fast compressed sensing MRI reconstruction via edge-enhanced dual discriminator generative adversarial network," *Magnetic resonance imaging*, vol. 77, pp. 124-136, 2021.

- [77] Y.-H. Dai and Y. Yuan, "A nonlinear conjugate gradient method with a strong global convergence property," *SIAM Journal on optimization*, vol. 10, pp. 177-182, 1999.
- [78] I. Daubechies, M. Defrise, and C. De Mol, "An iterative thresholding algorithm for linear inverse problems with a sparsity constraint," Communications on Pure and Applied Mathematics: A Journal Issued by the Courant Institute of Mathematical Sciences, vol. 57, pp. 1413-1457, 2004.
- [79] A. Beck and M. Teboulle, "A fast iterative shrinkage-thresholding algorithm for linear inverse problems," SIAM journal on imaging sciences, vol. 2, pp. 183-202, 2009.
- [80] J.-p. Huang, L.-k. Zhu, L.-h. Wang, and W.-l. Song, "Compressed sensing MRI using sparsity averaging and FISTA," *Applied Magnetic Resonance*, vol. 48, pp. 749-760, 2017.
- [81] J. Yang and Y. Zhang, "Alternating direction algorithms for \ell\_1-problems in compressive sensing," SIAM journal on scientific computing, vol. 33, pp. 250-278, 2011.
- [82] W. Yin, S. Osher, D. Goldfarb, and J. Darbon, "Bregman iterative algorithms for \\ell\_1-minimization with applications to compressed sensing," SIAM Journal on Imaging sciences, vol. 1, pp. 143-168, 2008.
- [83] J. Duan, Y. Liu, and L. Zhang, "Bregman iteration based efficient algorithm for mr image reconstruction from undersampled k-space data," *IEEE Signal Processing Letters*, vol. 20, pp. 831-834, 2013.

- [84] D. R. S. Saputro and P. Widyaningsih, "Limited memory Broyden-Fletcher-Goldfarb-Shanno (L-BFGS) method for the parameter estimation on geographically weighted ordinal logistic regression model (GWOLR)," in AIP Conference Proceedings, 2017, p. 040009.
- [85] D. C. Youla and H. Webb, "Image Restoration by the Method of Convex Projections: Part 1 Theory," *IEEE transactions on medical imaging*, vol. 1, pp. 81-94, 1982.
- [86] J. Shah, I. Qureshi, H. Omer, and A. Khaliq, "A modified POCS-based reconstruction method for compressively sampled MR imaging," *International journal of imaging systems and technology*, vol. 24, pp. 203-207, 2014.
- [87] L. Feng, T. Benkert, K. T. Block, D. K. Sodickson, R. Otazo, and H. Chandarana, "Compressed sensing for body MRI," *Journal of Magnetic Resonance Imaging*, vol. 45, pp. 966-987, 2017.
- [88] J. C. Ye, "Compressed sensing MRI: a review from signal processing perspective," *BMC Biomedical Engineering*, vol. 1, pp. 1-17, 2019.
- [89] K. G. Hollingsworth, "Reducing acquisition time in clinical MRI by data undersampling and compressed sensing reconstruction," *Physics in Medicine & Biology*, vol. 60, p. R297, 2015.
- [90] M. Blasche, C. Forman, and S. Healthineers, "Compressed sensing—the flowchart," MAGNETOM Flash, vol. 14, 2016.
- [91] O. N. Jaspan, R. Fleysher, and M. L. Lipton, "Compressed sensing MRI: a review of the clinical literature," *The British journal of radiology*, vol. 88, p. 20150487, 2015.

- [92] G. Shrividya and S. Bharathi, "A study of optimum sampling pattern for reconstruction of MR images using compressive sensing," in 2018 Second International Conference on Advances in Electronics, Computers and Communications (ICAECC), 2018, pp. 1-6.
- [93] J. Huang, L. Wang, and Y. Zhu, "Compressed Sensing MRI Reconstruction with Multiple Sparsity Constraints on Radial Sampling," *Mathematical Problems in Engineering*, vol. 2019, 2019.
- [94] L. Feng, R. Grimm, K. T. Block, H. Chandarana, S. Kim, J. Xu, et al., "Golden-angle radial sparse parallel MRI: combination of compressed sensing, parallel imaging, and golden-angle radial sampling for fast and flexible dynamic volumetric MRI," Magnetic resonance in medicine, vol. 72, pp. 707-717, 2014.
- [95] F. Krahmer and R. Ward, "Stable and robust sampling strategies for compressive imaging," *IEEE transactions on image processing*, vol. 23, pp. 612-622, 2013.
- [96] D. R. Thedens, P. Irarrazaval, T. S. Sachs, C. H. Meyer, and D. G. Nishimura, "Fast magnetic resonance coronary angiography with a three-dimensional stack of spirals trajectory," Magnetic Resonance in Medicine: An Official Journal of the International Society for Magnetic Resonance in Medicine, vol. 41, pp. 1170-1179, 1999.
- [97] K. T. Block, H. Chandarana, S. Milla, M. Bruno, T. Mulholland, G. Fatterpekar, et al., "Towards routine clinical use of radial stack-of-stars 3D gradient-echo sequences for reducing motion sensitivity," *Journal of the Korean Society of Magnetic Resonance in Medicine*, vol. 18, pp. 87-106, 2014.

- [98] Y. Pang, B. Yu, and X. Zhang, "Enhancement of the low resolution image quality using randomly sampled data for multi-slice MR imaging," *Quantitative imaging in medicine and surgery*, vol. 4, p. 136, 2014.
- [99] S. Datta, B. Deka, H. U. Mullah, and S. Kumar, "An efficient interpolated compressed sensing method for highly correlated 2D multi-slice MRI," in 2016 International Conference on Accessibility to Digital World (ICADW), 2016, pp. 187-192.
- [100] S. Datta and B. Deka, "Magnetic resonance image reconstruction using fast interpolated compressed sensing," *Journal of Optics*, vol. 47, pp. 154-165, 2018.
- [101] Y. Pang, J. Jiang, and X. Zhang, "Ultrafast fetal MR imaging using interpolated compressed sensing," in *Proc Intl Soc Mag Reson Med*, 2014.
- [102] L. Weizman, O. Rahamim, R. Dekel, Y. C. Eldar, and D. Ben-Bashat, "Exploiting similarity in adjacent slices for compressed sensing MRI," in 2014 36th Annual International Conference of the IEEE Engineering in Medicine and Biology Society, 2014, pp. 1549-1552.
- [103] C. Peng, "Towards Faster MRI Acquisition," Doctoral dissertation, University of Maryland, College Park, 2019.
- [104] C. Chen and J. Huang, "Compressive sensing MRI with wavelet tree sparsity," in Advances in neural information processing systems, 2012, pp. 1115-1123.
- [105] C. Chen and J. Huang, "Exploiting the wavelet structure in compressed sensing MRI," Magnetic resonance imaging, vol. 32, pp. 1377-1389, 2014.
- [106] C. Chen and J. Huang, "The benefit of tree sparsity in accelerated MRI," *Medical image analysis*, vol. 18, pp. 834-842, 2014.

- [107] J. Huang, S. Zhang, and D. Metaxas, "Efficient MR image reconstruction for compressed MR imaging," Medical Image Analysis, vol. 15, pp. 670-679, 2011.
- [108] A. Hirabayashi, N. Inamuro, K. Mimura, T. Kurihara, and T. Homma,

  "Compressed sensing MRI using sparsity induced from adjacent slice similarity,"

  in 2015 International Conference on Sampling Theory and Applications

  (SampTA), 2015, pp. 287-291.
- [109] M. Murad, M. Bilal, A. Jalil, A. Ali, K. Mehmood, and B. Khan, "Efficient Reconstruction Technique for Multi-Slice CS-MRI Using Novel Interpolation and 2D Sampling Scheme," *IEEE Access*, 2020.
- [110] S. Datta and B. Deka, "Multi-channel, multi-slice, and multi-contrast compressed sensing MRI using weighted forest sparsity and joint TV regularization priors," in *Soft Computing for Problem Solving*, ed: Springer, 2019, pp. 821-832.
- [111] S. Datta and B. Deka, "Efficient interpolated compressed sensing reconstruction scheme for 3D MRI," *IET Image Processing*, vol. 12, pp. 2119-2127, 2018.
- [112] "AANLIB database of Harward medical school".
  http://www.med.harvard.edu/aanlib/. Accessed March 2020.
- [113] Z. Wang, A. C. Bovik, H. R. Sheikh, and E. P. Simoncelli, "Image quality assessment: from error visibility to structural similarity," *IEEE transactions on image processing*, vol. 13, pp. 600-612, 2004.
- [114] L. Zhang, L. Zhang, X. Mou, and D. Zhang, "FSIM: A feature similarity index for image quality assessment," *IEEE transactions on Image Processing*, vol. 20, pp. 2378-2386, 2011.

- [115] A. Hore and D. Ziou, "Image quality metrics: PSNR vs. SSIM," in 2010 20th

  International Conference on Pattern Recognition, 2010, pp. 2366-2369.
- [116] J. Lee Rodgers and W. A. Nicewander, "Thirteen ways to look at the correlation coefficient," *The American Statistician*, vol. 42, pp. 59-66, 1988.
- [117] G. Blanchet and L. Moisan, "An explicit sharpness index related to global phase coherence," in 2012 IEEE International Conference on Acoustics, Speech and Signal Processing (ICASSP), 2012, pp. 1065-1068.
- [118] N. Venkatanath, D. Praneeth, M. C. Bh, S. S. Channappayya, and S. S. Medasani, "Blind image quality evaluation using perception based features," in 2015 Twenty First National Conference on Communications (NCC), 2015, pp. 1-6.
- [119] U. Sara, M. Akter, and M. S. Uddin, "Image quality assessment through FSIM, SSIM, MSE and PSNR—a comparative study," *Journal of Computer and Communications*, vol. 7, pp. 8-18, 2019.
- [120] M. Murad, A. Jalil, M. Bilal, S. Ikram, A. Ali, B. Khan, et al., "Radial Undersampling-Based Interpolation Scheme for Multislice CSMRI Reconstruction Techniques," BioMed Research International, vol. 2021, p. 6638588, 2021/04/13 2021.
- [121] R. W. Chan, E. A. Ramsay, E. Y. Cheung, and D. B. Plewes, "The influence of radial undersampling schemes on compressed sensing reconstruction in breast MRI," *Magnetic resonance in medicine*, vol. 67, pp. 363-377, 2012.
- [122] H. Jung, J. Park, J. Yoo, and J. C. Ye, "Radial k-t FOCUSS for high-resolution cardiac cine MRI," Magnetic Resonance in Medicine: An Official Journal of the

- International Society for Magnetic Resonance in Medicine, vol. 63, pp. 68-78, 2010.
- [123] J. M. Pauly, "Gridding & the NUFFT for non-cartesian image reconstruction,"

  ISMRM Educational Course on Image Reconstruction, vol. 45, 2012.
- [124] J. D. O'Sullivan, "A fast sinc function gridding algorithm for Fourier inversion in computer tomography," *IEEE transactions on medical imaging*, vol. 4, pp. 200-207, 1985.
- [125] R. Grimm, "Reconstruction Techniques for Dynamic Radial MRI," Friedrich-Alexander-Universitaet Erlangen-Nuernberg (Germany), 2015.
- [126] K. T. Block, M. Uecker, and J. Frahm, "Undersampled radial MRI with multiple coils. Iterative image reconstruction using a total variation constraint," Magnetic Resonance in Medicine: An Official Journal of the International Society for Magnetic Resonance in Medicine, vol. 57, pp. 1086-1098, 2007.
- [127] D. J. Winkel, H.-C. Breit, B. Shi, D. T. Boll, H.-H. Seifert, and C. Wetterauer,

  "Predicting clinically significant prostate cancer from quantitative image features
  including compressed sensing radial MRI of prostate perfusion using machine
  learning: comparison with PI-RADS v2 assessment scores," Quantitative imaging
  in medicine and surgery, vol. 10, p. 808, 2020.
- [128] N. Chauffert, P. Ciuciu, and P. Weiss, "Variable density compressed sensing in MRI. Theoretical vs heuristic sampling strategies," in 2013 IEEE 10th International Symposium on Biomedical Imaging, 2013, pp. 298-301.

- [129] J. Cao, S. Liu, H. Liu, and H. Lu, "CS-MRI reconstruction based on analysis dictionary learning and manifold structure regularization," *Neural Networks*, vol. 123, pp. 217-233, 2020.
- [130] J. Caballero, A. N. Price, D. Rueckert, and J. V. Hajnal, "Dictionary learning and time sparsity for dynamic MR data reconstruction," *IEEE transactions on medical* imaging, vol. 33, pp. 979-994, 2014.
- [131] S. Winkelmann, T. Schaeffter, T. Koehler, H. Eggers, and O. Doessel, "An optimal radial profile order based on the Golden Ratio for time-resolved MRI,"
  IEEE transactions on medical imaging, vol. 26, pp. 68-76, 2006.
- [132] K. L. Wright, J. I. Hamilton, M. A. Griswold, V. Gulani, and N. Seiberlich, "Non-Cartesian parallel imaging reconstruction," *Journal of Magnetic Resonance Imaging*, vol. 40, pp. 1022-1040, 2014.
- [133] J. A. Fessler and B. P. Sutton, "Nonuniform fast Fourier transforms using min-max interpolation," *IEEE transactions on signal processing*, vol. 51, pp. 560-574, 2003.
- [134] M. Murad, A. Jalil, M. Bilal, S. Ikram, A. Ali, K. Mehmeed, et al., "Gaussian-Radial Under-Sampling Based CSMRI Reconstruction using a Modified Interpolation Approach," in 2021 International Conference on Electrical, Communication, and Computer Engineering (ICECCE), 2021, pp. 1-6.

